Rapid semi-automated phenotypic assays for compound testing in patient-derived SPG4 neurons

Dissertation

zur Erlangung des Doktorgrades (Dr. rer. nat)

der

Mathematisch-Naturwissenschaftlichen Fakultät

der

Rheinischen Friedrich-Wilhelms-Universität Bonn

vorgelegt von

Kristina Rehbach (geb. Dobrindt)

aus

Bonn

Bonn, Juli 2018

Angefertigt mit Genehmigung der Mathematisch-Naturwissenschaftlichen Fakultät der
Rheinischen Friedrich-Wilhelms-Universität Bonn

1. Gutachter: Prof. Dr. Oliver Brüstle

2. Gutachter: Prof. Dr. Walter Witke

Mündliche Prüfung: 03.12.2018

Erscheinungsjahr: 2018

TABLE OF CONTENTS

Table of Contents I

Abstract V

1 Introduction 1

1.1 Neurite pathologies and axonal degeneration: common phenotypes in neurodegenerative diseases 1

1.2 Hereditary spastic paraplegia (HSP) 2

1.2.1 Introduction into HSP 2

1.2.2 Common molecular mechanisms of HSP 2

1.2.3 Spastic paraplegia 4 (SPG4): the most common form of HSP 4

1.2.4 The SPG4 protein spastin 5

1.2.5 Animal models and *in vitro* models of SPG4 6

1.3 Human pluripotent stem cells 9

1.3.1 Embryonic stem cells 9

1.3.2 Induced pluripotent stem cells 10

1.4 Neural development 11

1.5 The motor pathway 11

1.6 Neuronal differentiation 12

1.7 Cortical development and differentiation 12

1.8 Pharmacological screening 13

1.9 Aim of the study 14

2 Materials & Methods 15

2.1 Cell culture 15

2.1.1 Cell lines 15

2.1.1 Cell culture instruments 15

2.1.2 Cell culture materials 16

2.1.3 Cell culture media 16

2.1.4 Cell culture reagents 17

2.1.5 Cell culture coatings 19

2.1.6 Cell counting 19
2.1.7 Reprogramming of patient fibroblasts 19
2.1.8 Human pluripotent stem cell culture 20
2.1.9 Undirected differentiation 21
2.1.10 Teratoma assay 21
2.1.11 Directed differentiation into all three germ layers 21
2.1.12 Quality control of cell lines 22
2.1.13 Differentiation into glutamatergic cortical neurons 22
2.1.14 Differentiation into GABAergic forebrain neurons 23
2.2 Phenotypical assays 25
2.2.1 Neurite outgrowth and growth cone assay 25
2.2.1 Axonal swellings 25
2.3 Molecular biology 26
2.3.1 Molecular biology instruments 26
2.3.1 Molecular biology materials 26
2.3.2 Molecular biology reagents 27
2.3.3 Molecular biology kits 28
2.3.1 Molecular biology buffers 28
2.3.2 Primary antibodies and dyes 29
2.3.1 Secondary antibodies 29
2.3.1 Primer sequences 29
2.3.1 Analysis software 30
2.3.2 DNA preparation 31
2.3.3 RNA preparation 31
2.3.4 Complementary DNA (cDNA) preparation 31
2.3.5 SNP analysis 31
2.3.6 Genotyping 32
2.3.7 Scorecard analysis 32
2.3.8 Semi-quantitative PCR 33
2.3.9 Quantitative PCR 33

2.3.10 Immunocytochemistry 33
2.3.1 Automated image acquisition and image analysis 34
2.3.2 Western blot 35
3 Results 37
3.1 Generation and validation of SGP4 iPSCs 37
3.1.1 Validating genomic integrity of generated iPSC lines 37
3.1.2 Confirmation of the SPG4 mutation in generated iPSC lines 41
3.1.3 Assessment of pluripotency of generated iPSC lines 41
3.1.4 Transgene silencing 45
3.2 Differentiation and validation of cortical neurons 46
3.3 SPG4 neurons show reduced spastin levels 51
3.4 Assessment of disease-specific early phenotypes in cortical SPG4 neurons 53
3.4.1 Cortical SPG4 neurons display an impaired neurite outgrowth 53
3.4.2 Growth cones of cortical SPG4 neurons are significantly enlarged 54
3.4.3 Taxol treatment leads to rapid induction of TAU1-positive axons 55
3.4.4 Cortical SPG4 neurons show axonal swellings 56
3.5 Generation and validation of GABAergic neurons 57
3.6 GABAergic SPG4 neurons do not show disease-associated phenotypes 60
3.7 GABAergic neurons display elevated M1 *SPAST* levels 63
3.8 Compound evaluation in cortical SPG4 neurons 64
3.8.1 Read-through molecules fail to upregulate spastin levels 64
3.8.2 Automated analysis and selection of candidate compounds 65
3.8.3 Modulation of neurite outgrowth and growth cone area with small molecules 67
3.8.4 Modulation of axonal swellings using small molecules 72
3.8.5 Cryopreservation of the SPG4 neurite phenotype 75
4 Discussion 77
4.1 Generation and quality control of iPSCs 77
4.2 Derivation of highly enriched neuronal cultures with cortical identity 79
4.3 Spastin loss of function in SPG4 neurons 81
4.4 Identification of early, rapid phenotypes in SPG4 neurons 82

4.5 Subtype specificity of described phenotypes 83
4.6 Assay automation for compound screening 85
4.7 Identification of hit compounds rescuing SPG4 pathophenotypes 85
4.8 Outlook 87
5 References i
6 Figures xvii
7 Tables xix
8 Appendix xx
8.1 Abbreviations xx
8.2 Acknowledgements xxiii
8.3 Declaration xxv
8.4 Publications xxvii

ABSTRACT

Hereditary spastic paraplegia (HSP) is an inherited disease characterized by progressive spasticity in the lower limbs, caused by axonal degeneration of corticospinal motor neurons. Spastic paraplegia 4 (SPG4) is the most frequent, autosomal dominant subtype, responsible for >50% of all pure HSP cases. Affected patients carry mutations in the *SPAST* gene encoding the microtubule-severing enzyme spastin. So far, no curative treatment for HSP is available and drug discovery screens are hampered by the lack of suitable model systems. While SPG4-associated phenotypic alterations have been described in iPSC-derived neurons, development of these *in vitro* phenotypes typically requires several weeks of *in vitro* differentiation, limiting their exploitation for high-throughput assays. Therefore, developing a SPG4 model and enabling rapid phenotypic analyses within a few days is of great interest and became the focus of this study. To this end, fibroblasts of family members carrying a specific *SPAST* nonsense mutation were reprogrammed to a pluripotent state employing retroviruses or non-integrating Sendai viruses encoding *OCT4*, *KLF4*, *SOX2* and *c-MYC* yielding in several fully validated SPG4 iPSC lines. IPSCs from three patients carrying heterozygous *SPAST* nonsense mutations were differentiated into highly enriched neuronal cortical cultures comprising >80% glutamatergic neurons expressing the layer V/VI markers CTIP2 and TBR1. Spastin levels in SPG4 neuronal cultures were reduced by approximately 50% compared to controls. Focusing on the identification of early neuronal HSP-related phenotypes, SPG4 neurons exhibited a 51% reduction in neurite length compared to controls already 24 hours after plating. At that time point, enlarged growth cones suggestive of a cytoskeletal imbalance were observed as well. Moreover, axonal swellings a hallmark of the HSP pathology, could be reliably detected already five days after plating of SPG4 iPSC-derived cortical neurons. Swellings were 1-7µm in diameter and stained positive for the axonal markers TAU1 and acetylated tubulin. Furthermore, these disease specific early phenotypes appeared to be cell type specific and could not be found in GABAergic SPG4 forebrain neurons, which might be due to a higher expression of M1 *SPAST* in this cell type. However, the application of different read-through inducing molecules did not lead to an up-regulation of spastin levels in patient cultures. To identify new potentially therapeutic compounds, counteracting SPG4-associated neuronal phenotypes, all three fast phenotypic assays were transferred to an automated or semi-automated 96-well-setup. Indeed, the actin-destabilizing drug Latrunculin B and the liver X receptor (LXR) agonist GW3965 led to a significant increase in patient neurite length. And eight of the tested drugs achieved a significant reduction of patient growth cone areas, including Latrunculin B and GW3965. The most effective reduction of axonal swellings, accompanied by normal neuronal morphology was achieved by the bone morphogenetic protein (BMP) inhibitor DMH1 and the LXR agonist GW3965. In particular, GW3965 was able to rescue all three phenotypes of SPG4 neurons and had no effect on control neurons.

In summary, in this thesis several rapid phenotypic assays for disease modeling and drug screening in SPG4 neurons have been developed. In addition, the cortical neurons generated in this thesis are cryopreservable and prepared cell batches are readily available for future screening purposes. Taken together, the findings of this thesis provide an excellent basis for studying the underlying pathomechanisms as well as for drug development in hereditary spastic paraplegia.

1 INTRODUCTION

1.1 Neurite pathologies and axonal degeneration: common phenotypes in neurodegenerative diseases

Hereditary spastic paraplegia (HSP) is characterized by retrograde degeneration of upper motor neurons and axonal swellings, cellular phenotypes which are common to several motor neuron and neurodegenerative diseases (Blackstone 2018). Amyotrophic lateral sclerosis (ALS) is one of the most prominent motor neuron diseases, caused by degeneration of upper motor neurons and spinal motor neurons (Fischer-Hayes et al. 2013; Moloney et al. 2014). ALS patients often display additional symptoms of frontotemporal dementia (FTD) (Zago et al. 2011; Ferrari et al. 2011). In fact, these two neurodegenerative disorders seem to be closely related and can be caused by a hexanucleotide repeat expansion in the first intron of the same genomic locus: *C9ORF72*, which is the most common cause of ALS. This mutation can manifest in either ALS, FTD or both (Renton et al. 2011). In another motor neurons disease, spinal muscular atrophy (SMA), spinal motor neurons degenerate, leading to overall muscle weakness (Winkler et al. 2005; Heesen et al. 2016). Charcot Marie Tooth can be caused by myelopathy leading to axonopathy, or primarily by axonal degeneration of spinal motor neurons as well as sensory neurons. This group of disorders is associated with mutations in different genomic loci and is considered to be the most common hereditary polyneuropathy (Krajewski et al. 2000; Hoyle et al. 2015). Even though multiple sclerosis is mainly known to be caused by demyelination, evidence points towards a major role of axonal degeneration in disease onset, progression and severity (Su et al. 2009; Haines et al. 2011). Alzheimer's disease is characterized by progressive axonal degeneration, accompanied by the formation of axonal tau accumulations (Mertens et al. 2013; Kanaan et al. 2013; Kneynsberg et al. 2017). Parkinson's disease is caused by axonal and neuronal degeneration of dopaminergic neurons in the substantia nigra (Burke and O'Malley 2013; Tagliaferro and Burke 2016). *In vitro* iPSC models of Parkinson's disease could show additional neurite phenotypes, including reduced numbers of neurites, reduced neurite length and neurite arborization (Sánchez-Danés et al. 2012; Reinhardt et al. 2013). Overall, axonal degeneration and neurite pathologies are key pathological hallmark in a number of neurodegenerative diseases including HSP.

1.2 Hereditary spastic paraplegia (HSP)

1.2.1 Introduction into HSP

Hereditary spastic paraplegia is a group of disorders displaying a progressive degeneration of the upper motor neurons, manifesting by spastic weakness of the lower extremities (Tallaksen et al. 2001; Salinas et al. 2008; Lo Giudice et al. 2014). The genetic causes associated with HSP are steadily growing. Until now, 78 different spastic paraplegia disease-loci and 60 spastic paraplegia genes have been identified (Lo Giudice et al. 2014; Novarino et al. 2014; Solowska and Baas 2015; Estrada-Cuzcano et al. 2017). As indicated by the name, HSP is an inherited disease and has an overall prevalence of 1.8-9 /10^5, depending of the population at hand (Blackstone 2012; Ruano et al. 2014). The disease onset is highly variable, ranging from early childhood up to 70 years of age. Depending on the affected gene and form, HSP can be passed on in an autosomal dominant, autosomal recessive, X-linked, or mitochondrial mode (Schüle and Schöls 2011; Finsterer et al. 2012). The most common forms of HSP: SPG4 (Hazan et al. 1999) and SPG3A (Zhao et al. 2001) are both pure, uncomplicated forms, affecting only the upper motor neurons without additional symptoms (e.g. dementia, cerebellar ataxia, thin corpus callosum). Whereas SPG11, (Martínez Murillo et al. 1999; Stevanin et al. 2007) which is the most common cause of autosomal recessive HSP, (Lo Giudice et al. 2014) presents as a complicated form with additional symptoms.

1.2.2 Common molecular mechanisms of HSP

Genes that are mutated in HSP play a role in several essential cellular processes, many of which are of particular importance in neurons, a specialized cell type with long axons and thus an enlarged membrane compartment and enhanced trafficking needs. One of these membrane compartments is the endoplasmic reticulum (ER), which stretches throughout the whole axon from the soma to the distal synapses. Besides the ER, several other cellular compartments or processes have been implicated in the formation of HSP. Amongst these are lipid metabolism, myelination, mitochondria, axonal transport, endosomal trafficking, inhibition of BMP signaling, microtubule interaction, autophagy and developmental errors. Thus, the proteins involved in HSP are localized at several different cellular sites (Figure 1.1)

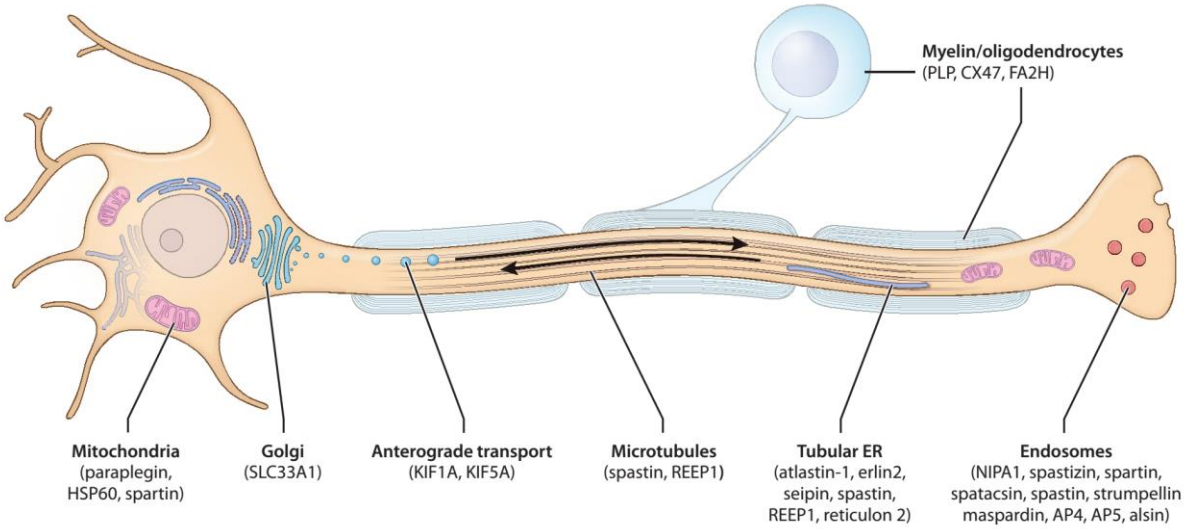

Figure 1.1 Illustration of HSP proteins and their cellular compartments (Blackstone et al. 2012)

Spastin (SPG4), atlastin (SPG3A), receptor expression-enhancing protein 1 (REEP1, SPG31) (Züchner et al. 2006), reticulon2 (SPG12) (Montenegro et al. 2012) and protrudin (SPG33) (Mannan et al. 2006; Hashimoto et al. 2014) are all located at the smooth tubular ER (Park et al. 2010; Goyal & Blackstone 2013) and mutations in these proteins cause more than 50% of all HSP cases. One important function of the ER is lipid -synthesis and -distribution. The HSP proteins spartin (SPG20) (Patel et al. 2002; Eastman et al. 2009; Edwards et al. 2009), seipin (SPG17) (Windpassinger et al. 2004; Szymanski et al. 2007), REEP1 (SPG31) (Falk et al. 2014) and spastin (SPG4) (Papadopoulos et al. 2015) play a role in lipid droplet biogenesis. Whereas several other HSP proteins are involved in lipid biosynthesis. They include the acetyl-CoA transporter (SPG42) (Lin et al. 2008), DDHD1 (SPG28) (Tesson et al. 2012), DDHD2 (SPG54) (Schuurs-Hoeijmakers et al. 2012), fatty acid 2-hydroxylase (FA2H; SPG35) (Dick et al. 2010), CYP2U1 (SPG56) (Tesson et al. 2012), neuropathy target esterase (NTE; SPG39) (Rainier et al. 2008; Read et al. 2009), cytochrome P450-7B1 (CYP7B1; SPG5) (Tsaousidou et al. 2008), β-1,4-N-acetyl-galactosaminyl transferase 1 (B4GALNT1; SPG26) (Boukhris et al. 2013), glucocerebrosidase GBA2 (SPG46) (Martin et al. 2013) and CPT1C (Rinaldi et al. 2015). The intracellular gap junction channel connexin–47 (SPG44) (Orthmann-Murphy et al. 2009), the proteolipid protein 1 (PLP1; SPG2) (Saugier-Veber et al. 1994) and FA2H (SPG35) on the other hand are expressed in oligodendrocytes and play an immediate role in the myelination process.
Mitochondrial function is another common theme among HSP-causing proteins. Mutations in paraplegin (SPG7) (Hansen et al. 2002), heat shock protein 60 (HSP60; SPG13) (Casari et al. 1998), acetyl-CoA transporter (SPG42) and DDHD1 (SPG28) (Tesson et al. 2012) lead to increased oxidative stress or alter mitochondrial form and function.

Mutations in the motor proteins KIF1A (SPG30) (Erlich et al. 2011) and KIF5A (SPG10) (Reid et al. 2002) lead to axonal transport abnormalities, which has in a more indirect manner also been implied for SPG4 (Kasher et al. 2009).

Endosomes play a major role in trafficking of membrane and cargo. Several HSP proteins e.g. protrudin (SPG33), maspardin (SPG21) (Simpson et al. 2003) and NIPA1 (SPG6) (Rainier et al. 2003) are known to be located at endosomes, even though their exact function is still unclear. Spatacsin (SPG11) (Stevanin et al. 2007), spastizin (SPG15) (Hanein et al. 2008) and KIAA0415 (SPG48) (Słabicki et al. 2010) on the other hand are part of a protein complex involved in endosomal vesicle trafficking, which has also been implicated in DNA repair. Strumpellin (SPG8) (Valdmanis et al. 2007) is part of the Wiskott–Aldrich syndrome protein and scar homolog (WASH) complex, which regulates endosomal trafficking (Freeman, Seaman, and Reid 2013).

Endosomal sorting complex required for transport (ESCRT) complexes also regulate trafficking of proteins from endosomes to lysosomes and other vesicles. HSP protein VPS37A (SPG53) (Zivony-Elboum et al. 2012) is part of the ESCRT–I complex, whereas spastin (SPG4) and spartin (SPG20) interact with the ESCRT–III complex (Renvoisé and Blackstone 2010; Allison et al. 2013) through a common microtubule interacting and trafficking (MIT) domain (Ciccarelli et al. 2003). Likely due to its function in endosomal sorting, spartin (SPG20) is also involved in epidermal growth factor receptor (EGFR) regulation (Bakowska et al. 2007). Endosomal sorting might also play a role in the inhibitory function of atlastin (SPG3A), spastin (SPG4), (SPG6) and Spartin (SPG20) on BMP signaling (Tsang et al. 2009).

Tectonin beta propeller repeat containing protein 2 (TECPR2; SPG49) (Oz-Levi et al. 2012) was the first HSP protein discovered that is part of the autophagic machinery, a very important cellular degradation mechanism. Only recently two additional proteins spatacsin (SPG11) and spastizin (SPG15) have been implicated in impaired autophagy (Renvoisé et al. 2014; Chang et al. 2014; Varga et al. 2015).

Only two forms of HSP are known, that are definitely due to developmental errors: NCAM (SPG1) (Jouet et al. 1994) plays an important role in axon pathfinding and MCT8 (SPG22) (Schwartz et al. 2005) is a membrane transporter involved in axon development. Besides SPG1 and SPG22, developmental involvement is only discussed for SPG3A which might play a role in axon elongation during development (Zhu et al. 2006). Overall, several important cellular functions are implicated in the disease mechanism of HSP, they include ER function, lipid biosynthesis, myelination, mitochondrial function, axonal transport, endosomal sorting and trafficking, BMP inhibition and autophagy.

1.2.3 Spastic paraplegia 4 (SPG4): the most common form of HSP

SPG4 is the most common form of hereditary spastic paraplegia (Finsterer et al. 2012; Ruano et al. 2014). Over 50% of the autosomal dominant and >25% of all HSP cases are due to mutations

in the *SPAST* gene (Schüle et al. 2016). SPG4 manifests as pure, uncomplicated form, affecting only the upper motor neurons without additional symptoms (e.g. dementia, cerebellar ataxia, thin corpus callosum). Patients display a spastic paraplegia of the lower limbs, leading to spastic gait and immobility. The age of onset is usually around 30 years of age, but it may vary from early childhood to old age, even if the same mutation is present. The *SPAST* gene is located on chromosome 2p22.3, spans a region of about 90 kb and contains 17 exons.

SPG4 can be caused by a variety of mutations in the *SPAST* gene including missense, nonsense, splice site, deletions and insertions. Most of these mutations lead to a loss of protein expression, which indicates that the most common mode of action is haploinsufficiency. Only very few cases are reported where a dominant negative active mode of action is implied (Solowska et al. 2010). Remarkably, about 6% of individuals carrying a *SPAST* mutation are completely asymptomatic (Dürr et al. 2012). Genetic modifiers are likely to play a role but have not yet been discovered.

1.2.4 The SPG4 protein spastin

Spastin is one of the central HSP proteins, which is due to the frequency of SPG4 mutations, its various cellular functions and the fact that it interacts with several other HSP causing proteins.

The main function of spastin is a severing of microtubules carried out by the AAA (ATPase associated with various cellular activities) enzyme domain (Figure 1.2). It is present in all isoforms, makes up most of the protein (spanning amino acids 342 – 599) and becomes active upon hexamerization (White et al. 2007). Especially negatively charged polyglutamylated tubulin stimulates spastin-mediated severing (Lacroix et al. 2010). Spastin has two different start codons leading to different isoforms of the protein. The first start codon is initiating the M1 isoform, expressed to a minor degree due to a weaker Kozak sequence (Claudiani et al. 2005). The predominantly and ubiquitously expressed spastin isoform is the shorter M87 isoform (Solowska et al. 2010). Besides the 616 amino acid (68 kDa) long M1 isoform and the 530 amino acid (60 kDa) long M87 isoform, two additional isoforms, generated by mRNA splicing of exon 4 (shaded in black), exist (Figure 1.2). Although the M87 is in general more abundantly expressed, the M1 isoform is thought to be predominantly expressed in the spinal cord (Solowska et al. 2010).

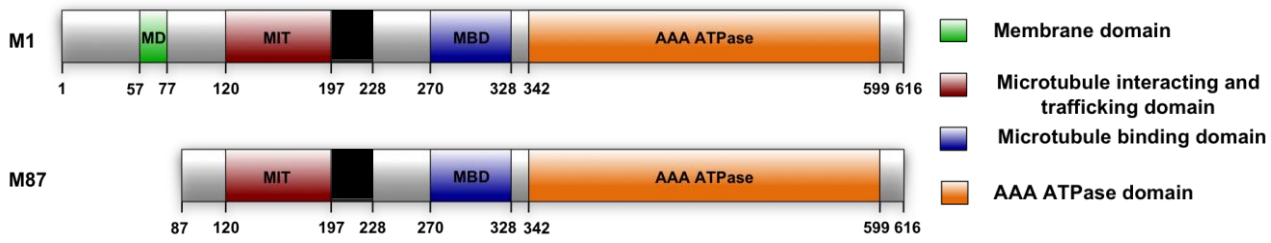

Figure 1.2 Scheme of the microtubule severing protein spastin

Besides the AAA domain, a microtubule-binding domain (MTBD) spanning amino acids 270 to 328, is essential for hexamerization of spastin and breaking of microtubules. The microtubule interacting and trafficking domain (MIT) made up of amino acids 120-197 on the other hand, is a protein interacting domain. Through the MIT domain spastin interacts with two ESCRT-III complex proteins: charged multi-vascular body protein 1B (CHMP1B) and the increased sodium tolerance (IST1) protein. ESCRT-III, CHMP1B and spastin act together to complete abscission during cytokinesis, which is delayed in HeLa KO lines (Reid et al. 2005; Connell et al. 2009). *In vivo* this effect cannot be observed, pointing towards a compensation mechanism. The interaction with IST1 on the other hand, seems to promote fission of recycling tubes from endosomes, controlling the balance between degradation and recycling of receptors *in vitro* in HeLa cells but also *in vivo* in zebrafish (Allison et al. 2013). This regulatory function might explain spastin's role as inhibitor of BMP signaling (Tsang et al. 2009), a pathway involved in developmental patterning, differentiation, axonal guidance and axon outgrowth (Liu et al. 2005). However, it is yet unclear, through which mechanism spastin achieves a down-regulation of BMP signaling.

In spastin, a hydrophobic region stretches from amino acids 57 to 77, which is unique to the longer M1 isoform and forms a hairpin that can intercalate as a wedge into the ER membrane (Park et al. 2010). In addition, this hydrophobic domain can interact with the hydrophobic hairpins of atlastin and REEP1, other HSP causing proteins, and the endoplasmic reticulum shaping protein reticulon 1 (RTN1) (Mannan et al. 2006). Together these proteins are involved in shaping the smooth endoplasmic reticulum. More specifically, they mediate the formation of three-way junctions responsible for the polygonal structure of the tubular ER (Park et al. 2010; Goyal et al. 2013). Due to spastin's role as a microtubule severing enzyme, it can in addition mediate lipid droplet formation and abscission from the ER (Papadopoulos et al. 2015). Furthermore, spastin is a binding partner of protrudin (SPG33) and promotes protrudin-dependent neurite outgrowth (Zhang et al. 2012). However, it is still uncertain if the M1 isoform, the M87 isoform or both isoforms are accountable for disease formation.

1.2.5 Animal models and *in vitro* models of SPG4

Several disease models with mutated spastin have been generated and described to further understand the molecular basis of SPG4. These disease models range from HeLa cell culture models, to zebrafish-, drosophila- and mouse models to more advanced human pluripotent stem cell-based cell culture models. Even a bovine model exists, carrying mutations in the *SPAST* gene and causing a recessive neurodegenerative disease called bovine spinal demyelination (Thomsen et al. 2010).

In SPG4 patients, the most prominent molecular phenotype that could be found postmortem are axonal swellings in the spinal cord (Kasher et al. 2009). This phenotype was for the first time recapitulated in a mouse model expressing mutated spastin carrying a premature stop codon.

Even though the motor defects were mild, the mice exhibited axonal swellings with abnormal accumulation of organelles and cytoskeletal components (Tarrade et al. 2006). Axonal swellings, which contain cytoskeletal proteins can also be observed in another SPG4 mouse model, where pathogenic splice site mutations lead to a loss of protein (Kasher et al. 2009). In two human iPSC models with decreased spastin expression, axonal swellings filled with mitochondria, TAU protein (Denton et al. 2014) and disrupted microtubules (Havlicek et al. 2014) were found. In one of the mouse models and one of the iPSC models, a rescue of axonal swellings with low concentrations of microtubule targeting drugs Nocodazole, Vinblastine, Taxol (Fassier et al. 2013) or only Vinblastine (Denton et al. 2014) could be shown. The authors speculated, that the occurrence of axonal swellings might be due to insufficient microtubule severing by mutated spastin.

Spastin's ability to sever microtubules was first suspected due to its sequence homology with the microtubule severing enzyme katanin and its colocalization with microtubules (Connell et al. 2009). This was confirmed by cell culture models, which could also show that mutations within spastin's ATPase domain can severely impair microtubule severing (Evans et al. 2005). A proposed disease mechanism is a traffic jam caused by disrupted microtubules and axonal swellings that leads to impaired axonal transport. Evidence for this hypothesis could be found in a mouse model in 2009 and in three human SPG4 models. However, the results are somewhat controversial, since all studies show different impairments. In the mouse model a reduced anterograde transport was observed (Kasher et al. 2009). The first published iPSC disease model reported an overall decreased mitochondrial transport (Denton et al. 2014), whereas the second iPSC disease model could only show a slight imbalance of axonal transport with less retrograde movement (Havlicek et al. 2014). In a disease model using patient olfactory mucosa cells, marginally slower moving peroxisomes were observed (Abrahamsen et al. 2013), a phenotype that could be rescued by low concentrations of the microtubule binding drugs: Taxol, Vinblastine, EpothiloneD or Noscapine (Fan et al. 2014). Similar observations have been made in mouse neuroblastoma cells, which exhibited slightly reduced velocity of vesicles, upon overexpression of certain *SPAST* mutations (Fuerst et al. 2011).

Comparable controversy prevails in the question whether reduced spastin levels lead to more or less of stable, acetylated tubulin. One would expect more stable microtubules, but for olfactory mucosa derived cells the opposite effect was reported, i.e. slight down-regulation of acetylated tubulin. This was explained by compensatory upregulation of stathmin, a microtubule-destabilizing enzyme (Abrahamsen et al. 2013). Denton et al. found the expected upregulation of acetylated microtubule in patient iPSC derived neurons, however the sample size of one patient and one control is very low. In contrast Havlicek et al. did not see any difference regarding stabilized tubulin levels in their patient iPSC derived neurons compared to controls. Here, the difference to the expected result is explained by an observed upregulation of the microtubule severing enzyme p60 katanin.

In addition, spastin seems to have an impact on neurite length and morphology. Even though normal viability and neurite density were reported for cultured cortical neurons of the 2006 mouse model (Tarrade et al. 2006), spastin knockdown in developing zebrafish embryos led to dramatic defects in motor axonal outgrowth (Wood et al. 2006; Butler et al. 2010). Likewise, in cultured mouse hippocampal neurons, spastin depletion led to abnormal neuronal morphology, dystrophic neurites, axonal growth defects and reduced microtubule assembly rate (Riano et al. 2009). In human iPSC-derived neurons, reduced neurite complexity and neurite length was observed after 6 weeks of culture, phenotypes that could be rescued by spastin overexpression (Havlicek et al. 2014). However, the right spastin dose seems to be very important, indicated by decreased motor function in Drosophila and neurite outgrowth defects in primary rat cortical neurons upon overexpression of spastin (Solowska et al. 2014).

Since there is no developmental aspect known for SPG4, a mechanism in which spastin is important for axon maintenance and regeneration seems likely. The only evidence regarding regeneration has been reported in a drosophila model (with one mutated spastin allele) where mutant flies exhibited defective axon regeneration from the dendrite and the stump, but normal axon and dendrite outgrowth (Stone et al. 2012).

One hypothesis to explain the selectivity and late onset of SPG4, is the differential isoform expression. In rats, spastin is highly expressed in all embryonic neural tissues but downregulated in the adult nervous system. Interestingly, in rats, the M1 isoform is almost absent from developing neurons and most adults neuron, but is more strongly expressed in the adult spinal cord (Solowska et al. 2008). From this observation the hypothesis was derived that the rare M1 isoform is responsible for disease formation. Due to its hydrophobic domain, the M1 isoform has some unique functions, it localizes to the early secretory pathway and the ER, where it can sort to pre- and mature lipid droplets. Since, downregulation of spastin led to decreased lipid droplet number in Drosophila nerves, spastin seems to play a role in lipid droplets formation (Papadopoulos et al. 2015). In an overexpression scenario, the M1 isoform is believed to interrupt normal axon growth and inhibit fast axonal transport due to decreased microtubule dynamics caused by a gain of function mechanism of mutated M1 spastin (Solowska et al. 2008; Solowska et al. 2014).

Membrane modeling might be another common theme in SPG4 pathology. HeLa cells and zebrafish lacking spastin exhibit increased tubulation of the endosomal tubular recycling compartments leading to defective receptor sorting (Allison et al. 2013). Through this mechanism, lack of spastin could lead to BMP receptor downregulation. Spastin's role as inhibitor of BMP signaling has been shown previously in HeLa cells, together with NIPA1s ability to promote endocytosis and lysosomal degradation of the BMPRII (Tsang et al. 2009).

Especially in models where only one motor neuron exists, defects in neuromuscular junctions (NMJs) and synapses have been reported. Spastin-null Drosophila larvae have more numerous and clustered NMJ synaptic boutons and the adult flies cannot fly or jump and have fewer

microtubule bundles within the NMJs (Sherwood et al. 2004). Drosophila carrying a spastin knock-out in neural cells show an excessive stabilization of microtubules in the NMJ synapse, which can be attenuated by Vinblastine treatment (Orso et al. 2005). Even flies that lack drosophila spastin and have a humanized heterozygous genotype (one active, one inactive human spastin), have an aberrant distal synapse morphology. Comparable to the drosophila knock-out, the synaptic boutons are more numerous and the microtubule distribution is altered (Du et al. 2010). In zebrafish, spastin knock-out leads to reduced growth cone activity *in vivo* combined with altered microtubule dynamics. However, Nocodazole a microtubule destabilizing substance similar to Vinblastine enhances the severity of the phenotype (Butler et al. 2010).
Until now, there is no specific therapy known for SPG4. In cellular models only microtubule modulating drugs, which are approved as cancer treatments, were able to alleviate phenotypes. One other, rather surprising strategy proven successful in a drosophila SPG4 model was cooling of the organism. Decreased temperature improved mobility, survival and a synaptic phenotype in the flies (Baxter et al. 2014).

1.3 Human pluripotent stem cells

1.3.1 Embryonic stem cells

Pluripotent cells have the ability to self- renew as well as the potential to differentiate into every cell of the organism, thus into all three germ layers. The concept of pluripotency was first discovered in teratocarcinoma (also named teratoma), tumors consisting of differentiated cells of all three germ layers. In 1964, Kleinsmith and Pierce identified embryonal carcinoma cells, capable of teratoma formation after single cell transplantation in mice (Kleinsmith et al. 1964). These cells were competent of both unlimited self-renewal and multilineage differentiation, thus fulfilling the definition of pluripotency. This was the foundation for the isolation of embryonic stem cells from the inner cell mass of mouse preimplantation blastocysts in 1981 (Evans and Kaufman 1981; Martin 1981). These mouse embryonic stem cells (ESCs) were cultured on irradiated feeder cells (mouse embryonic fibroblasts) in the presence of leukemia inhibitory factor (Lif) and fetal call serum (FCS), grew in colonies and had a tightly packed dome-shaped morphology. The isolation of human embryonic stem cells from the blastocysts was finally achieved in 1998 (Thomson et al. 1998). Even though mouse and human ESC lines are pluripotent, human ESC-colonies have a flattened morphology and are fibroblast growth factor (FGF) - rather than Lif -dependent. It is now believed, that human ESCs are actually derived from the post-implantation epiblast, which is one step further in embryogenesis, and are already primed towards a lineage. Human ESCs are randomly methylated and are now often referred to as epiblast derived stem cells (EpiSCs) or primed ESCs (Nichols and Smith 2009). Further understanding of pluripotency led to more defined medium and culture conditions. Human ESCs are now most commonly cultured in a feeder-free

manner on growth factor reduced (GFR) Matrigel (MG), a gelatinous extracellular matrix protein mixture derived from Engelbreth-Holm-Swarm (EHS) mouse sarcoma, consisting of approximately 60% laminin, 30% collagen IV, and 8% entactin (Xu et al. 2001). The dissociation reagent collagenase, that lifted whole colonies from the feeder layer, has been replaced by the much faster acting accutase in combination with a Rho-associated protein kinase (ROCK) inhibitor, that is used to increase survival of the gained single cells (Watanabe et al. 2007). The alternative EDTA acts even faster, but maintains small cell clumps that can survive without ROCK inhibitors (Beers et al. 2012). The most popular defined media for human ESCs are mTeSR and Essential 8 (E8), both based on the growth factors FGF2 and transforming growth factor beta (TGF-β) (Ludwig et al. 2006a; Ludwig et al. 2006b; Chen et al. 2011; Beers et al. 2012). FGF2 is acting as a survival factor for ESCs and promotes long-term self-renewal, whereas TGF-β promotes pluripotency by upregulating the pluripotency genes *OCT4* and *NANOG* (Xu et al. 2005; Darr et al. 2006; Johnson et al. 2008). Besides *OCT4* and *NANOG*, *SOX2* belongs to the core pluripotency factors, which enforce each other through auto regulatory circuits, promote self-renewal and pluripotency and down-regulate differentiation genes (Boyer et al. 2005; Kashyap et al. 2009).

1.3.2 Induced pluripotent stem cells

In 2006, the group of Yamanaka revolutionized the stem cell field by dedifferentiating mouse fibroblasts into pluripotent stem cells, called induced pluripotent stem cells (iPSCs), by lentiviral overexpression of four factors (Takahashi and Yamanaka 2006). These potent pluripotency inducing factors, now known as Yamanaka factors are Oct4, Sox2, Klf4 and c-Myc. Only one year later, reprogramming was also achieved in the human system generating human iPSCs, highly similar to human ESCs (Takahashi et al. 2007; Yu et al. 2007). This new development made a widespread research on human pluripotent stem cells and derived patient specific cells possible, since there was no longer a need for human blastocysts and the involved ethical concerns. Reprogramming started off with integrating viruses e.g. lentiviruses and retroviruses, which integrate randomly into the genome and might cause additional mutations in coding regions. To avoid genomic aberrations, incomplete silencing or reactivation of the transgenes in differentiated cells, non-integrating systems were developed. Early strategies like repeated plasmid transfection (Okita et al. 2008), protein mediated reprogramming (Zhou et al. 2009) and adenoviral transduction (Stadtfeld et al. 2008) were soon replaced by simpler and more efficient methods including transfection of synthetic modified mRNA (Warren et al. 2010) and Sendai virus transduction. Especially Sendai RNA viruses carrying the four Yamanaka factors are very efficient for reprogramming of primary cells (Fusaki et al. 2009). Human iPSCs are essentially indistinguishable from human ESCs, they can be cultured using the same media and coatings. However, to make sure that iPSCs are fully reprogrammed and truly pluripotent, they have to go

through a profound validation process. Since iPSCs are generated from adult somatic cells, clones have to be screened for pre-existing mutations as well as newly acquired ones, which might mask the cellular phenotype. To correct for minor mutations, that cannot be seen in standard genome analysis, e.g. karyotyping or single nucleotide polymorphism (SNP) analysis, disease modeling studies use two to three clones of one genetic background. Furthermore, iPSC clones are analyzed regarding morphology, growth rate, pluripotency marker expression, transgene silencing and their differentiation potential (Park and Daley 2009; Maherali and Hochedlinger 2008). Pluripotent cells should per definition be able to differentiate into all three germ layers; this can be tested *in vivo* by teratoma formation in mice or *in vitro* by directed or undirected differentiation followed by immunostaining or real-time qPCR analysis on a so-called scorecard array (Bock et al. 2011). Especially the possibility to differentiate iPSCs into all tissues of the body allows research on authentic cell types like neurons or cardiomyocytes, whose availability is otherwise very limited, with a wild type or disease genotype. Overall, the field of iPSC research offers exciting opportunities for disease modeling, drug screening and developmental research.

1.4 Neural development

The nervous system is derived from the ectoderm. First, the neural plate forms which invaginates to form the neural tube during neurulation. All cells of the central nervous system develop from the walls of the neural tube. The neural crest gives rise to the peripheral nervous system and lies adjacent to the neural tube. During early differentiation, three primary vesicles are formed, the prosencephalon (forebrain), the mesencephalon (midbrain) and the rhombencephalon (hindbrain), which is connected to the caudal neural tube (spinal cord). The prosencephalon develops further into the telencephalic vesicles, the diencephalon and the optic vesicles. The telencephalon gives rise to the cerebral cortex and the basal telencephalon, whereas the diencephalon forms the thalamus and the hypothalamus. The patterning into different brain regions is mediated by growth factors and their concentration gradients. In general, retinoic acid and FGF signaling posteriorize, BMP signaling dorsalizes and sonic hedgehog (Shh) signaling ventralizes (Bear et al. 2007; Briscoe and Novitch 2008).

1.5 The motor pathway

The motor pathway, also called the corticospinal pathway is responsible for voluntary movement. Movement instructions originate from the cerebral cortex, more specifically the layer V of the motor cortex and follow the corticospinal tract to the spinal cord to finally trigger muscle contraction and movement. The axons of the upper motor neurons are the longest in the human body and form glutamatergic, excitatory synapses. Originating in the motor cortex, they mostly cross over in the medula and descend down to the spinal cord, where they establish synapses either directly with lower motor neurons or with spinal interneurons, which then connect with the

lower, spinal motor neurons. These spinal or alpha motor neurons innervate the large skeletal muscle fibers. Due to extensive branching, one motor neuron can form countless neuromuscular junctions to excite up to several hundred muscle fibers. The length and complexity of the motor pathway is especially challenging for its components, particularly the upper motor neurons with their uniquely long axons (Guyton and Hall 2006; Blackstone 2012).

1.6 Neuronal differentiation

To effectively model human diseases with ESCs or iPSCs, it is necessary to differentiate a pure population of the affected neuronal subtype, to be able to exclude effects from contaminating cell types. When the concept of neural differentiation first emerged, undirected differentiating embryoid bodies (EBs) or neural lineage inducing stromal feeder cells were used. These protocols had a high variability of outcome and poor yield of the desired cell type. SMAD signaling, which is activated by members of the TGF-beta superfamily has been identified as a key factor during early neural development (Smith and Harland 1992; Sasai et al. 1994; Wrana and Attisano 2000). Accordingly, the BMP inhibitor noggin enhanced neural induction in early human ESC differentiation protocols (Lee et al. 2007; Elkabetz et al. 2008). Moreover, inhibition of nodal, another member of the TGF-beta family, promoted neural induction in an EB-based differentiation protocol (Smith et al. 2008). Combining noggin and SB431542, an inhibitor of nodal, led to almost complete neural induction and revolutionized the field of neural differentiation (Chambers et al. 2009). Intrinsic differentiation propensities of pluripotent stem cells (PSCs) could be overcome to achieve an even better neural induction by replacing nodal with the small molecule inhibitor Dorsomorphin (Kim et al. 2010).

1.7 Cortical development and differentiation

The default program for neural differentiation is the forebrain fate, but specific induction of cortical neuroepithelial stem cells seems to be dependent on retinoid signaling (Shi et al. 2012). Complete cortical differentiation from human PSCs takes approximately 80 days and goes through different progenitor stages. By the means of paracrine signaling, the cells induce each other's proliferation and dorsalization. Besides neuroepithelial stem cells, two later progenitor populations: the basal progenitor cells and the outer radial glial cells exist and lead to the formation of the cortex (Lui et al. 2011). The cortex consists mainly of glutamatergic, excitatory projection neurons and only to 20% of GABAergic interneurons that are generated in the striatum and migrate into the cortex during development (Wonders and Anderson 2006). The six layers of cortical excitatory neurons are generated in a specific order, first the deep layer neurons (V and VI) followed by the upper layer neurons. Layer V and layer VI of the cortex are characterized by their expression of the marker CTIP2 and TBR1, respectively. Whereas, in the upper layers BRN2, SATB2 and CUX1 expression is predominant (Hansen, Rubenstein, and Kriegstein 2011).

1.8 Pharmacological screening

Traditionally, early drug discovery was based on historical knowledge, for example in the case of aspirin. Due to advances in molecular biology, animal models and overexpression systems were employed to find a candidate drug or to randomly test several hundred thousands of chemical compounds (Heilker et al. 2014). It turned out that candidates that were highly successful in early drug discovery phases often failed to show efficacy in clinical trials. Considering the time (>10 years) and the immense costs (often exceeding $1 billion) invested into every drug candidate that reaches late stage drug development, it is essential to develop reliable preclinical biological models (Hughes et al. 2011). Here, a physiological human disease model for phenotypic screening which is nonetheless standardized, would be highly desirable. IPSC derived disease models could make this possible. However, it is crucial that the affected cell type is employed and that the readout is as close to the *in vivo* phenotype as possible. To exclude drugs that have random, disease unrelated effects, it is advisable to use more than one phenotypic assay. For high-throughput analysis it is essential that the assay is amenable to upscaling combined with an automated analysis (Heilker et al. 2014). But this alone is not enough, in addition the assay has to achieve low experimental variability and good separation between populations. Based on means and standard deviations of both the positive and negative controls, the z-factor can be calculated and provides information on whether or not the assay is amenable for high throughput screening (Figure 1.3).

$$\text{Z-factor} = 1 - \frac{3(\sigma_p + \sigma_n)}{|\mu_p - \mu_n|}.$$

Figure 1.3 Formula for the z-factor

The Z-factor is a statistical measure for assay performance often used in high-throughput screening. It is defined by four parameters: the means (μ) and standard deviations (σ) of both the positive (p) and negative (n) controls (μ_p, σ_p, and μ_n, σ_n).

A set-up with a z-factor between 0.5 and 1.0 qualifies as an excellent assay worth pursuing further (Bray and Carpenter 2013). A z-factor below 0.5 would disqualify the assay, if the separation between populations is too low. However, if the Z-factor is below 0.5 due to a high experimental variability, the assay could be optimized further to achieve a reduction in the standard deviation.

1.9 Aim of the study

HSP is a hereditary neurodegenerative disease, without a known disease mechanism and without curative treatment. Since corticospinal neurons are the affected cell type, accessibility of patient neurons for research is very limited. IPSC derived cortical neurons are a suitable tool to overcome the lack of SPG4 neurons and to accelerate research towards medical treatment.

Thus, the aim of the study is the generation of a standardized human neuronal model for the most common form of hereditary spastic paraplegia, i.e. SPG4.

For this purpose, fibroblasts of three patients will be reprogrammed into iPSCs. To ensure the quality of generated iPSCs, the cell clones will be extensively validated regarding their pluripotency and differentiation potential. To study SPG4 in authentic patient neurons, iPSCs have to be differentiated into the disease affected cell type, i.e. cortical deep layer projection neurons. Therefore, a neuronal differentiation protocol yielding high quality cortical neurons will be developed. Using these neurons, cellular phenotypes unique to SPG4 patient cortical neurons will be identified. These phenotypic assays can be further used to implement a drug screening to approach treatment. To make this possible, a standardized *in vitro* model showing early and severe phenotypes has to be implemented and adapted to automation. Overall, SPG4 iPSC-derived cortical neurons might provide a unique opportunity to study cellular phenotypes in SPG4 patient derived neurons *in vitro* and could be envisioned for drug screening and treatment.

2 MATERIALS & METHODS

2.1 Cell culture

2.1.1 Cell lines

Cell line	Description	Source
HSP22f	Female SPG4 fibroblast cell line	AG Schöls (Tübingen)
HSP23m	Male SPG4 fibroblast cell line	AG Schöls (Tübingen)
HSP24m	Male SPG4 fibroblast cell line	AG Schöls (Tübingen)
HSP22f-1	iPSC clone 1 of patient HSP22f	Generated during this thesis
HSP22f-11	iPSC clone 11 of patient HSP22f	Generated during this thesis
HSP23m-1	iPSC clone 1 of patient HSP23m	Generated during this thesis
HSP23m-19	iPSC clone 19 of patient HSP23m	Generated during this thesis
HSP24m-3	iPSC clone 3 of patient HSP24m	Generated during this thesis
HSP24m-6	iPSC clone 6 of patient HSP24m	Generated during this thesis
Control 1	iPSC lines of control COII	Generated by Swetlana Ritzenhofen Fibroblasts: AG Schöls (Tübingen)
Control 2	iPSC lines of control COIII	Generated by Swetlana Ritzenhofen Fibroblasts: AG Schöls (Tübingen)
Control 3	iPSC lines of control AK1	Generated by Matthias Brandt
HEK293T	Human Embryonic Kidney 293 cells containing the SV40 Large T-antigen	Life technologies

Table 2.1 Cell lines

2.1.1 Cell culture instruments

Instruments	Manufacturer
Mr. Frosty 5100 Cryo 1°C	Nalgene
-150°C freezer	Panasonic
-80°C freezer U570 Premium	New Brunswick
Autoclave DX-150	Systec
Axiovert 40C microscope	Carl Zeiss
Casey automatic cell counter	Innovatis
Cell counter	VWR
Digital Camera Canon Power Shot G5	Canon
DMLL LED microscope	Leica
Fuchs-Rosenthal counting chamber	Faust
HERAguard horizontal cell culture hood	Kendro
HERAsafe vertical cell culture hood	Kendro
Incubator: HERAcell 150	Heraeus
Megafuge 1.0R	Kendro
Megafuge 16R	Thermo Fisher Scientific
Refrigerator KGEE36A	Bosch

Table 2.2 Cell culture instruments

2.1.2 Cell culture materials

Material	Manufacturer
µ 96-well plate	ibidi
Cell scraper	Costar/ Corning
Cellsieve Cell Strainer 40µM Nylon	BD Biosciences
Cryovials (1ml, 1.8ml)	Nunc
Falcon tissue culture dish (3.5cm, 6cm)	BD Biosciences
Falcon tubes (15ml, 50ml)	BD Biosciences, Corning, Greiner Bio
Parafilm	BRAND
Plastic pipettes (5ml, 10ml, 25ml)	Sarstedt
Reaction tubes (0.5ml, 1.5ml)	Sarstedt
Syringe (10ml, 20ml, 50ml)	BD Biosciences
Syringe filter (0.2µm)	PALL Corporation
Syringe filter (0.45µm)	Whatman Schleicher & Schuell
Tissue culture dish (10cm)	TPP
Tissue culture flask (T75, T175)	Corning
Tissue culture plate (24-well, 96-well)	Costar/ Corning
Tissue culture plate (6-well, 12-well)	Nunc

Table 2.3 Cell culture materials

2.1.3 Cell culture media

MEF medium
88% DMEM (high glucose)
10% FCS
1% NEAA
1% Sodium pyruvate

Reprogramming medium 1
93% Advanced DMEM
5% FCS
1mM L-Glutamine
1% Pen/Strep

Reprogramming medium 2
79% DMEM/F12
19% KO Serum Replacement
1% NEAA
400µM L-Glutamine
0.1mM β-Mercaptoethanol
1% Pen/Strep
7ng/ml FGF2

iPSC medium (feeder-cell culture)
79% Knockout-DMEM
20% KO Serum Replacement
1% NEAA
0.1mM β-Mercaptoethanol
1mM L-Glutamine
10ng/ml FGF2

iPSC medium (feeder-free cell culture)
100% DMEM/F12
19.4µg/ml Insulin
10.7µg/ml Holo-Transferrin
14ng/ml Sodium selenite
64µg/ml L-Ascorbic-Acid-2-Phosphat
2ng/ml TGFβ
10ng/ml FGF2
100ng/ml Heparin

EDTA dissociation solution
100% PBS
0.5M EDTA (pH 8.0)
1.8mg/ml NaCl

Spontaneous differentiation medium
79% Knockout-DMEM
20% KO Serum Replacement
1% NEEA
1mM L-Glutamine

iPSC freezing medium (feeder-free cell culture)
80% iPSC medium
20% DMSO

iPSC freezing medium
90% Serum replacement
10% DMSO

Mesoderm medium 1
100% DMEM/F12
19.4µg/ ml Insulin
10.7µg/ml Holo-Transferrin

Mesoderm medium 2
100% DMEM/F12
19.4µg/ ml Insulin
10.7µg/ml Holo-Transferrin

14ng/ml Sodium selenite 64µg/ml L-Ascorbic-Acid-2-Phosphat 100ng/ml Activin A 2µM CHIR99021 50nM PI-103	14ng/ml Sodium selenite 64µg/ml L-Ascorbic-Acid-2-Phosphat 10ng/mL BMP4 () 3µM CHIR99021
Endoderm medium 1	**Endoderm medium 2**
98% STEMdiff Definitive Endoderm Basal Medium 1% STEMdiff Definitive Endoderm Supplement A 1% STEMdiff Definitive Endoderm Supplement B	99% STEMdiff Definitive Endoderm Basal Medium 1% STEMdiff Definitive Endoderm Supplement B
Ectoderm medium / Neuro induction medium (GABA)	**Neuro medium (GABA)**
100% Neuro medium (GABA) 500nM LDN-193189 15µM SB431542	49% DMEM/F12 49% Neurobasal 1% B27 supplement 0.5% NEAA 0.5mM L-Glutamine 1% Pen-Strep 50µM ß-Mercaptoethanol 0.5% N2 Supplement
Neuro-medium (cortical)	**Neuro induction medium (cortical)**
49% DMEM/F12 49% Neurobasal 1% B27 supplement 0.5% NEAA 0.5mM L-Glutamine 1% Pen-Strep 50µM ß-Mercaptoethanol 10nM Progesterone 50µM Putrescine 30nM Sodium selenite 50ng/ml Apo-Transferrin 12,5µg/ml Insulin 0.8mg/ml Glucose	100% Neuro medium 10µM SB431542 1µM Dorsomorphin **Freezing medium** 90% Serum replacement 10% DMSO **Neuro freezing medium** 70% Serum replacement 20% Trehalose 10% DMSO

Table 2.4 Cell culture media

2.1.4 Cell culture reagents

Reagent	Manufacturer	Catalog number	Stock Concentration
2-Propanol	Carl Roth	AE73.2	ready to use
Accutase	Thermo Fisher Scientific	A1110501	ready to use
Activin A	PeproTech	AF-120-14E	100µg/ml
Advanced DMEM	Thermo Fisher Scientific	12634010	ready to use
Amlexanox	Tocris	4857	100mM
Apo-Transferrin	Sigma-Aldrich	T2036	10µg/ml in H_2O
AraC	Sigma-Aldrich	C6645	10mM in H_2O
B27 supplement	Thermo Fisher Scientific	17504044	50x
BDNF	Cell guidance	GFH1	10µg/ml in 0.1% BSA
BMP4	PeproTech	120-05	10µg/ml in 0.1% BSA (4mM HCl)
CHIR 99021	Axon Medchem	Axon 1386	10mM in DMSO
Collagenase Typ IV	Thermo Fisher Scientific	17104019	1mg/ml in KODMEM
Cytochalasin B	Sigma-Aldrich	C6762	10mM in DMSO
DAPT	Tocris bioscience	2634	10mM in DMSO

D-Glucose	Sigma-Aldrich	G8270	160mg/ml
DMEM (high glucose)	Thermo Fisher Scientific	41965039	ready to use
DMEM/F-12	Thermo Fisher Scientific	11320074	ready to use
DMEM/F-12 (HEPES)	Thermo Fisher Scientific	31330038	ready to use
DMH1	Sigma-Aldrich	D8946	10mM in DMSO
DMSO	Sigma-Aldrich	67-68-5	ready to use
Dorsomorphin	Sigma-Aldrich	P5499	5mM in DMSO
EDTA	Sigma-Aldrich	60-00-4	0.5M in PBS
FBS (fetal bovine serum)	Thermo Fisher Scientific	10270106	ready to use
FGF2 (iPSC medium)	Thermo Fisher Scientific	RFGFB50	10µg/ml in 0.1% BSA
FGF2 (neural diff.)	R&D systems	233-FB	1g/ml or 10µg/ml in 0.1% BSA
FuGENE HD	Roche	04709713001	ready to use
GDNF	Cell guidance	GFH2	10µg/ml in 0.1% BSA
Gelatin	Sigma-Aldrich	9000-70-8	0.1% in H_2O
Geltrex	Thermo Fisher Scientific	A1413202	1:100 in KO DMEM
Gentamicin	Thermo Fisher Scientific	15750060	50mg/ml
GW3965	Sigma-Aldrich	G6295	10mM in DMSO
Heparin	Sigma-Aldrich	H3149	1mg/ml in PBS
Holo-Transferrin	Merck Millipore	616397	10µg/ml in H_2O
IGF-1	R&D Systems	AFL291	100mg/ml
Insulin	Sigma-Aldrich	91077C	5mg/ml in 1% acetic acid (PBS)
Jasplakinolide	Millipore/Calbiochem	420107	100µM in DMSO
Knockout DMEM	Thermo Fisher Scientific	10829018	ready to use
KO Serum Replacement	Thermo Fisher Scientific	A3181502	ready to use
Laminin	Sigma-Aldrich	L2020	1mg/ml
L-Ascorbic-Acid-2-Phosphat	Sigma-Aldrich	A8960	64mg/ml in H_2O
Latrunculin B	Sigma-Aldrich	L5288	10mM in DMSO
LDN-193189	Axon Medchem	Axon 1509	2mM in DMSO
L-Glutamine	Thermo Fisher Scientific	25030081	100mM
Matrigel	BD Biosciences	354230	ready to use
mTeSR™1	STEMCELL Technologies	05850	ready to use
N2 supplement	Thermo Fisher Scientific	17502001	100x
NEAA	Thermo Fisher Scientific	11140050	100x
Neurobasal medium	Thermo Fisher Scientific	21103049	ready to use
Noscapine	Sigma-Aldrich	363960	100mM in DMSO
OptiMEM	Thermo Fisher Scientific	31985062	ready to use
PBS	Thermo Fisher Scientific	14190094	ready to use
PD0325901	Tocris bioscience	4192	10mM in ethanol
Pen/Strep	Thermo Fisher Scientific	15140122	100x
PI-103	Tocris bioscience	2930	500µM in DMSO
Progesteron	Sigma-Aldrich	P8783	20µM in ethanol
PTC124 (Ataluren)	Selleckchem	S6003	35,2mM
Putrescin	Sigma-Aldrich	P5780	100mM in H_2O
ROCK-Inhibitor (Y-27632)	Tocris	1254	10mM in H_2O
SB431542	Axon Medchem	1661	50mM in DMSO
Scriptaid	Biomol	Cay10572	10mM in
Sodium selenite	Sigma-Aldrich	S5261	14µg/ml in H_2O
Taxol (Paclitaxel)	Sigma-Aldrich	T7191	30µM in DMSO
TGFβ1	PeproTech	100-21	1µg/ml in 0.1% BSA
TRO19622	Sigma-Aldrich	T3077	0.5mM in DMSO
Tryphan Blue	Thermo Fisher Scientific	T8154	ready to use
TrypLE™ Express	Thermo Fisher Scientific	12605010	ready to use
Vinblastine	Sigma-Aldrich	V1377	1µM in DMSO
β-Mercaptoethanol	Thermo Fisher Scientific	21985023	50mM
STEMdiff™ Definitive Endoderm kit	STEMCELL Technologies	05110	For details go to cell culture media

Table 2.5 Cell culture reagents

2.1.5 Cell culture coatings

For culture on feeder cells, plates were first coated with gelatin for 30 minutes at 37°C and then covered with 3-4x10^4 feeder cells per cm^2 in MEF medium.
During feeder-free iPSC culture, plates were coated with Geltrex. Plates were prepared at least 30 minutes before splitting by diluting one 200µl Geltrex aliquot quickly in 18ml ice-cold KnockOut-DMEM and spreading 1ml solution per well of a 6-well plate. Plates were incubated at 37°C for 30-60 minutes and stored at 4°C for up to one week.
Neurons and differentiating neural cultures were cultured on Matrigel (MG) coated plates. MG-coated plates were prepared at least one day prior to splitting. One 1ml aliquot of MG was thawed slowly on ice at room temperature (RT) for at least three hours or at 4°C over-night. Pipetted with a pre-cooled 5ml plastic pipette, the MG was diluted in 30ml ice-cold DMEM-F12 (without Hepes) and used to cover the desired plates and dishes (1ml on one well of a 6-well plate). MG-coated plates were stored at 4 °C for up to two weeks.

2.1.6 Cell counting

Cells were mostly counted in a Fuchs-Rosenthal counting chamber. 20µl cell solution was mixed with 20µl Tryphan blue in a 1.5ml tube. 20µl of this solution were transferred to a counting chamber. A minimum of four large squares ($1mm^2$) were counted manually under a bright field microscope. The counted cell number was divided by the number of squares, times the depth of the chamber (0.1mm) times the dilution factor to acquire the cell number per microliter. In some instances, the CASEY cell counter was employed for automated counting. 10µl cell suspension were diluted in 10ml CASEY buffer and measured with a suitable protocol that was generated according to the manual.

2.1.7 Reprogramming of patient fibroblasts

Patient fibroblasts were cultured in MEF medium supplemented with 10ng/ml FGF2 prior to reprogramming. The youngest possible passage was used and cells were cultured at densities between 50% and 90%. One day prior to infection, 150,000 fibroblasts were plated on one MG-coated well of a 12-well cell culture plate in MEF medium. All four Sendai virus preparations, each containing one of the Yamanaka reprogramming factors: OCT4, SOX2, KLF4 and c-MYC, were diluted in 4ml Reprograming medium 1. 0.5ml of this virus solution was centrifuged on one well of the previously seeded fibroblasts for 45 minutes at 32°C and 1,500xg. Starting the next day, the medium was changed daily to fresh Reprogramming medium 1 for six days. After seven days, fibroblasts already changed morphology and were harvested with 0.025% TrypLE™ Express

reagent. Cells were resuspended in Reprogramming medium 1 supplemented with 5µM ROCK inhibitor, counted and 100,000 infected fibroblasts were seeded on previously prepared feeder covered 10cm cell culture dishes. The next day, the medium was switched to Reprogramming medium 2. Subsequently, the medium was changed every other day for 3-6 weeks until the appearing colonies were large enough for manual picking. To establish clonal lines, 100µl pipette tips were used to transfer single colonies into wells of a feeder-covered 12-well plate. From thereon, medium was changed daily to fresh Reprogramming medium 2. After the clonal cell lines were successfully established, coating was switched to Geltrex and medium to iPSC medium for feeder-free culture.

2.1.8 Human pluripotent stem cell culture

At the beginning of this work, human pluripotent stem cells were cultured on irradiated mouse fibroblasts, called feeder cells, in iPSC medium based on KnockOut DMEM. The splitting procedure was done enzymatically, by incubating the cells in 1mg/ml Collagenase Typ IV solution at 37°C. After one hour, the colonies were washed off carefully with medium and centrifuged for 3 minutes at 800rpm in a 15ml Falcon tube. Subsequently, the cell pellet was crushed by resuspension with a 1000µl micropipette, further diluted with fresh iPSC medium and plated on feeder coated 6-well tissue culture plates that were prepared on the previous day.

For feeder-free iPSC cultivation, cells were cultured on Geltrex-coated tissue culture plates in self-made E8 medium (Chen et al. 2011) or mTeSR medium. The iPSC medium was changed daily and the cells were grown until they reached 70-80% confluence.

The cultures were split every 3-4 days with EDTA dissociation solution by washing once with PBS, adding 1ml EDTA dissociation solution per well and incubating for 3-5 minutes at room temperature, while check the progress of dissociation under the microscope. When the cultures started to dissociate, EDTA dissociation solution was removed, the cells were washed off with medium and transferred onto a new Geltrex-coated plate using a split ratio of 1:3-1:5 without centrifugation.

For experiments that required single cell solutions, or homogeneous monolayer cultures, feeder-free iPSC cultures were split enzymatically using accutase. The cultures were washed once with PBS and then dissociated by incubating accutase for 10 minutes at 37°C. The cells were washed off with medium, transferred into a Falcon tube and centrifuged for 5 minutes at 1200rpm. During centrifugation, the cell number was determined using a Fuchs-Rosenthal counting chamber. The iPSCs were resuspended in iPSC medium supplemented with 10µM ROCK inhibitor and seeded in the desired density on the desired plate format.

To generate backups, iPSCs were cryopreserved. After splitting and centrifugation, cells were resuspended in ice-cold SR-based iPSC freezing medium and quickly filled in previously prepared cryovials. Following an EDTA split, cells were rinsed off with 0.5 ml medium per well and then

quickly mixed with 0.5ml iPSC freezing medium (feeder-free) and filled in previously prepared cryovials. The cryovials were placed in Mr. Frosty cryo containers, stored at -80°C over-night and moved to -150°C freezers or into liquid nitrogen tanks on the next day.

2.1.9 Undirected differentiation

Human iPS cell colonies were lifted enzymatically by collagenase treatment, without further dissociation of the colonies with a micropipette. Colonies were transferred to a falcon tube and centrifuged at 800xg for 3 minutes followed by careful resuspension in EB1 medium and transferal to a Petri dish to promote embryoid body (EB) formation. The medium was changed every other day by collecting the EBs in a 15ml tube, letting them settle at the bottom of the tube, carefully aspirating the supernatant, gently resuspending the EBs in fresh EB1 medium and returning the solution to a Petri dish. Seven days after colony detachment, EBs were plated on gelatin-coated tissue culture dishes in either EB1 medium (ectoderm) or MEF medium (endoderm and mesoderm) to promote outgrowth of differentiated cells. The medium was changed every other day and cultures were fixed for immunocytochemistry after seven days.

2.1.10 Teratoma assay

One six-well plate of undifferentiated iPSCs was pre-incubated with 10µM ROCK inhibitor for one hour. IPSCs were dissociated with collagenase and carefully washed off the plate with 0.5 ml medium without breaking up the colonies. Cell suspension was quickly transferred to the mouse house for transplantation in the testis of SCID beige mice. Three mice per cell line were transplanted by Anke Leinhaas.

2.1.11 Directed differentiation into all three germ layers

For directed differentiation into all three germ layers, iPSCs were cultured in mTeSR medium for one week to enable endoderm differentiation. Reaching 80% confluency, the cultures were dissociated with accutase, centrifuged and counted. The iPSCs were resuspended in mTeSR medium supplemented with 10µM ROCK inhibitor and 1 mio cells were seeded per well of a MG-coated 12-well plate. The following day, one well of each cell line was treated with endoderm medium, one with ectoderm medium and one with mesoderm medium 1. After 24 hours, medium was changed to endoderm medium 2, mesoderm medium 2 and fresh ectoderm medium. The medium was exchanged daily and the cells were harvested after five days for RNA preparation. Cultures were washed off with ice-cold PBS and the ectoderm, mesoderm and endoderm differentiation of every cell line was pooled and centrifuged for 5 minutes at 1400 rpm. The cell pellets were frozen at -80 °C for later RNA isolation.

2.1.12 Quality control of cell lines

Cell lines in culture were checked every day regarding contaminations, purity and normal cell growth. Contaminated cultures and cell lines with an abnormal morphology or growth rate were immediately discarded. Mycoplasma tests were performed every two weeks using DNA prepared with quick extract and subsequent PCR analysis.

2.1.13 Differentiation into glutamatergic cortical neurons

For the cortical differentiation, iPSCs were cultured in mTeSR or StemBrew medium. Undifferentiated iPSCs were split two days prior to initial seeding at a split ratio of 1:2 to acquire a large amount of high quality iPSCs. To induce neural fate, a homogenous, very high-density culture is beneficial. Thus, iPSC cultures were split using accutase and 7-10 mio cells were seeded on one well of a 6-well plate in iPSC medium supplemented with 10µM ROCK inhibitor. The next day, an over-confluent cell layer had formed and the cortical differentiation was started by switching the medium to neural induction medium (day 0). The medium was changed daily and the volume was increased, depending on the metabolic activity, indicated by a pH sensor in the medium. On day 10, the neural induction medium was supplemented with 20ng/ml FGF2 to promote proliferation. On the next day, the cultures were washed once with PBS and dissociated as clumps using accutase treatment for 7 minutes at 37°C. The cells clumps were carefully rinsed off, transferred to a falcon tube and centrifuged for 3 minutes at 1200rpm. After centrifugation, the cell pellet was carefully resuspended in neuro medium supplemented with 20ng/ml FGF2 and 10µM ROCK inhibitor and seeded at a split ratio of 1:3 onto MG-coated 6-well plates. The cultures were cultivated in neuro medium supplemented with 20ng/ml FGF2 until day 13, with daily medium changes. Starting on day 14, the medium was switched to Neuro medium supplemented with 10ng/ml FGF2 and 100ng/ml heparin and was changed every other day. On day 17, the cultures were dissociated as clumps using accutase treatment for 6 minutes and seeded at a split ratio of 1:2 on fresh MG-coated plates in neuro medium supplemented with 10ng/ml FGF2, 100ng/ml Heparin and 10µM ROCK inhibitor. The medium was replaced with medium without ROCK inhibitor the next day. The same splitting procedure was repeated on day 22. On day 31, the cultures were dissociated by incubating accutase supplemented with 10µM ROCK inhibitor for 20 minutes at 37°C. The cells were washed off with medium and collected in one 50 ml Falcon tube to freeze the cultures down as one batch. After centrifugation for 3 minutes at 1400rpm, the cell pellet was resuspended in ice-cold freezing medium (one ml per well). 1ml cell solution was quickly filled in previously prepared cryovials, placed in Mr. Frosty cryo containers and stored at -80°C over-night. The next day, the cryovials were moved to -150°C freezers or into liquid nitrogen tanks.

For maturation of the precursors, one vial was thawed quickly in a 37°C water bath until only a small clump of ice remained. The cell solution was diluted with 9ml medium, transferred to a 15ml falcon tube and centrifuged for 3 minutes at 1200rpm. Subsequently the pellet was resuspended in neuro medium supplemented with 10µM ROCK inhibitor and seeded on 3 wells of a MG-coated 6-well plate. The medium was replaced with neuro medium without ROCK inhibitor the next day and cultures were cultivated with medium changes on every other day until day 44. On day 44, cultures contain a large fraction of neurons and can be dissociated for final maturation by treating the cultures with 0.75ml accutase supplemented with 10µM ROCK inhibitor for 60-75 minutes at 37°C. Tapping against the plate promotes the dissociation further. Cells were washed off with medium and carefully dissociated by pipetting up and down with a 10ml plastic pipette. The solution was transferred to a 15ml falcon tube and centrifuged at 1300rpm for 5 minutes. At the same time the cell number was determined by counting manually or employing the CASEY cell counter. After centrifugation, the cell pellet was carefully resuspended in neuro medium supplemented with 10µM ROCK inhibitor and the cells were seeded in the desired cell number on different MG-coated plates. For immunocytochemical analysis, 1-2mio cells were seeded on one 3.5cm dish and 0.02-0.2mio cells on one well of a 96-well plate. For protein, DNA or RNA harvest 10mio cells were plated per well of a 6-well plate. On the next day, the medium was changed to neuro medium supplemented with 10µM PD0325901 and 10µM DAPT to force differentiation of remaining precursors. The same medium was refreshed on day 47. On day 49, the cultures were mitotically inactivated by treatment with 5µM AraC (Cytosine β-D-arabinofuranoside hydrochloride), to prevent further proliferation. The medium was removed from the cultures on the following day and discarded in a specialized waste container. Until analysis, the cells were cultured further in neuro medium with medium changes every other day, without aspirating the medium completely.

2.1.14 Differentiation into GABAergic forebrain neurons

For the GABAergic forebrain differentiation, iPSCs were cultured in E8 medium. Undifferentiated iPSCs were split using accutase and 2 mio cells were seeded on one well of a 6-well plate in iPSC medium supplemented with 10µM ROCK inhibitor. The next day, a confluent cell layer had formed and the GABAergic differentiation was started by switching the medium to neural induction medium (d0). The medium was changed daily. On day 9, the neural induction medium was supplemented with 20ng/ml FGF2 to promote neural rosette formation. On the next day, the cultures were washed once with PBS and dissociated as clumps using accutase treatment for 7 minutes at 37°C. The cells clumps were carefully rinsed off, transferred to a Falcon tube and centrifuged for 3 minutes at 1200rpm. After centrifugation, the cell pellet was carefully resuspended in neuro medium supplemented with 20ng/ml FGF2 and 10µM ROCK inhibitor and seeded at a split ratio of 1:3 onto MG-coated 6-well plates. The cultures were cultivated in neuro

medium supplemented with 20ng/ml FGF2 until day 12, with daily medium changes. Starting on day 13, the medium was switched to neuro medium and was changed every other day. On day 20, the cultures were dissociated by incubating accutase supplemented with 10µM ROCK inhibitor for 20 minutes at 37°C. The cells were washed off with medium and collected in one 50ml Falcon tube to freeze the cultures down as one batch. After centrifugation for 3 minutes at 1400rpm, the cell pellet was resuspended in ice-cold freezing medium (one ml per well). 1 ml cell solution was quickly filled in previously prepared cryovials, placed in Mr. Frosty cryo containers and stored at -80°C over-night. On the next day, the cryovials were moved to -150°C freezers or into liquid nitrogen tanks.

For maturation of the frozen precursors, one vial was thawed quickly in a 37°C water bath until only a small clump of ice remained. The cell solution was diluted with 9ml medium, transferred to a 15ml falcon tube and centrifuged for 3 minutes at 1200rpm. Subsequently the pellet was resuspended in neuro medium supplemented with 10µM ROCK inhibitor and seeded on 3 wells of a MG-coated 6-well plate. The medium was replaced with neuro medium without ROCK inhibitor the next day and cultures were cultivated with medium changes on every other day until day 27. On day 27, cultures contain a large fraction of neurons and can be dissociated for final maturation by treating the cultures with 0.75ml accutase supplemented with 10µM ROCK inhibitor for 60-75 minutes at 37°C. Tapping against the plate promotes the dissociation further. Cells were washed off with medium and carefully dissociated by pipetting up and down with a 10ml plastic pipette. The solution was transferred to a 15ml Falcon tube and centrifuged at 1300rpm for 5 minutes. At the same time, the cell number was determined by counting manually or employing the CASEY cell counter. After centrifugation, the cell pellet was carefully resuspended in neuro medium supplemented with 10µM ROCK inhibitor and the cells were seeded in the desired cell number on different MG-coated plates. For example, 2 mio cells on one 3.5cm or 0.2 mio cells on one well of a 96-well plate for immunocytochemical analysis and 10 mio per well of a 6-well plate for protein/ DNA or RNA harvest. On the next day, the medium was changed to neuro medium supplemented with 10µM PD0325901 and 10µM DAPT to force differentiation of remaining precursors. The medium was refreshed on day 30 and day 32. On day 33, the cultures were mitotically inactivated by treatment with 5µM AraC to prevent further proliferation. The medium was removed from the cultures on the following day and discarded in a specialized waste container. Until analysis, the cells were cultured further in neuro medium with medium changes every other day.

2.2 Phenotypical assays

2.2.1 Neurite outgrowth and growth cone assay

The neurite outgrowth assay was performed on cortical glutamatergic cultures on day 57 and GABAergic cultures on day 37, thus on post-mitotic neurons of 2 weeks of age. Neuronal cultures were washed once with 1ml PBS and were subsequently incubated with 0.75ml accutase supplemented with 10µM ROCK Inhibitor for a minimum of 60 minutes at 37°C. The status of dissociation was checked regularly by tapping against the plate. When the neuronal network had dissociated into small clumps and single cells, the cells were rinsed off with neuron medium 3 to 4 times to further dissociate remaining cell clumps. The cell solution was transferred into a falcon tube and centrifuged at 200xg for 5 minutes at 4°C. In the meantime, the number of viable cells was counted via Tryphan blue staining in a Fuchs-Rosenthal counting chamber. After centrifugation, the cells were resuspended in neuro medium supplemented with 10µM ROCK Inhibitor and passed through a 40µm cell strainer before seeding. To achieve low density cultures with single neurons, 200.000 or 20.000 cells were seeded on MG-coated 3.5cm dishes or 96-well plates, respectively. Control and patient cell lines were split and plated simultaneously to avoid time differences. Cells were evenly distributed on dishes or plates and returned to the incubator. After exactly 24 hours, cultures were fixed with 4% PFA and stained with DAPI and ActinRed 555 and against beta-III-tubulin. Images were acquired with a 20x objective. For the analysis of neurite length, initially ImageJ together with the NeuronJ plugin were used (Popko et al. 2009). This semi-automated analysis was later replaced by image acquisition with the INCell Analyzer 2200 and the image analysis software INCell Developer toolbox. Growth cone analysis was performed in a semi-automated manner with the CellProfiler software or automated with the InCell Developer toolbox.

2.2.1 Axonal swellings

Axonal swellings were analyzed by immunocytochemical stainings against axonal TAU1. To achieve an expression of axonal TAU1 in young neurons, cortical cultures were seeded in neuro medium supplemented with 3nM Taxol and 10µM ROCK inhibitor after dissociation on day 44. The medium was removed the next day and replaced by neuro medium supplemented with 10µM PD0325901 and 10µM DAPT, with was renewed on day 47. Cultures were fixed with 4% PFA and stained against TAU1 and Map2 on day 50. Random images were taken with a 20x objective and used to quantify TAU1 positive swellings >1µm. counted numbers were normalized to length of TAU1 positive axons, acquired by ImageJ with the Neurite tracer macro (Pool et al. 2008) or the InCell Developer toolbox.

2.3 Molecular biology

2.3.1 Molecular biology instruments

Instruments	Manufacturer
-80°C freezer U570 Premium	New Brunswick
Centrifuge 5424 R	Eppendorf
Centrifuge: Megafuge 1.0r	Heraeus
Chemidoc XRS+	Bio-Rad
Eppendorf realplex 4 Mastercycler ep gradient	Eppendorf
Fluorescence microscope: Axio Imager.Z1	Carl Zeiss
Fluorescence microscope: Axioskop 2	Carl Zeiss
Fluorescence microscope: Axiovert 200M	Carl Zeiss
GelDoc 2000	Bio-Rad
INCell Analyzer 2200	GE Healthcare
Inverse light microscope: Axiovert 40 CFL	Carl Zeiss
Microbial incubator	Heraeus
Micro-tabletop-centrifuge	Biozym
Microwave 800	Severin
Mini tabletop centrifuge 5424	Eppendorf
NanoDrop UV/Vis spectral photometer 1000	Thermo Fisher Scientific
Overhead shaker Rotoshake Genie	Scientific Industries
Plate reader Envision Multi label	Perkin Elmer
Power supply Standard power pack P25	Biometra
Power supply Power Pac 300	Bio-Rad
Refrigerator G 2013 Comfort	Liebherr
T3 Thermo cycler	Biometra
Thermomixer Compact	Eppendorf
ViiA™ 7 Real-Time PCR System	Thermo Fisher Scientific
Western blot running chamber Mini Trans-Blot Cell	Bio-Rad
XCell SureLock® Mini-Cell Electrophoresis System	Thermo Fisher Scientific

Table 2.6 Molecular biology instruments

2.3.1 Molecular biology materials

Material	Manufacturer
96-well qPCR plate	PEQLAB
Falcon tubes (15ml, 50ml)	BD Biosciences, Corning, Greiner
NuPAGE™ Novex™ 10% Bis-Tris Protein Gels, 1.5mm, 15-well	Thermo Fisher Scientific
NuPAGE™ Novex™ 4-12% Bis-Tris Protein Gels, 1.5mm, 15-well	Thermo Fisher Scientific
Parafilm	BRAND
PCR reaction tubes	Carl Roth
PCR cooler	Eppendorf
PCR plate seal	PEQLAB
PCR stripes, 0.2ml	Biozym
Plastic pipettes (5ml, 10ml, 25ml)	Sarstedt
Reaction Tubes (0.5ml, 1.5ml)	Sarstedt

Table 2.7 Molecular biology materials

2.3.2 Molecular biology reagents

Reagent	Manufacturer	Catalog number
Bromphenolblue NaCl	Carl Roth	A512.
Chromatography paper (whatman paper)	Whatman	3030917
Complete™, Mini Protease Inhibitor Cocktail	Roche	11836153001
DABCO	Carl Roth	0718.1
DNA ladder 100 bp	NEB	N3231L
DNAse	Qiagen	79254
dNTPs peqGOLD	PEQLAB	20-2011
ECL Classico	Millipore	WBLUC0100
ECL Crescendo	Millipore	WBLUR0100
ECL SuperSignal	Thermo Fisher Scientific	34095
EDTA	Carl Roth	X986.3
Ethanol	Carl Roth	9065.4
Ethidium bromide	Carl Roth	2218.2
FBS (fetal bovine serum)	Thermo Fisher Scientific	10270106
Fluorescein	BioRad	170-8780
Glutaraldehyde	Carl Roth	4995
Glycerin	Carl Roth	3783
Glycine	Carl Roth	3908.3
HCl (37%)	Carl Roth	X942.1
Leupeptin	Sigma-Aldrich	L2884
Methanol	Carl Roth	HN41.2
Milk powder	Carl Roth	T145.3
Mowiol 4-88	Carl Roth	0713.1
NaCl	Carl Roth	9265.2
Nitrocellulose (0.2µM) Protran membrane	Whatman	1037353
Tergitol® NP-40	Sigma-Aldrich	127087-87-0
NuPAGE® LDS Sample Buffer (4X)	Thermo Fisher Scientific	NP0007
NuPAGE® MOPS SDS Running Buffer (20X)	Thermo Fisher Scientific	NP0001
PBS	Life technologies	14190-094
PeqGOLD Agarose	PEQLAB	35-1020
PFA	Sigma-Aldrich	P6148
Phenylmethylsulfonylfluorid (PMSF)	Sigma-Aldrich	P7626
Ponceau solution	Sigma-Aldrich	P7170-1L
QuickExtract DNA Extraction Solution	Biozym	101094 (QE09050)
Sharp Novex prestained Ladder	Thermo Fisher Scientific	LC5800
Sodium deoxycholate	Sigma-Aldrich	D6750
Sodium fluoride (NaF)	Carl Roth	4503
Sodium phosphate (Na3PO4)	Sigma-Aldrich	342483
SYBR Green nucleic acid gel stain	Sigma-Aldrich	S-9430
TRIS	Carl Roth	5429.3
TRIS base	Carl Roth	5429.1
TRIS-HCl	Carl Roth	9090.3
Triton X-100	Sigma-Aldrich	9002-93-1
Trypsin Inhibitor	Thermo Fisher Scientific	17075-029
Tween-20	Carl Roth	9127.1
Xylencyanol	Carl Roth	A513
β-mercaptoethanol	Sigma-Aldrich	M7522

Table 2.8 Molecular biology reagents

2.3.3 Molecular biology kits

Kit	Manufacturer	Catalog number
DNeasy Blood & Tissue kit	Qiagen	69504
GoTaq Flexi DNA polymerase kit	Promega	M8305
iScript reverse transcriptase kit	Bio-Rad	170-8891
Pierce BCA kit	Thermo Fisher Scientific	PI-23228
QIAquick Gel Extraction Kit	Qiagen	28704
RNeasy Mini Kit	Qiagen	74104
Taq DNA polymerase kit	Thermo Fisher Scientific	18038042
TaqMan® hPSC Scorecard™ Kit, 384-well	Thermo Fisher Scientific	A15872

Table 2.9 Molecular biology kits

2.3.1 Molecular biology buffers

Supermix for semiquantitative PCR	**Supermix for quantitative PCR (GoTaq)**
30.4% ddH_2O	30.23% ddH_2O
40% 5x GoTaq Flexi buffer (green)	40% 5x GoTaq buffer (clear)
20% $MgCl_2$ (25mM)	20% MgCl2 (25mM)
1.6% dNTPs (100mM, 0.4% each)	8% DMSO
8% DMSO	1.6% dNTPs (100mM, 0.4% each)
	0.15% SYBR green (1000x)
	0.02% Fluorescein (100µM)
Supermix for quantitative PCR (Taq)	**10x DNA loading buffer**
65.03% ddH_2O	70% ddH_20
20% 10x PCR buffer	30% Glycerin
12% MgCl2 (50mM)	1mg/ml Bromphenolblue NaCl
1.6% dNTPs (100mM, 0.4% each)	1mg/ml Xylencyanol
0.15% SYBR green (1000x)	
0.02% Fluorescein (100µM)	
50x TAE buffer	**TE-4 buffer (pH 8)**
242g/l TRIS base	10mM TRIS base
10% 0.5M EDTA (pH 8.0)	0.1mM EDTA
5.71% Acetic acid	
RIPA buffer (pH 7.4)	**10x Western transfer buffer**
50mM TRIS-HCL	29g/l Glycine
150mM NaCl	59g/l TRIS base
1mM EDTA	
1% NP-40	**1x Western transfer buffer**
0.25% Sodium deoxycholate	10% 10x Western transfer buffer
Add freshly:	20% Methanol
1mM Na3PO4	70% ddH_2O
1mM NaF	
10µg/ml Leupeptin	**Western blocking solution**
10µg/ml Trypsin Inhibitor	5% milk powder
1mM PMSF	95% TBS-T
1x Complete™, Mini Protease Inhibitor Cocktail	
10x TBS buffer (pH 7.6)	**1x TBS-T buffer (pH 7.6)**
24g/l TRIS HCl	10% 10x TBS
5.6g/l TRIS base	89.9% ddH_2O
88g/l NaCl	0.1% Triton X-100

Table 2.10 Molecular biology buffers

2.3.2 Primary antibodies and dyes

Antigen	Host	Manufacturer	Catalog number	Dilution
Acetylated tubulin	ms IgG	Sigma	T7451	1:1000
AFP	rb IgG	Dako	A0008	1:200
Brn2	gt IgG	Santa Cruz	sc-6029	1:500
CTIP2	rat IgG	abcam	ab18465	1:500
FEZF2	rb IgG	antikoerper-online	ABIN1386712	1:500
FOXG1	rb, IgG	abcam	ab18259	1:500
GABA	ms IgG	Sigma	A0310	1:1000
GABA	rb IgG	Sigma	A-2052	1:1000
GFAP	rb IgG	DAKO	A000829-2	1:1000
MAP2	rb IgG	Millipore	AB5622	1:500
MAP2ab	ms IgG	Sigma	M1406	1:500
Nestin	ms IgG	Millipore	AB5922	1:300
SMA	ms IgM	Dako	M0851	1:200
Spastin	ms IgG	Santa Cruz	sc-81624	1:1000
TAU1	ms IgG	Millipore	MAB3420	1:500
TAU	rb IgG	Millipore	MAB10417	1:300
TBR1	rb IgG	proteintech	20932-1-AP	1:1000
TRA1-60	ms IgM	Millipore	MAB4360	1:500
TRA1-81	ms IgG	Millipore	MAB4381	1:500
TUJ1 (TUBB3)	ms IgG	Covance	MMS-435P	1:1000
TUJ1 (TUBB3)	rb IgG	Covance	PRB-435P	1:2000
TUJ1 (TUBB3)	chk IgY	Millipore	AB9354	1:500
vGlut1	rb IgG	synaptic systems	135303	1:1000
ActinRed 555 ReadyProbes reagent		Life technologies	R37112	According to manual
Vector® Blue AP Substrate Kit		Vector laboratories	SK-5300	According to manual
DAPI		Sigma-Aldrich	D9542	1:10000

Table 2.11 Primary antibodies and dyes

2.3.1 Secondary antibodies

Fluorophore	Target species	Manufacturer	Catalog number	Dilution
Alexa Fluor® 488	ms IgG	Thermo scientific	A11001	1:1000
Alexa Fluor® 488	rb IgG	Thermo scientific	A11008	1:1000
Alexa Fluor® 555	ms IgG	Thermo scientific	A21424	1:1000
Alexa Fluor® 555	rb IgG	Thermo scientific	A21429	1:500
Alexa Fluor® 555	rat IgG	Thermo scientific	A21434	1:1000
Alexa Fluor® 555	gt IgG	Thermo scientific	A21432	1:1000
Alexa Fluor® 555	ms IgM	Thermo scientific	A21426	1:1000
Alexa Fluor® 647	ms IgG	Thermo scientific	A21235	1:500
Alexa Fluor® 647	chk IgG	Thermo scientific	A21449	1:500
HRP-linked	ms IgG	Cell Signaling	#7076	1:1000

Table 2.12 Secondary antibodies

2.3.1 Primer sequences

Primer target	Sequence	Originator
18S forward	TTCCTTGGACCGGCGCAAG	Lodovica Borghese
18S reverse	GCCGCATCGCCGGTCGG	Lodovica Borghese
c-MYC endogenous forward	TTCGGGTAGTGGAAAACCAC	Johannes Jungverdorben
c-MYC endogenous reverse	CCTCCTCGTCGCAGTAGAAA	Johannes Jungverdorben

c-MYC total forward	AAGACTCCAGCGCCTTCTCT	Johannes Jungverdorben
c-MYC total reverse	TCTTGTTCCTCCTCAGAGTCG	Johannes Jungverdorben
CTIP2 forward	AGAACTGCAGCAACTTGACG	Kristina Rehbach
CTIP2 reverse	GTACACCTCCTTGCCGATCT	Kristina Rehbach
FEZF2 forward	ACCAACTGTGGCGTGTGC	Kristina Rehbach
FEZF2 reverse	GAGGTGGCCGCTGAGGA	Kristina Rehbach
FOXG1 forward	CTGGCGGCTCTTAGAGAT	Lodovica Borghese
FOXG1 reverse	CCCTCCCATTTCTGTACGTTT	Lodovica Borghese
GAD1 forward	CTTGTGAGTGCCTTCAAGGAG	Lodovica Borghese
GAD1 reverse	TGCTCCTCACCGTTCTTAGC	Lodovica Borghese
GAD2 forward	CTCGAAGGTGGCTCCAGTG	Vesselina Semkova
GAD2 reverse	CTCCCAAGGGTTGGTAGCTG	Vesselina Semkova
KLF4 endogenous forward	GACCAGGCACTACCGTAAACA	Johannes Jungverdorben
KLF4 endogenous reverse	CTGGCAGTGTGGGTCATATC	Johannes Jungverdorben
KLF4 total forward	CCCAATTACCCATCCTTCCT	Johannes Jungverdorben
KLF4 total reverse	ACGATCGTCTTCCCCTCTTT	Johannes Jungverdorben
M1 spastin forward	ACCCGCTGTTTGTAGGCTTC	Kristina Rehbach
M1 spastin reverse	TCTCATCCTCATCGATGCGC	Kristina Rehbach
M87 spastin forward	GCGTCCGAGTCTTCCACAAA	Kristina Rehbach
M87 spastin reverse	CCATTCCACAGCTTGCTCCT	Kristina Rehbach
OCT4 endogenous forward	GACAGGGGGAGGGGAGGAGCTAG	Johannes Jungverdorben
OCT4 endogenous reverse	GTTCCCTCCAACCAGTTGCCCCAAAC	Johannes Jungverdorben
OCT4 total forward	GTGGAGGAAGCTGACAACAA	Johannes Jungverdorben
OCT4 total reverse	TTCTCCAGGTTGCCTCTCA	Johannes Jungverdorben
SOX2 endogenous forward	GTATCAGGAGTTGTCAAGGCAGAG	Johannes Jungverdorben
SOX2 endogenous reverse	TCCTAGTCTTAAAGAGGCAGCAAAC	Johannes Jungverdorben
SOX2 total forward	GCCGAGTGGAAACTTTTCTCG	Johannes Jungverdorben
SOX2 total reverse	GCAGCGTGTACTTATCCTTCTT	Johannes Jungverdorben
SPAST forward	GACAAGGGGTTGTGCTCCT	Kristina Rehbach
SPAST reverse	GCCTTTCTTCTTCCCTCGTC	Kristina Rehbach
SPAST Seq forward	CCACAACACCTGGCCTAAAG	Kristina Rehbach
SPAST Seq reverse	ACAGAGCAAGCGTCCATCTC	Kristina Rehbach
TBR1 forward	TCTCGACCACTGACAACCTG	Kristina Rehbach
TBR1 reverse	CCGTCCAAGACAGGAGAGAG	Kristina Rehbach
vGlut1 forward	GGGCCATGACTAAGCACAAG	Lodovica Borghese
vGlut1 reverse	CTCCTCGCTCATCTCCTCAG	Lodovica Borghese
vGlut2 forward	TCAGATTCCGGGAGGCTACA	Vesselina Semkova
vGlut2 reverse	TGGGTAGGTCACACCCTCAA	Vesselina Semkova

Table 2.13 Primer Sequences

2.3.1 Analysis software

Software	Purpose	Manufacturer
Axiovision LE	Image acquisition	Carl Zeiss
CellProfiler	Image analysis	The Broad Institute Imaging Platform
CLC Sequence Viewer 7	DNA sequence analysis	CLC bio
CorelDraw Graphics Suite X5	Figure design	Corel
GenomeStudio	SNP analysis	Illumina
GraphPad Prism 6	Statistical analysis	Graphpad
Image Lab	Western Blot quantification	Bio-Rad
ImageJ	Image analysis	Wayne Rasband, NIH
INCell Analyzer 2200 software	Automated image acquisition	GE Healthcare
INCell developer toolbox	Automated image analysis	GE Healthcare
Neurite Tracer	Image J macro	(Pool et al. 2008)
NeuronJ	Image J plugin	(Ho et al. 2011)
Powerpoint	Figure design	Microsoft

Primer3Plus	Primer design	Andreas Untergasser
Quantity One	Agarose gel documentation	Bio-Rad

Table 2.14 Analysis software

2.3.2 DNA preparation

DNA was usually extracted from one well of a 6-well plate using the Qiagen DNeasy Blood & Tissue kit according to the manual. To prepare DNA for mycoplasma tests, 20µl of cell solution that was left over during routine splitting procedures were mixed with 100µl quick extract in a 0.5ml PCR reaction tube followed by heating in a PCR cycler. DNA concentration was measured with the NanoDrop 1000.

Temperature	Time
68°C	15min
95°C	8min

Table 2.15 Quick Extract cycle program

2.3.3 RNA preparation

RNA was usually extracted from one well of a 6-well plate and prepared with the Quiagen RNeasy Mini Kit according to the manual including on column DNAse treatment. RNA concentration was measured with the NanoDrop 1000.

2.3.4 Complementary DNA (cDNA) preparation

RNA was transcribed into cDNA with iScript reverse transcriptase according to the manual.

Reverse transcription reaction mix	Reverse transcription cycle program	
2µg RNA	5min	at 25°C
8µl 5x iScript reaction mix	30min	at 42°C
2µl iScript reverse transcriptase	5min	at 85°C
Fill up with ddH_20 to 40µl	∞	at 4°C

Table 2.16 Reverse transcription

2.3.5 SNP analysis

For SNP analysis, DNA was prepared with the Qiagen DNeasy Blood & Tissue kit and eluted in 100µl TE-4 buffer. The DNA concentration was measured with the NanoDrop 1000 and subsequently adjusted to 60ng/ml. The samples were processed by members of the AG Nöthen at the Institute of Human Genetics at the University of Bonn on the Illumina BeadChip HumanOmniExpress-12v1.0. The generated SNP data was analyzed with the Illumina Genome Studio and Genome Viewer.

2.3.6 Genotyping

Genotyping of the patient iPSC lines was done via Sequencing PCR. For this purpose, a PCR reaction flanking the mutation was designed using the SPAST Seq primer pair.

	Sequencing PCR cycle program		
Sequencing PCR reaction mix	**Cycle number**	**Time**	**Temperature**
1µl DNA (100ng)	1	1min	98°C
2.5µl Primer mix (3.33µM each)	2	30s	98°C
31µl ddH_20	3	30s	60°C
10µl HF 5x buffer	34x from cycle 2	30s	72°C
4µl DMSO	5	5min	72°C
1µl dNTPs (10mM)	6	∞	4°C
0.5µl Phusion DNA polymerase			

Table 2.17 Sequencing PCR

The PCR product was mixed with 10x DNA loading buffer run via gel electrophoresis on a 1% agarose gel with 1µg/ml ethidium bromide in 1x TAE buffer. Subsequently, the band of the PCR product was cut out with a scalpel under UV-light and purified with the QIAquick Gel Extraction Kit according to the manual. 5,3µl eluted DNA (>700ng) were mixed with 1µl forward SPAST Seq primer (10µM) and 0.7µl 100mM TRIS-HCl pH 8 and sent to Seqlab for extended Hotshot sequencing. Sequence data was analyzed with the CLC Sequence viewer.

2.3.7 Scorecard analysis

The Scorecard analysis is a TaqMan array, which analyses the expression of genes associated with pluripotency and differentiation of all three germ layers. To determine the differentiation potential of analyzed iPSC lines, the acquired data can be compared to pluripotent and differentiated reference profiles online (Bock et al. 2011). The Scorecard kit includes one 384-well plate, already prepared with primers, a TaqMan Master Mix and an optical adhesive film.
For this assay, RNA from directed differentiations was prepared and transcribed into cDNA. In each vial of one 8x PCR stripe, 2µl cDNA were mixed with 68µl ddH2O and 70µl TaqMan Master Mix. Of this solution, 10µl were loaded into each well of the first six columns of the 384-well plate. This procedure was repeated three times per plate. The PCR was performed with the ViiA™ 7 Real-Time PCR System.

Scorecard PCR reaction mix (12 wells)	**Cycle number**	**Time**	**Temperature**
2µl cDNA	1	20s	50°C
70µl TaqMan Master Mix	2	60s	95°C
68µl ddH_20	39x from cycle 2	20s	60°C

Table 2.18 Scorecard PCR

2.3.8 Semi-quantitative PCR

For semi-quantitative PCR, cDNA was prepared and diluted 1:30 with ddH_2O. The PCR solution was prepared with the GoTaq Flexi Kit using the green buffer, that already contains loading buffer and 18S was used as a loading control. The reaction was run according to the Semi-quantitative PCR cycle program on a T3 Thermo cycler. Subsequently, the PCR was analyzed via gel electrophoresis on a 1% agarose gel with 1µg/ml ethidium bromide in 1x TAE buffer. A picture was acquired with the Chemidoc XRS+.

	Semi-quantitative PCR cycle program		
Semi-quantitative PCR reaction mix	**Cycle number**	**Time**	**Temperature**
1µl cDNA	1	5min	95°C
1µl Primer mix (3.33 µM each)	2	60s	95°C
10.375µl ddH_20	3	60s	60°C
12.5µl Supermix	20x-34x from cycle 2	40s	72°C
0.125µl GoTaq Flexi DNA polymerase	5	5min	72°C

Table 2.19 Semi-quantitative PCR (GoTaq)

2.3.9 Quantitative PCR

For quantitative PCR, cDNA was prepared and diluted 1:30 with ddH_2O. For the silencing PCR, the PCR solution was prepared with the GoTaq Flexi Kit using the translucent buffer. The M1 spastin, M87 spastin, vGlut1 and GAD PCR reactions were performed by Monika Veltel using the Taq polymerase kit. All PCRs were run in triplicates on the Eppendorf realplex 4 Mastercycler and analyzed using 18S as reference gene.

	quantitative PCR cycle program		
Quantitative PCR reaction mix	**Cycle number**	**Time**	**Temperature**
1µl cDNA	1	5min	95°C
1µl Primer mix (3.33 µM each)	2	60s	95°C
10.375µl ddH_20	3	60s	60°C
12.5µl Supermix	39x from cycle 2	40s	72°C
0.125µl GoTaq Flexi DNA polymerase	5	5min	72°C

Table 2.20 quantitative PCR (GoTaq)

Quantitative PCR reaction mix	**Cycle number**	**Time**	**Temperature**
1µl cDNA	1	3min	95°C
0.8µl Primer mix (3.33 µM each)	2	15s	95°C
7.08µl ddH_20	3	20s	60°C
10µl Supermix	39x from cycle 2	30s	72°C
0.12µl Taq polymerase	5	60s	95°C

Table 2.21 quantitative PCR (Taq)

2.3.10 Immunocytochemistry

Cell cultures were washed once with PBS and fixed with 4% PFA for 10-15 minutes at room temperature under a laminar flow hood designated for PFA work. For the fixation of GABA, the PFA solution was supplemented with 0.04% Glutaraldehyde. Subsequently, PFA was replaced by PBS and removed from the flow hood. Prior to staining, cultures were blocked with 10% FBS

in PBS + 0.1% Triton X-100 for one hour. The primary antibodies were diluted in 10% FBS in PBS + 0.1% Triton X-100 and incubated over night at 4°C. Subsequently, the cultures were washed three times with PBS for 2-5 minutes each. Afterwards, adequate secondary antibodies were diluted in 10% FBS in PBS + 0.1% Triton X-100 and incubated for one hour. Following, the cultures were incubated with DAPI solution for 3 minutes and afterwards washed three times with PBS for 2-5 minutes each. 96-well plates were kept at 4°C covered with PBS and wrapped in parafilm. Cultures on 3.5cm dishes were mounted in Mowiol with DABCO and covered with a glass cover slip and subsequently stored at 4°C.

2.3.1 Automated image acquisition and image analysis

To acquire large amounts of images of many cell lines or different condition, cells were seeded on 96-well plates. Positive and negative conditions were included on every plate. After fixation and staining, at least 10-20 images were acquired per well and subsequently analyzed. DAPI positive nuclei were segmented by object recognition. To separate nuclei within close proximity, an erosion image of the recognized nuclei was used as nuclear seed. Dead cells were excluded via size exclusion of nuclei. Neurites were identified by intensity segmentation of the TUBB3 channel. To avoid exclusion of fine neurites, the TUBB3 signal was enhanced prior to analysis. To exclude the soma and to count the length of single neurites and not the total neurite length of the cell, the nuclei signal was dilated and subtracted from the neurite channel. Neurite length was determined with an algorithm included in the INCell Developer toolbox.

For growth cone analysis, object recognition was used on the actin channel. Only the area of signals, that co-localized with the TUBB3 signal, but did not co-localize with a dilated nucleus were included in the analysis.

For the quantification of layer markers, DAPI, TBR1 and CTIP2 were segmented via object recognition and separated with a nuclear seed. Only TBR1 and CTIP2 signals, which co-localized with DAPI nuclei were counted. TBR1 and CTIP2 double positive cells were determined by co-localization of both with DAPI.

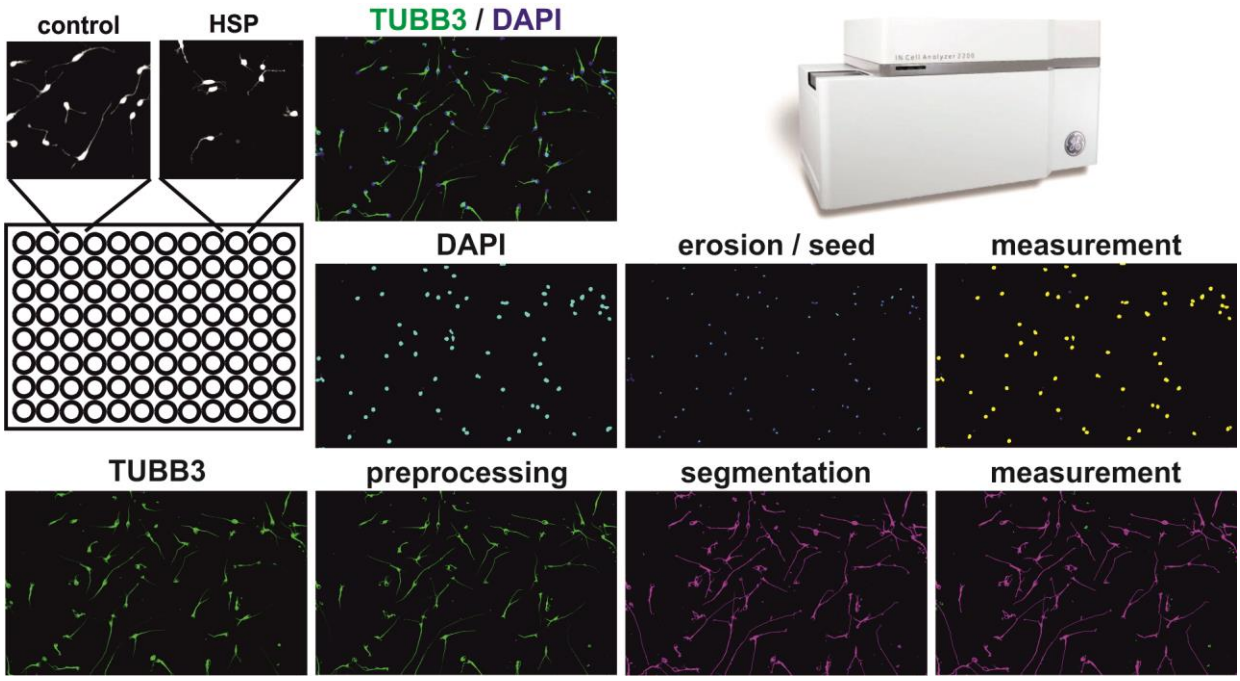

Figure 2.1 INCell analysis
Automated analysis was performed with the INCell Analyzer and Developer system. To ensure comparability, control and HSP cell lines were plated on the same thin-bottom 96-well plate. For analysis, the plates were fixed after 24 hours and stained against TUBB3 and the DAPI. Images were taken on the INCell Analyzer 2200. An analysis protocol was established on the INCell Developer platform, containing seeding and measuring of nuclei and enhancement, abstraction of nuclei, segmentation and measurement of neurites.

2.3.2 Western blot

For protein analysis, cells were washed off with ice-cold PBS and centrifuged at 4000rpm for 10 minutes and 4°C. The pellet was resuspended in 50-100 µl RIPA buffer, homogenized with a 100µl pipette and transferred to a 1.5ml tube. The cells were further lysed on an overhead shaker for 30 minutes at 4°C. Subsequently, the probes were centrifuged at 16000rpm for 30 minutes at 4°C. The supernatant was transferred to a new 1.5ml tube and weighed to determine the volume. For protein measurement was performed on 96-well plates with the Pierce BCA kit. Triplicates of the protein probes (1µl each) and a BSA dilution series (10µl each) were mixed with 200µl of the BCA solution and incubated at 37°C for 30 minutes. Following, the absorbance at 595nm was measured with a plate reader. Protein lysates were diluted with RIPA buffer and 4x LDS buffer was added to obtain a final concentration of 2µg/µl. The samples were incubated for 10 minutes at 70°C and afterwards aliquoted a 20µl and stored at -80°C.

For SDS-PAGE, precast NUPAGE Novex 4-12% Bis-Tris Mini Gels were used with MOPS running buffer. The samples were slowly thawed on ice and vortexed before loading. For spastin 40µg protein were loaded per lane, for all other western blots, 10µg. A protein marker was always included. The electrophoresis was performed with 200V for 45 minutes. Subsequently, the gels were incubated in western transfer buffer for 10-15 minutes together with the western blot membrane. Blotting sandwiches were assembled in western transfer buffer, starting on the dark

plastic side: Sponge, 2x whatman paper, gel, membrane, 2x whatman paper, sponge. During the assembly, the components were kept moist and air bubbles were carefully squeezed out The sandwiches were positioned in the western blot running chamber, which was filled with western transfer buffer and was placed in an ice box. The protein transfer was carried out at 100V for one hour. After blotting, membranes were washed with TBS-T. To visualize the proteins on the membrane, they were stained with ponceau solution for 30 s and afterwards, rinsed off with ddH_2O. The membrane was placed in foil and imaged with the Chemidoc. The remaining Ponceau staining was washed off with TBS-T. The membranes were blocked for one hour with blocking solution on the rotator. The primary antibody was diluted in blocking solution and transferred with the membrane to a 50ml falcon tube and place on a rotator at 4°C over-night. Afterwards, the membrane was washed 3x for 5 minutes with TBS-T. The HRP-coupled secondary antibody was likewise diluted in blocking solution and incubated on the membrane for one hour at room temperature. Afterwards, the membrane was washed 3x for 5 minutes with TBS-T. Before detection, the membrane was rinsed off with ddH_2O. The imaging was performed on the Chemidoc after incubating the membranes with ECL substrate. The signal was first detected with the ECL substrate Classico, which has the lowest sensitivity, then with Crescendo and as a last resort with a two-component substrate Femto super signal.

The quantification of western blot signals was performed with the Image lab software using the lanes and bands tool. To account for differentially loaded lanes, the signals were normalized against Ponceau, which was quantified using the volume tool of the image lab software.

3 RESULTS

3.1 Generation and validation of SGP4 iPSCs

To establish a patient specific SPG4 model, patient fibroblasts were reprogrammed into iPSCs. Prof. Ludger Schöls (Department for Neurodegenerative Diseases, University of Tübingen) kindly provided skin fibroblasts of three SPG4 patients. The classic reprogramming approach is based on the introduction of the four Yamanaka factors *OCT4*, *SOX2*, *KLF4* and *C-MYC* into fibroblast resulting in the generation of iPSCs *in vitro* (Takahashi et al. 2007). These factors can be delivered into the cell using integrating viruses, or non-integrating systems. Initially, iPSCs from the female patient HSP22f were generated using four FLAG-tagged retro-viruses containing the Yamanaka factors. Later, non-integrating Sendai RNA viruses have been chosen for reprogramming of fibroblasts from two male family members, i.e. HSP23m and HSP24m (as developed by Fusaki et al. 2009). The patients participating in this study belong to one family and carry an identical nonsense mutation in the SPAST gene. Interestingly, the age of onset differs, which might be either due to diagnostics or to actual differences in disease severity. An overview of generated iPSC clones, including the patient age at which the fibroblasts were retrieved, the gender, the mutation, the age of onset, the number of derived clones, the number of clones which failed to meet the quality control (QC) criteria and the virus vectors used for reprogramming is presented in Table 3.1.

Name	Age	Gender	Mutation	Age of Onset	Derived Clones	Failed QC	Virus Vector	Validation
HSP22f	40	female	UAG in exon 3 of the *SPAST* gene (Q193X)	18	12	3	Retro	2 validated clones
HSP23m	44	male	UAG in exon 3 of the *SPAST* gene (Q193X)	32	16	5	Sendai	1 validated clones
HSP24m	69	male	UAG in exon 3 of the *SPAST* gene (Q193X)	40	7	5	Sendai	2 validated clones

Table 3.1 Generation of SPG4 patient iPSC clones

3.1.1 Validating genomic integrity of generated iPSC lines

To ensure the suitability of the generated clonal iPSC lines, an extensive validation had to be performed. First of all, additional genomic aberrations had to be excluded. This is often done using simple G-banding. To achieve a higher resolution and detect smaller mutations, single nucleotide polymorphism (SNP)-array analysis was employed. Two measures, namely Log R ratio (LRR) and B allele frequency (BAF) allow the analysis of copy number changes and homozygosity (Simon-Sanchez et al. 2007). LRR visualizes the logged ratio of the observed versus the expected hybridization intensity, which is around 0 in diploid SNPs. Deletions lead to

a lower ratio, whereas duplications result in a LRR larger than 0. The BAF visualizes the proportion of a specific allele, the B allele and thus its variations. The expected proportion in a normal sample is 0.0 (A/A), 0.5 (A/B) and 1.0 (B/B), hence deviant numbers are indicative of copy number variations, whereas loss of heterozygosity leads to a missing 0.5 value.

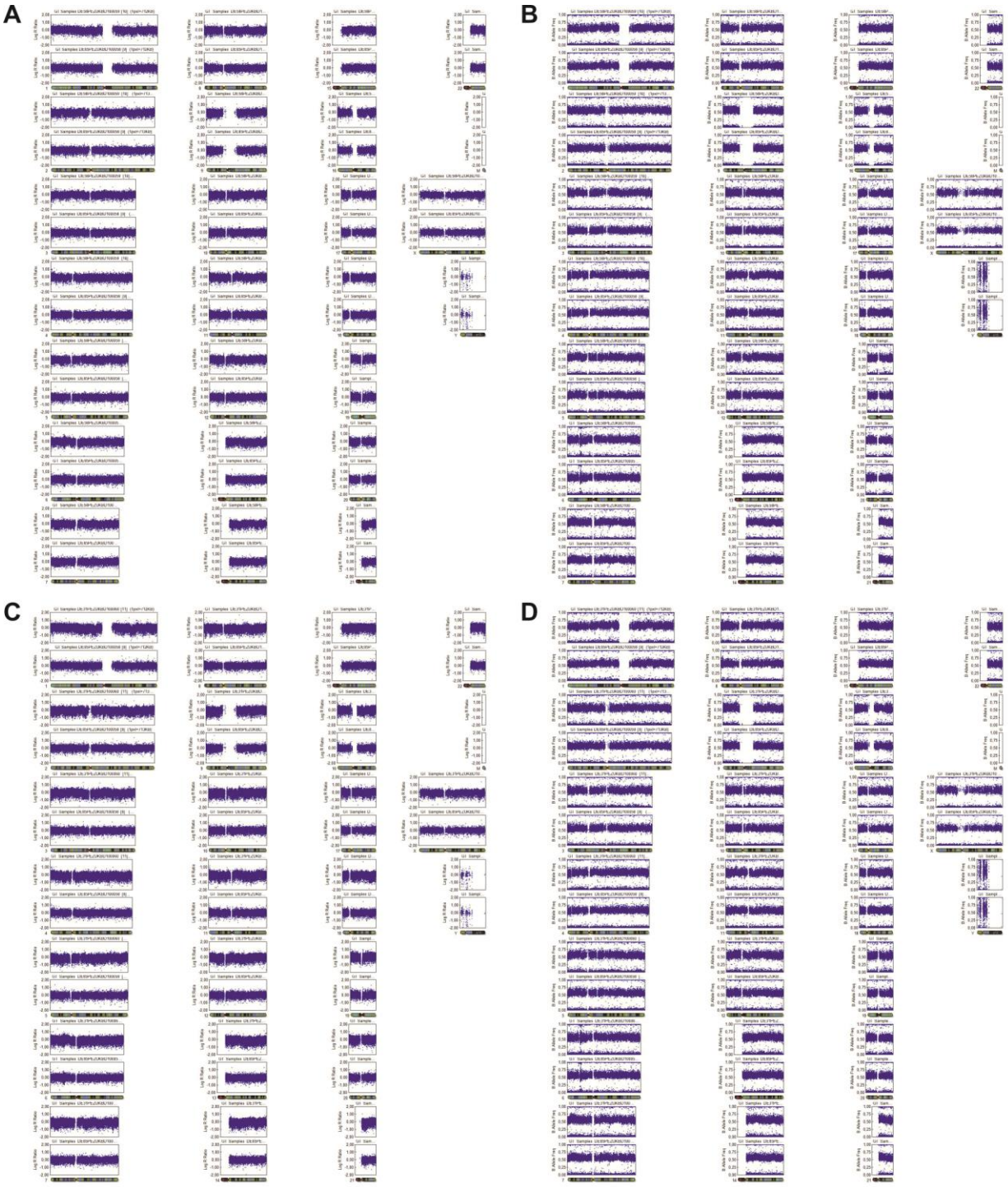

Figure 3.1 SNP analyses of HSP22f iPSC lines
SNP-array analyses of DNA from patient HSP22f, showing the iPSC SNP-array analysis in the upper panels and the fibroblast SNP-array analysis (passage 11) in the lower panels, to directly compare for aberrations. Chromosomes 1-22 and the X and Y chromosomes are displayed separately. The chromosome Y is being empty, due to the female nature of the samples. (A) LRR and (B) BAF of iPSC clone HSP22f-1 passage 9 show no major aberrations or differences to the SNP-array analysis of the fibroblast. (C) LRR and (D) BAF

of iPSC clone HSP22f-11 passage 8 show no major aberrations or differences to the SNP-array analysis of the fibroblast.

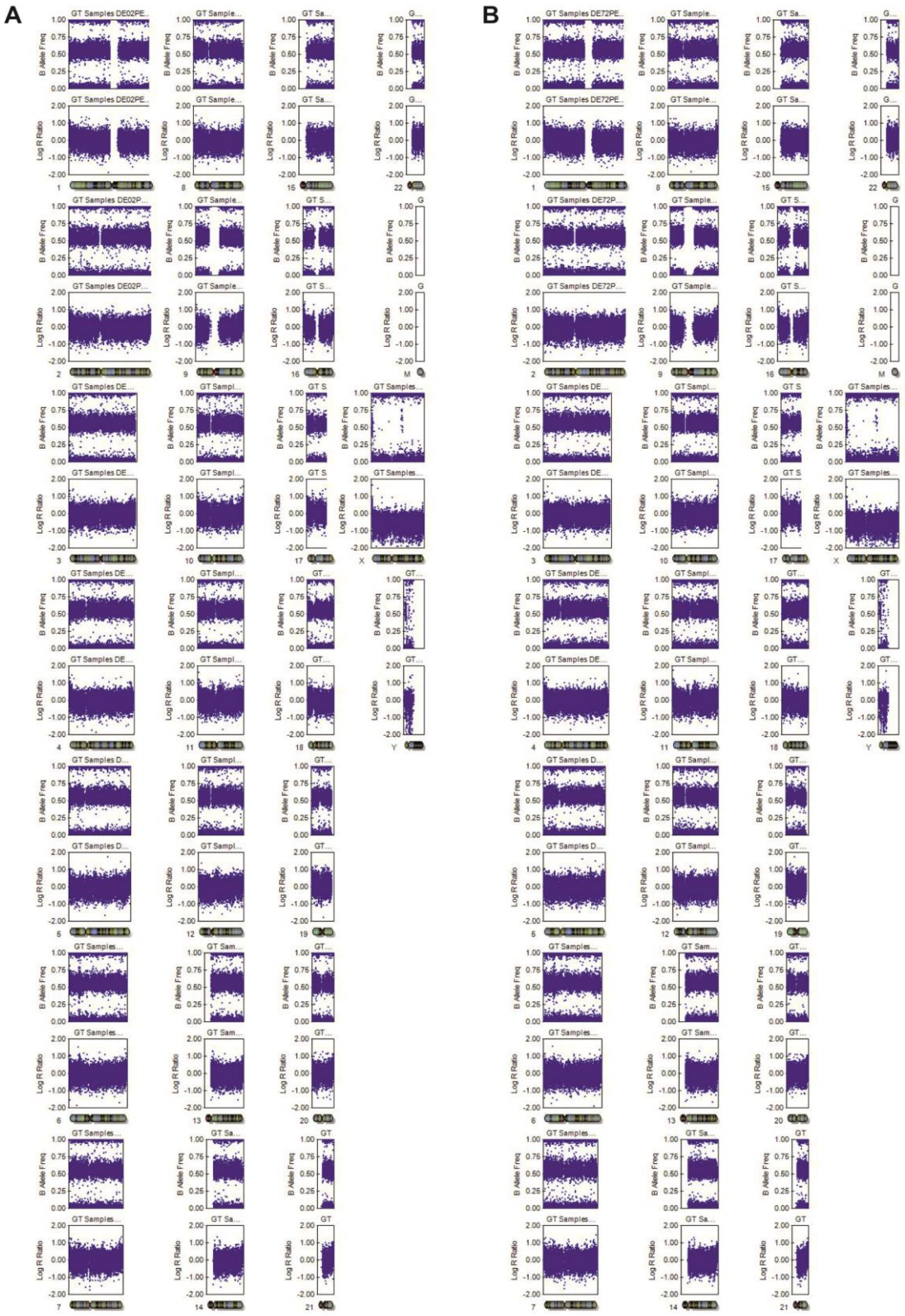

Figure 3.2 SNP analysis of HSP23m iPSC line

SNP-array analyses of DNA from patient HSP23m. Chromosomes 1-22 and the X and Y chromosomes are displayed separately, chromosome X displaying a Log R ratio below 0, which is due to the male nature of the samples. SNP-array analyses of (A) HSP23m fibroblast DNA passage 7 and (B) HSP23m-1 iPSC DNA

passage 8 are depicted, showing the BAF in the upper panels and the LRR in the lower panels, to directly compare these two modes of display. IPSC clone HSP23m-1 shows no major aberrations or differences to SNP-array analysis of the fibroblast.

Figure 3.3 SNP analyses of HSP24m iPSC lines

SNP-array analyses of DNA from patient HSP24m. Chromosomes 1-22 and the X and Y chromosomes are displayed separately. The chromosome X displays a Log R ratio below 0, which is due to the male nature of the samples. SNP-array analyses of (A) HSP24m fibroblast DNA passage 12, (B) HSP24m-3 iPSC DNA passage 6 and (C) HSP24m-6 iPSC DNA passage 7 are depicted, showing the BAF in the upper panels and the LRR in the lower panels, to directly compare these two modes of display. IPSC clones HSP24m-3 and HSP24m-6 show no major aberrations or differences to the SNP-array analysis of the fibroblast.

SNP genotyping of iPSC clones HSP22f-1, HSP22f-11 (Figure 3.1), HSP23m-1 (Figure 3.2), HSP24m-3 and HSP24m-6 (Figure 3.3) showed no major aberrations (> 300 kb) or copy number variations, whereas several other clones (Table 3.1) that displayed deletions and duplications were discarded from further use (data not shown).

3.1.2 Confirmation of the SPG4 mutation in generated iPSC lines

To ensure that generated iPSC clones carry an HSP causing mutation in the SPAST gene, the affected genomic region was analyzed via Sanger sequencing. All five lines were found to carry the heterozygous nonsense mutation in exon 3 at position 577 C>T, leading to a change in amino acids from glutamine (Q) to a termination codon at position 193 of the protein spastin.

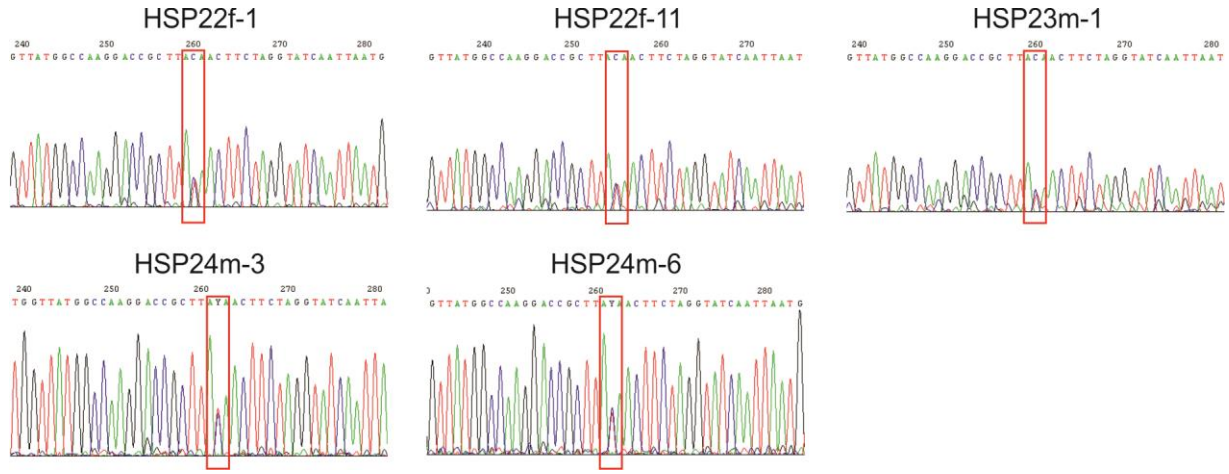

Figure 3.4 Sequencing analysis of mutated region in the *SPAST* gene
Sanger sequencing confirms the HSP causing nonsense mutation in the *SPAST* gene of all five iPSC lines.

3.1.3 Assessment of pluripotency of generated iPSC lines

A basic step in confirming pluripotency, is the presence of stem cell and pluripotency markers. The enzyme alkaline phosphatase is active in all stem cells, but is especially highly expressed in pluripotent stem cells (Štefková et al. 2015). In addition, pluripotent stem cells express a distinct marker set associated with pluripotency, such as the core pluripotency factors OCT4, SOX2 and NANOG as well as pluripotency associated transcription factors REX1 and LIN28 and the enzyme telomerase, which elongates telomeres in stem cells. In addition, the two cell surface antibodies TRA-1-60 and TRA-1-81, which bind to proteoglycans that are specifically expressed on the surface of pluripotent stem cells are widely used to show pluripotency (Andrews et al. 1984; Wright and Andrews 2009). All iPSC lines used in this study show alkaline phosphatase activity and stain positive for TRA-1-60 and TRA-1-81 (Figure 3.5).

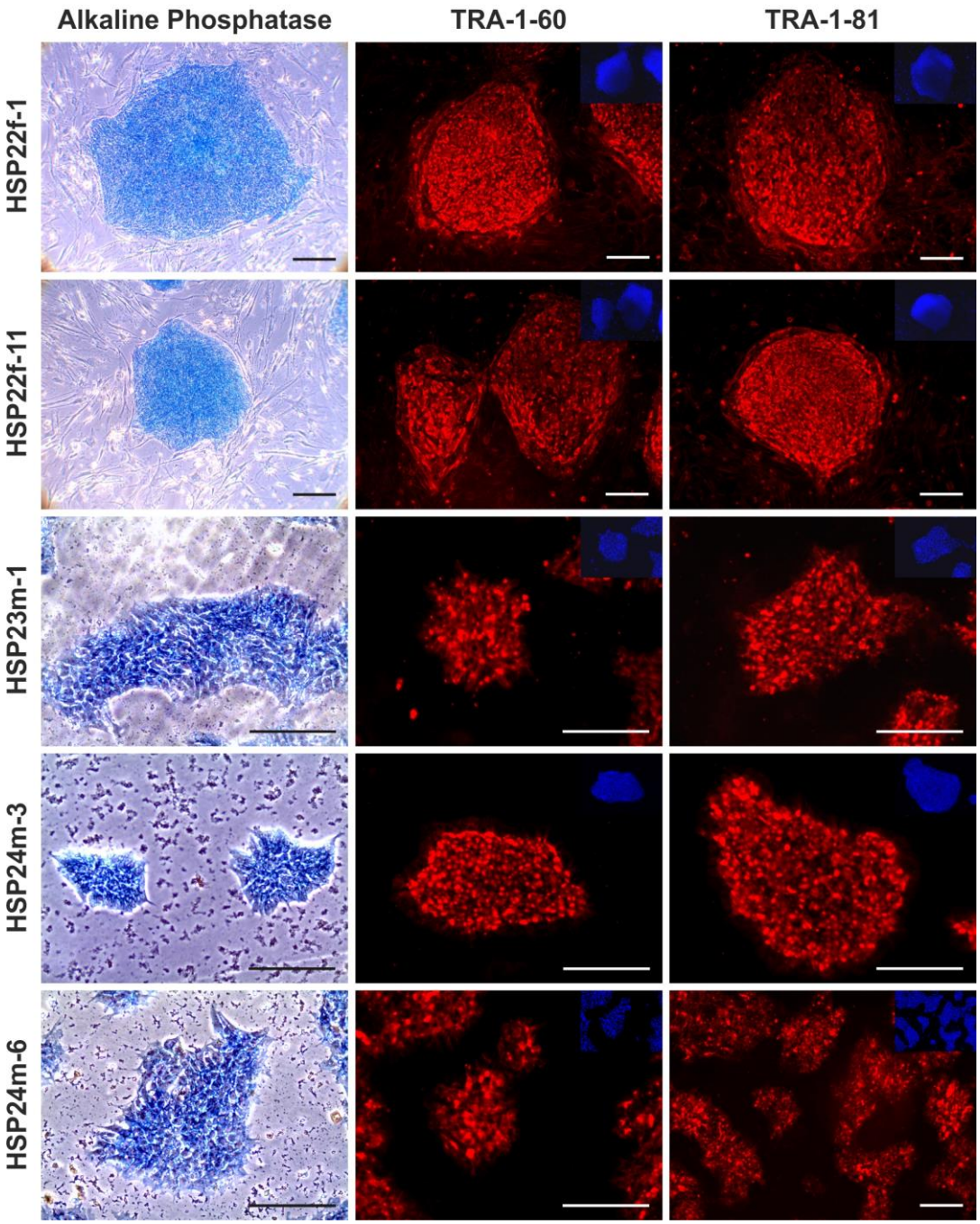

Figure 3.5 Pluripotency-associated markers
The iPSC clones HSP22f-1, HSP22f-11, HSP23m-1, HSP24m-3 and HSP24m-6 show alkaline phosphatase activity (bright field staining) and stain positive for the pluripotency associated surface markers TRA-1-60 and TRA-1-81 (Immunofluorescence staining). Nuclear DAPI staining is shown in the upper right corner. IPSC lines HSP22f-1 and HSP22f-11 were cultivated on mouse irradiated feeder cells in KOSR-medium, whereas iPSC lines HSP23m-1, HSP24m-3 and HSP24m-6 were cultivated on MG in E8 medium. Scale bar: 200µm.

While the expression of pluripotency markers is a strong indicator of pluripotency, the differentiation potential of the cells has to be verified. The gold standard for proving pluripotency in mouse pluripotent stem cells is the tetraploid complementation assay, where an embryo is formed solely out of iPSCs (De Los Angeles et al. 2015). Since this test is not possible with human iPSCs, the closest approximation is the test of teratoma formation in mice. For teratoma formation,

potentially pluripotent stem cells are transplanted into the testis of mice and analyzed for tumor formation after 6 to 10 weeks. If these tumors contain tissues of all three germ layers and thus qualify as teratomas, the donor iPSCs are considered to be pluripotent. Over the last years, it was discovered that assessing *in vitro* differentiation potential can give comparable results without the need for time-consuming and ethically arguable animal experiments. Hence embryoid body (EB) *in vitro* differentiation followed by immunofluorescence stainings or quantitative TaqMan analysis were established as alternatives to teratoma analysis (Bock et al. 2011).

For the first two retrovirally generated iPSC lines, i.e. HSP22f-1 and HSP22f-11, teratomas were generated, which contained endodermal gland structures, mesodermal cartilage and ectodermal neural rosettes (Figure 3.6).

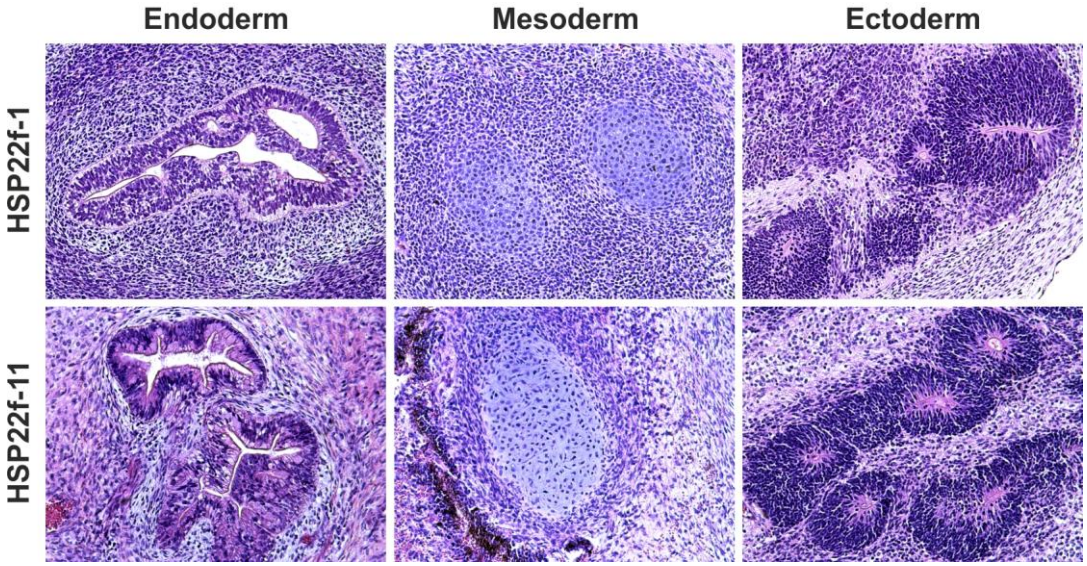

Figure 3.6 *In vivo* differentiation potential of SPG4 iPSCs
The iPSC clones HSP22f-1, HSP22f-11 were transplanted into the testis of SCID/beige mice to assess their differentiation potential *in vivo*. After 6-8 weeks, teratomas were harvested, embedded in paraffin and stained against HE. Teratomas of both iPSC lines formed teratomas, which contained endodermal gland structures, mesodermal cartilage and ectodermal neural rosettes and thus demonstrated that they contain cells of all three germ layers.

Furthermore, differentiation potential of generated iPSCs was tested *in vitro*, employing undirected EB formation. The iPSC clones were differentiated as EBs in the absence of FGF for 5 days, followed by an additional two weeks of adherent differentiation. Resulting cultures contained cells that stained positive for endodermal α-fetoprotein (AFP), mesodermal smooth muscle actin (SMA) and ectodermal β-III-tubulin (TUBB3). Thus, all tested iPSC lines gave rise to cells of all three germ layers *in vitro* (Figure 3.7).

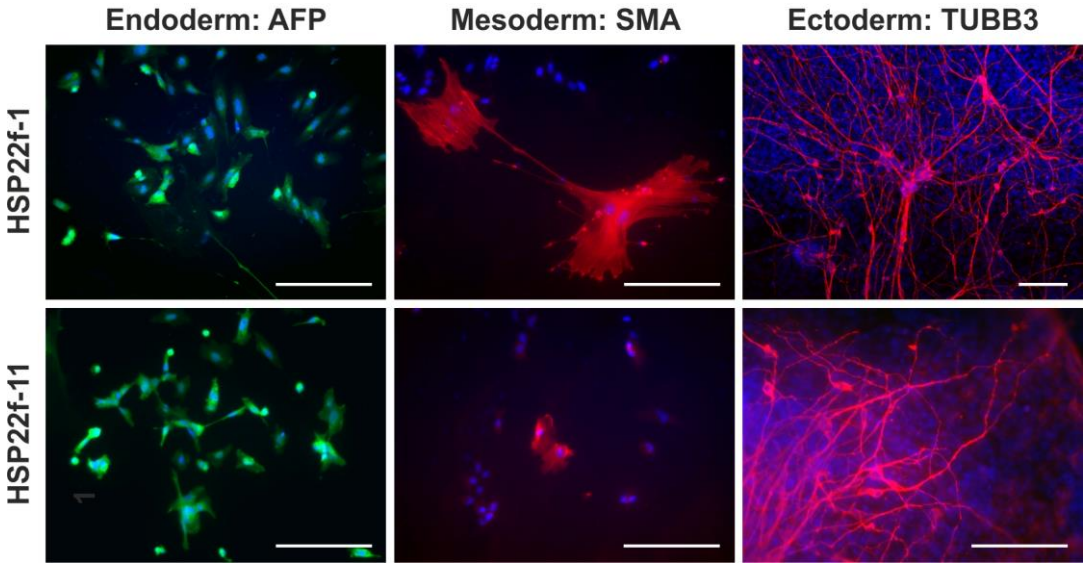

Figure 3.7 ***In vitro*** **differentiation potential of SPG4 iPSCs**
The iPSC clones HSP22f-1, HSP22f-11 were differentiated in the absence of FGF as EB structures for 5 days followed by an additional two weeks of adherent differentiation. Both cell lines gave rise to all three germ layers: α-fetoprotein (AFP)-positive endoderm, smooth muscle actin (SMA)-positive mesoderm and β-III-tubulin (TUBB3)-positive ectoderm. Scale bar: 200µm.

These teratoma-validated iPSC lines were used as control for the evaluation of the novel TaqMan-based Scorecard assay, which is in contrast to the teratoma and EB formation a quantitative measurement that might replace the traditionally used assays. In the first trial, the iPSC lines were differentiated as EBs in FGF-free basic medium for two weeks, followed by RNA preparation and cDNA generation, which was used for the Scorecard assay. However, in this undirected differentiation, endoderm and ectoderm were detectable but underrepresented and did not meet the cut-off values of the internal Scorecard assay quality control (data not shown). Thus, another differentiation approach had to be used to generate enough material to overcome these cut-off values. To that end, short directed differentiation protocols were established. Starting with confluent iPSCs, differentiation into each germ layer was induced in parallel for just five days. Afterwards, all three layer-specific directed differentiations of one line were pooled and subjected to the Scorecard assay. The previously tested lines HSP22f-1 and HSP22f-11 as well as the later generated lines HSP23m-1, HSP24m-3 and HSP24m-6 all successfully down-regulated pluripotency associated genes and self-renewal genes while upregulating germ-layer specific genes upon differentiation (Figure 3.8A). The expression of pluripotency genes and differentiation genes, was compared to the data of a large pool of undifferentiated PSCs, represented in Figure 3.8B by gray boxes. All tested iPSC lines achieved values that reside outside of the parameters for undifferentiated cells indicating that they were able to downregulate self-renewal markers and upregulate differentiation markers and are thus pluripotent. In addition to the differentiation potential, the Scorecard also tests whether residual Sendai virus is present in the samples, which would appear as a red flag in Figure 3.8B. No Sendai signal could be detected in the later three

iPSC lines, which were generated with Sendai viral vectors. In conclusion, this improved method leads to a fast and quantitative readout regarding the pluripotency of iPSC lines.

A

Sample Name	Self-renewal	Ectoderm	Mesoderm	Endoderm
HSP22f-1	-2.71	1.62	4.38	1.54
HSP23m-1	-2.72	1.28	4.73	2.18
HSP22f-11	-4.21	0.86	3.56	0.59
HSP24m-6	-3.55	0.81	5.25	1.05
HSP24m-3	-3.93	1.65	4.82	1.43

Figure 3.8 Scorecard analysis
The iPSC lines HSP22f-1, HSP22f-11, HSP23m-1, HSP24m-3 and HSP24m-6 were differentiated for five days in a directed manner into all three germ layers. Derived cell material of each cell line was pooled, to prepare RNA and cDNA, which was analyzed with the TaqMan® hPSC Scorecard™ Assay. (A) All tested iPSC lines showed an upregulation of markers of all three germ layers and downregulation of self-renewal markers. (B) Compared to a large pool of undifferentiated PSCs, represented by the gray box-whisker plots, the tested iPSC lines are able to downregulate self-renewal markers and upregulate differentiation markers and are thus defined pluripotent. Furthermore, the Scorecard is able to detect the presence of Sendai virus. Since no red flag appeared, all of the tested iPSC lines are free of Sendai virus.

3.1.4 Transgene silencing

Sendai virus is a non-integrating RNA virus and the temperature sensitive variants used for reprogramming, are usually eliminated upon cell division. On the contrary, retroviruses integrate as provirus into the host genome and will persist in the generated iPSC lines. However, the retroviral genes are usually inactivated through epigenetic silencing during the first ten passages (Hotta and Ellis 2008). In the retrovirally generated iPSC clones HSP22f-1 and HSP22f-11, transgene silencing was assessed by qPCR analysis with primers binding in the 5'-UTR of the endogenous reprogramming factors, and another set of primers detecting the total amount of

OCT4, *SOX2*, *KLF4* and *C-MYC*, respectively. Both iPSC lines show comparable amounts of endogenous and total transcripts, therefore confirming transgene inactivation through silencing (Figure 3.9).

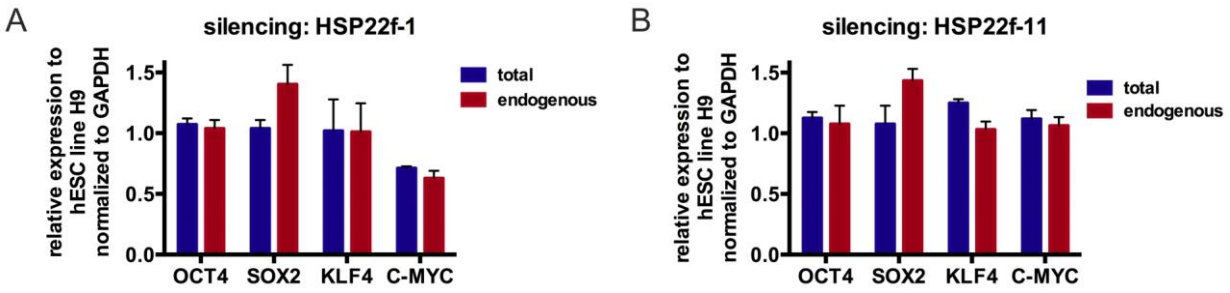

Figure 3.9 Validation of transgene silencing
QPCR analysis of iPSC clones HSP22f-1 (A) and HSP22f-11 (B) was performed to check for residual retroviral activity. Total (blue) versus endogenous (red) expression levels of *OCT4*, *SOX2*, *KLF4* and *C-MYC* were analyzed and normalized to the expression levels of the ESC line H9 and GAPDH. Error bars show SEM of triplicates.

3.2 Differentiation and validation of cortical neurons

The main phenotype of hereditary spastic paraplegia is a retrograde degeneration of the corticospinal motor neurons - glutamatergic projection neurons which reside in the layer V of the motor cortex. Other neuronal subtypes seem to be unaffected. Since the disease phenotype is restricted to such a specialized cell type, it is crucial to generate an almost similar neuronal cell type *in vitro* to be able to observe disease related phenotypes. For the generation of cortical neurons, a protocol published by Shi and colleagues in 2012 (Shi et al. 2012) was adapted (Figure 3.10). It is important to know, that the cortical differentiation *in vitro* resembles the *in vivo* development. This means, that the cortical layer V and layer VI are generated early on, followed by the upper cortical layers.

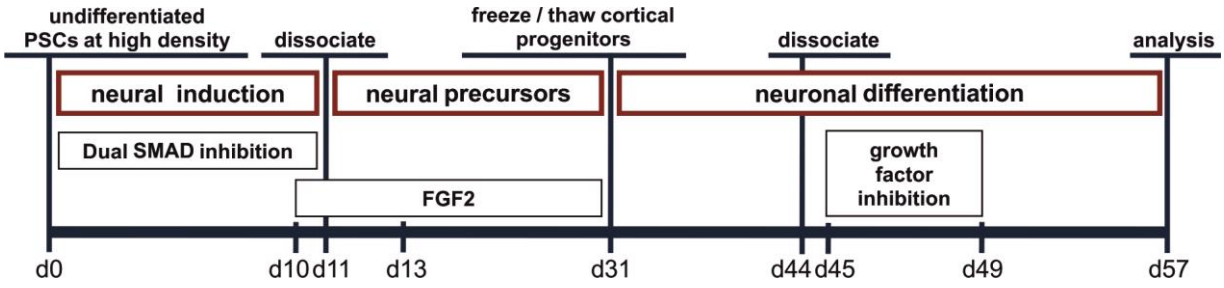

Figure 3.10 Cortical differentiation scheme

It is crucial to start the *in vitro* differentiation with homogeneous iPSCs to achieve a complete neuro induction. Therefore, the quality of the used iPSCs was determined by morphology and exemplary by staining for pluripotency marker TRA1-81 (Figure 3.11). Prior to differentiation, cells were singularized with Accutase and seeded at very high density to generate a monolayer. Neuroectoderm was induced by dual SMAD inhibition (Chambers et al. 2009) for 11 days. The

generated neural precursors were kept in a proliferative state with FGF2-treatment starting from day 10 and regular splitting starting on day 11. During this time, neural precursors had a homogeneous rosette-like morphology and stained positive for the neural stem cell marker nestin and the forebrain marker FOXG1 (Figure 3.11). On day 31 late cortical precursors were frozen down as one batch to ensure comparability between vials. Cultures were differentiated for 13 days without additional factors, dissociated on day 44 with Accutase and seeded in the desired final density. To avoid generation of higher cortical layers and astrocytes, complete differentiation was induced by treating the cultures with growth factor inhibitors targeting the FGF and Notch pathways (10µM PD0325901 and 10µM DAPT, respectively) for four days. For final analysis, neurons were matured until day 57 (Figure 3.10).

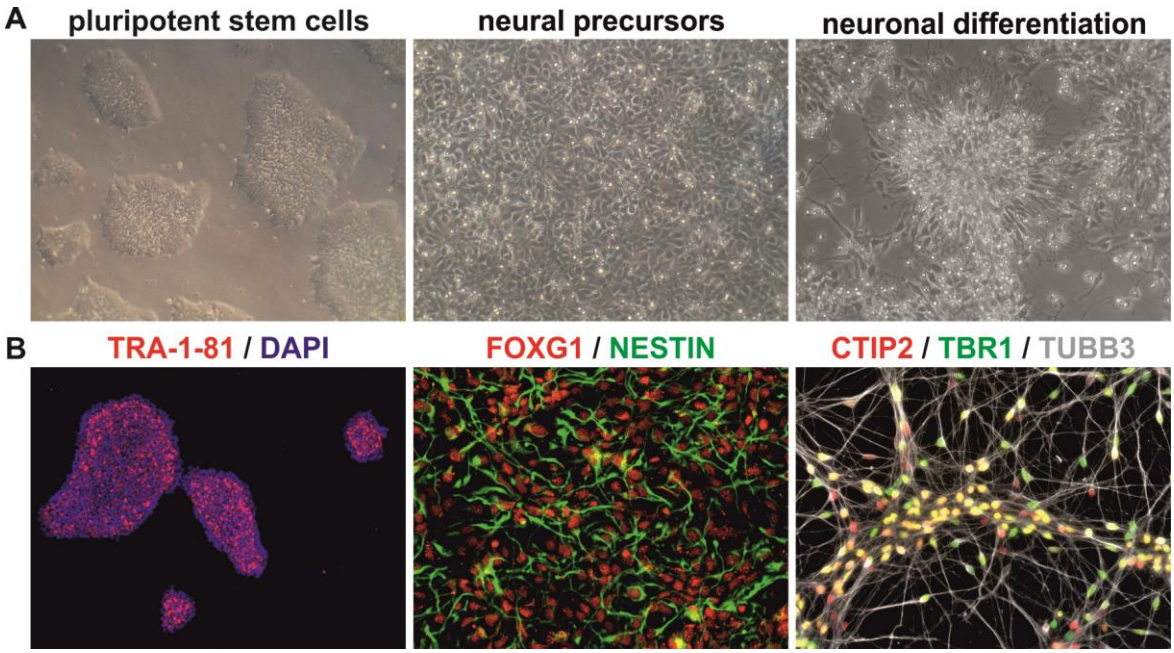

Figure 3.11 Differentiation of iPSCs to cortical progenitors and neurons
Overview over different stages in the cortical differentiation. (A) Bright field images show the typical morphology of iPSCs, early rosette and late rosette progenitors, which produce cortical neurons. (B) Differentiation is started with TRA-1-81 positive iPSCs, early progenitors are positive for the forebrain marker FOXG1 and the neural stem cell marker nestin. Cortical neurons produced by late rosettes are positive for the layer markers TBR1 and CTIP2 and the neuronal marker TUBB3.

Due to growth factor inhibition at a time when layer V is being generated, the cultures consisted almost entirely of cortical neurons positive for the layer V marker CTIP2 and the layer VI marker TBR1. The layer IV marker BRN2 was barely detectable (Figure 3.12A). Furthermore, almost all neurons stained positive for the vesicular glutamate transporter 1 (vGLUT1), which is only expressed in glutamatergic neurons, as well as the forebrain marker FOXG1. In addition, the even more specific marker FEZF2, which specifies corticospinal motor neurons (CSMN) (Lodato et al. 2014), was expressed in the majority of neurons (Figure 3.12B). The cortical identity of the generated neurons was further confirmed by semiquantitative RT-PCR analysis of *FOXG1*, *FEZF2*, *CTIP2* and *TBR1* expression (Figure 3.12C).

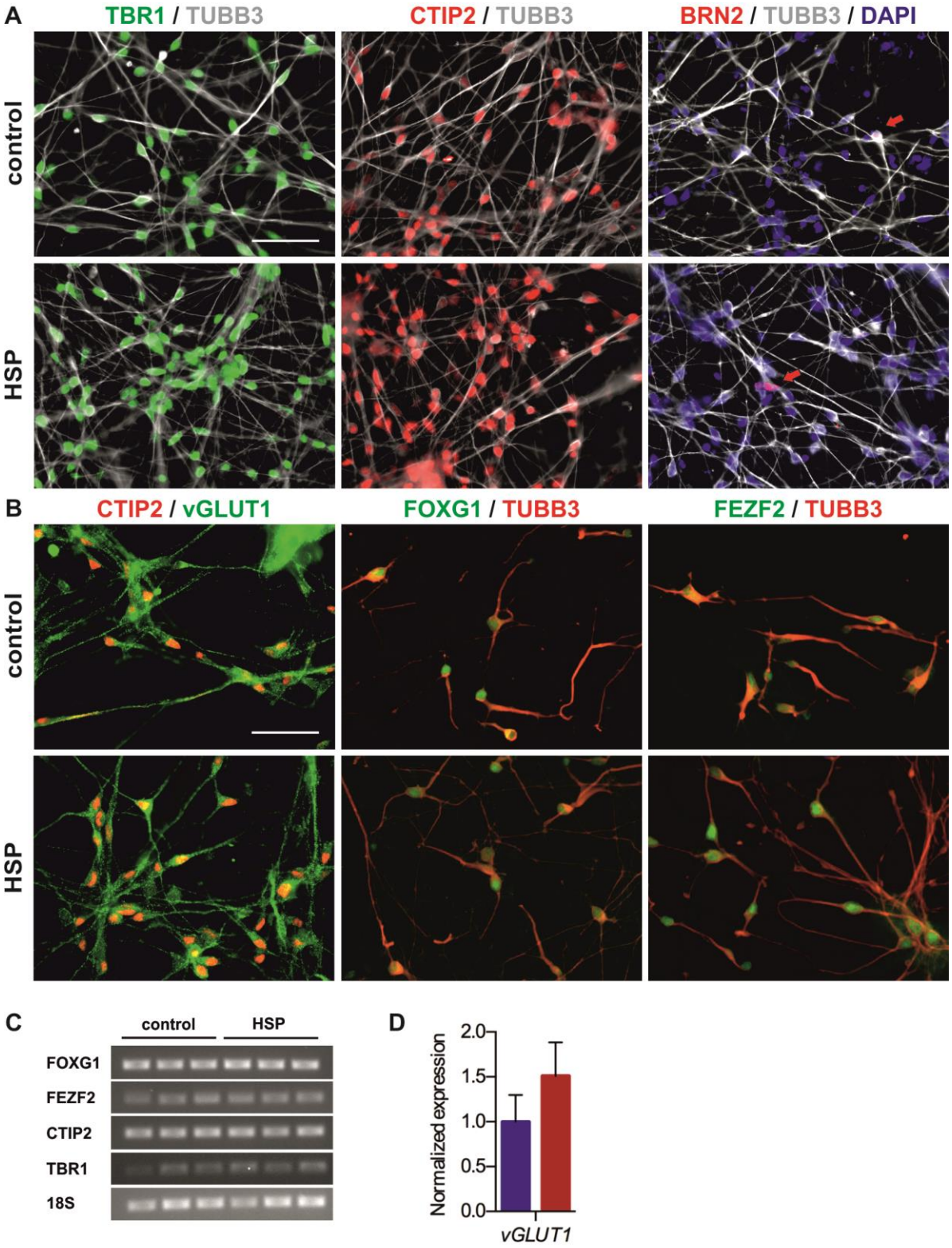

Figure 3.12 Validation of iPSC-derived cortical neurons

Cortical neurons of SPG4 patients and controls were fixed, stained and analyzed on day 57. (A) Cortical neurons stained positive for the layer VI marker TBR1, the layer V marker CTIP2 and the neuronal marker TUBB3, while the cultures were nearly devoid of the layer IV marker BRN2. (B) Immunofluorescence staining against vesicular glutamate transporter 1 (vGLUT1) confirms glutamatergic identity of cortical layer neurons, which are also positive for the forebrain marker FOXG1 and FEZF2, a marker expressed in corticospinal neurons. Scale bar: 50µm. (C) In addition, cortical forebrain identity of SPG4 patient and control neurons was confirmed by semiquantitative RT-PCR against *FOXG1*, *FEZF2*, *CTIP2* and *TBR1*, using 18S as loading control. (D) Q-PCR analysis confirms *VGLUT1* expression (control: n=6, HSP: n=6).

On day 57, every cortical batch generated from either SPG4 patient iPSCs or iPSCs of three healthy controls, was validated for the fraction of TUBB3 positive neurons and to confirm the absence of astroglia and other contaminating cell types. Since non-neuronal cells can introduce a lot of experimental variation, batches with less than 85% neurons were discarded from further use. However, most batches consisted typically of almost 100% TUBB3 positive neurons (control1: 99.9%, control2: 97.3%, control3: 88.8%, HSP22f: 98.8%, HSP23m: 100%, HSP24m: 99.5%) (Figure 3.13A). To estimate the amount of deep layer projection neurons present in the cultures, CTIP2 and TBR1 were quantified. Only cultures with at least 80% CTIP2 and/or TBR1 positive neurons were used for later analysis to ensure comparability between patient and control cell lines (control1: 97.3%, control2: 94.1%, control3: 81.5%, HSP22f: 92.0%, HSP23m: 93.1%, HSP24m: 90.3%) (Figure 3.13B).

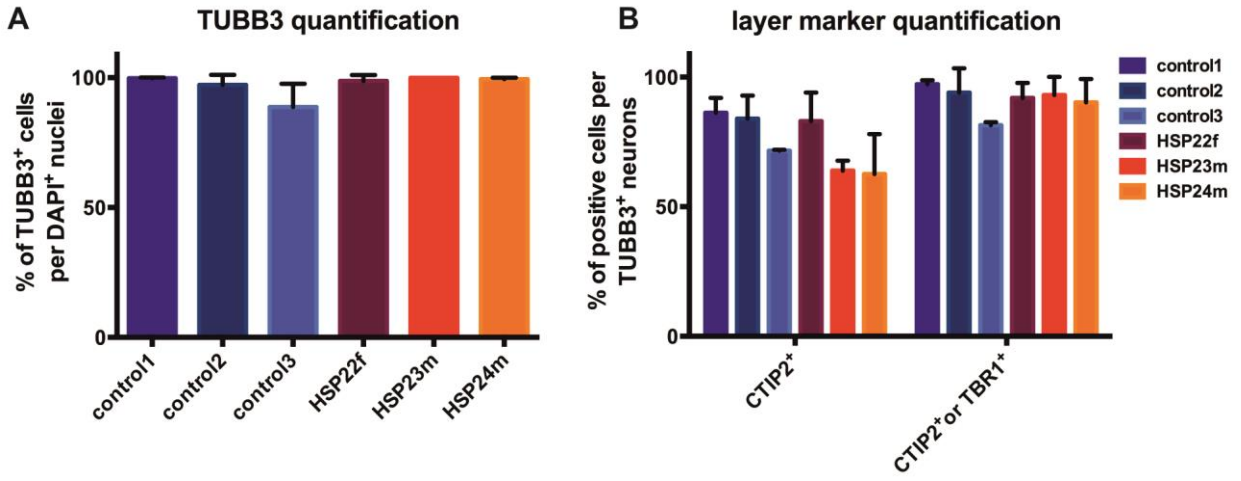

Figure 3.13 Marker quantification of cortical neurons
Immunofluorescence stainings of the neuronal marker TUBB3 and the layer markers TBR1 and CTIP2 were quantified to validate cortical cultures on day 57. (A) Control and SPG4 cortical cultures were highly enriched for neurons. (B) Cortical differentiation yields large fractions of CTIP2-positive neurons and even more either CTIP2 and/or TBR1 positive deep layer neurons. (C-61f: n=4, C-62m: n=3, C-31f: n=3, HSP-22f: n=6, HSP-23m: n=4, HSP-24m: n=3). Error bars show SD.

On day 57 most of the generated cortical neurons are double-positive for the layer VI marker TBR1 and the layer V marker CTIP2. However, at this early stage the neurons are still considered to be embryonal and not yet electrophysiological active. There is evidence that such double-positive neurons exist in the human fetal brain, but it is unknown if one of the transcription factors is down-regulated in the adult brain (Ip et al. 2011). To obtain mature functional neurons which are able to fire action potentials, the neurons were cultured on chemically inactivated mouse astrocytes for three months. Thereafter, neurons displayed arborized dendritic trees and still co-expressed the transcription factors CTIP2 and TBR1 (Figure 3.14).

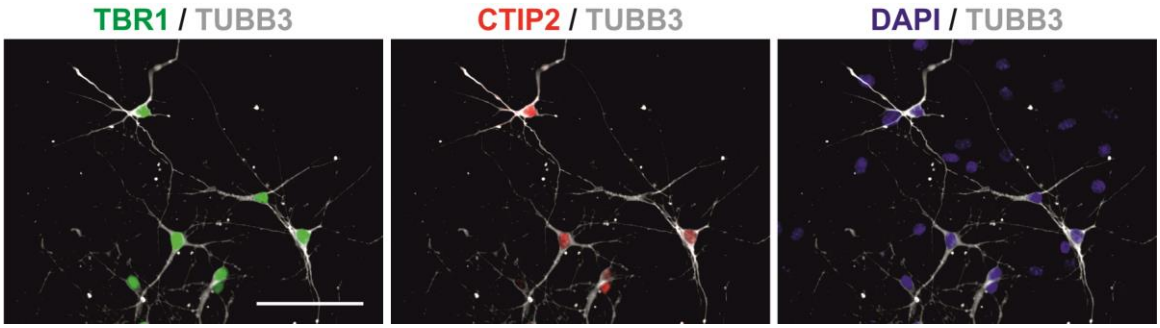

Figure 3.14 Layer identity of cortical neurons after three months on mouse astrocytes
In preparation for electrophysiology analysis, cortical neurons were dissociated and seeded on chemically inactivated mouse astrocytes on day 54. After two months, neurons stained positive for the cortical layer markers TBR1 and CTIP2 and thus conserved their deep layer cortical identity. Scale bar: 100µm.

To confirm that the neurons show functional properties, electrophysiological activity was assessed after three months of maturation on astrocytes (data obtained by Dr. Jaideep Kesavan). Current-clamp recording uses a current that is injected into the cell to induce membrane potential changes, which can be subsequently recorded. During current-clamp, both control and SPG4 neurons fired repetitive action potentials in response to 500 ms depolarizing current. Using whole-cell voltage-clamp, voltage-gated sodium and potassium channels were studied by controlling the voltage, while measuring the current through a cell membrane. The fast inactivating inward current was reversibly blocked by the application of Tetrodotoxin. In addition, spontaneous postsynaptic currents could be measured, confirming the presence of synapses and demonstrating an active neuronal network (Figure 3.15).

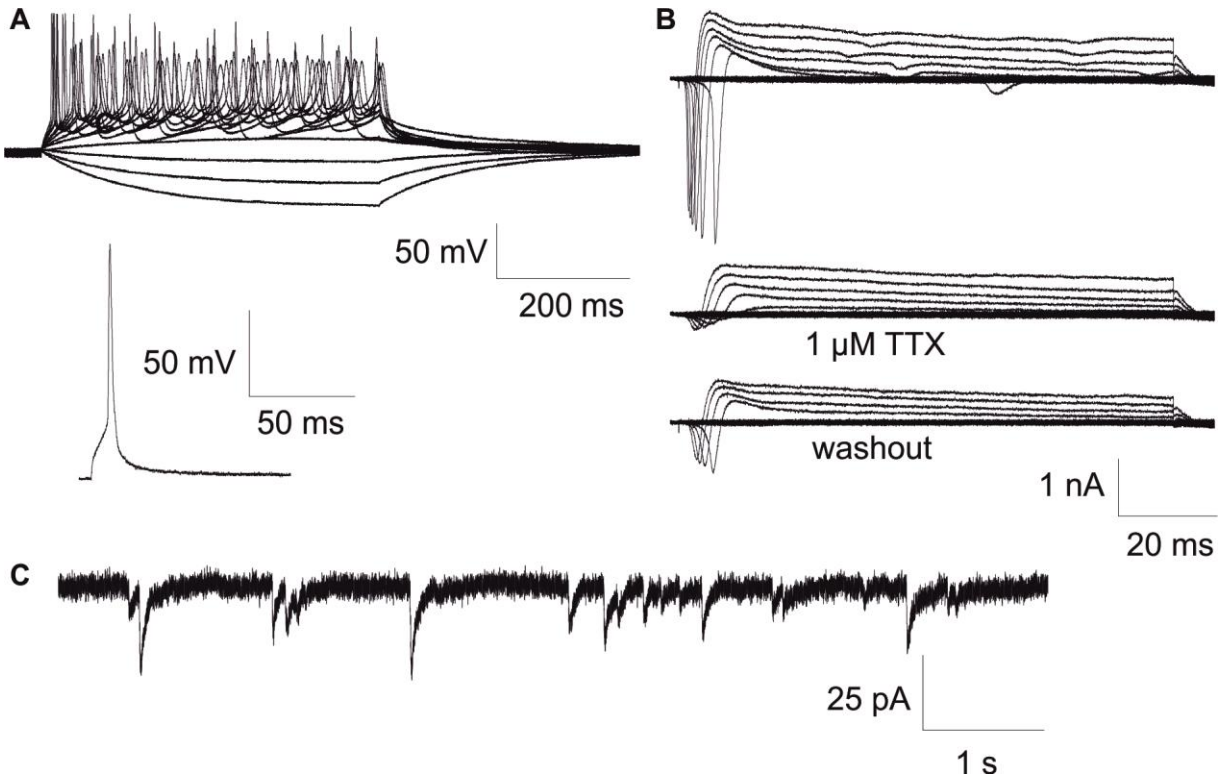

Figure 3.15 Electrophysiological properties of cortical neurons

Cortical neurons were cultured on mouse astrocytes for three months to mature *in vitro*. (A) Repetitive traces of action potentials recorded from cortical neurons in response to 500 ms depolarizing current injection. (B) Representative trace of fast inactivating inward current and sustained outward current in response to depolarizing voltage steps. Fast inactivating inward current and sustained outward current were blocked upon application of Tetrodotoxin (TTX) and recovered after washout. (C) Representative trace of spontaneous postsynaptic currents.

3.3 SPG4 neurons show reduced spastin levels

Spastin is the protein encoded by the gene *SPAST*, the genetic basis of the disease SPG4. Two translational start sites exist generating two main isoforms: M87 and the longer M1 isoform, which has an additional membrane binding domain. Splice variants of both isoforms exist, where exon 4 (shaded in black) is missing; those are called M87* and M1* (Figure 3.16A). The patient cells used in the study carry a premature stop codon at position 193 in exon three of the spastin gene, which is responsible for disease penetrance. Haploinsufficiency and a dominant negative mode of action have been discussed as disease mechanisms. To evaluate expression levels of spastin and shed a light on the disease mechanism, western blot analysis was performed with protein samples of control and SPG4 neurons. The M87 isoforms (60kDa) and its splice variant were detectable after a short exposure time, whereas the M1 isoform (68 kDa) and its splice variant are only visible after prolonged exposure. To be able to show both isoforms despite the close proximity, the M1 image had to be cut at the height of 60kDa, to separate them from the overexposed M87 bands (Figure 3.16B). Thus, the M87 isoforms are expressed at much higher levels compared to the M1 isoforms. A quantification of spastin M87 and M1 bands, normalized to ponceau, which labels the total protein, reveals an approximately 50% reduction of spastin levels in SPG4 neurons compared to levels in control neurons (Figure 3.16C). This reduction and the fact that signals of truncated spastin could never be detected on western blot, support haploinsufficiency as disease mechanism. Furthermore, semiquantitative RT-PCR and quantitative PCR analysis exhibit a reduction of *SPAST* mRNA levels of both isoforms in SPG4 neurons, a sign of nonsense-mediated mRNA decay (Figure 3.16D, E). Since the M87 *SPAST* isoform shares 100 % identity with the M1 isoform, primers designed to detect the M87 isoform, will always detected the M1 isoform as well, therefore the data is referred to as M87+M1. However, the M87 *SPAST* isoform is more abundant and contributes the majority of the signal.

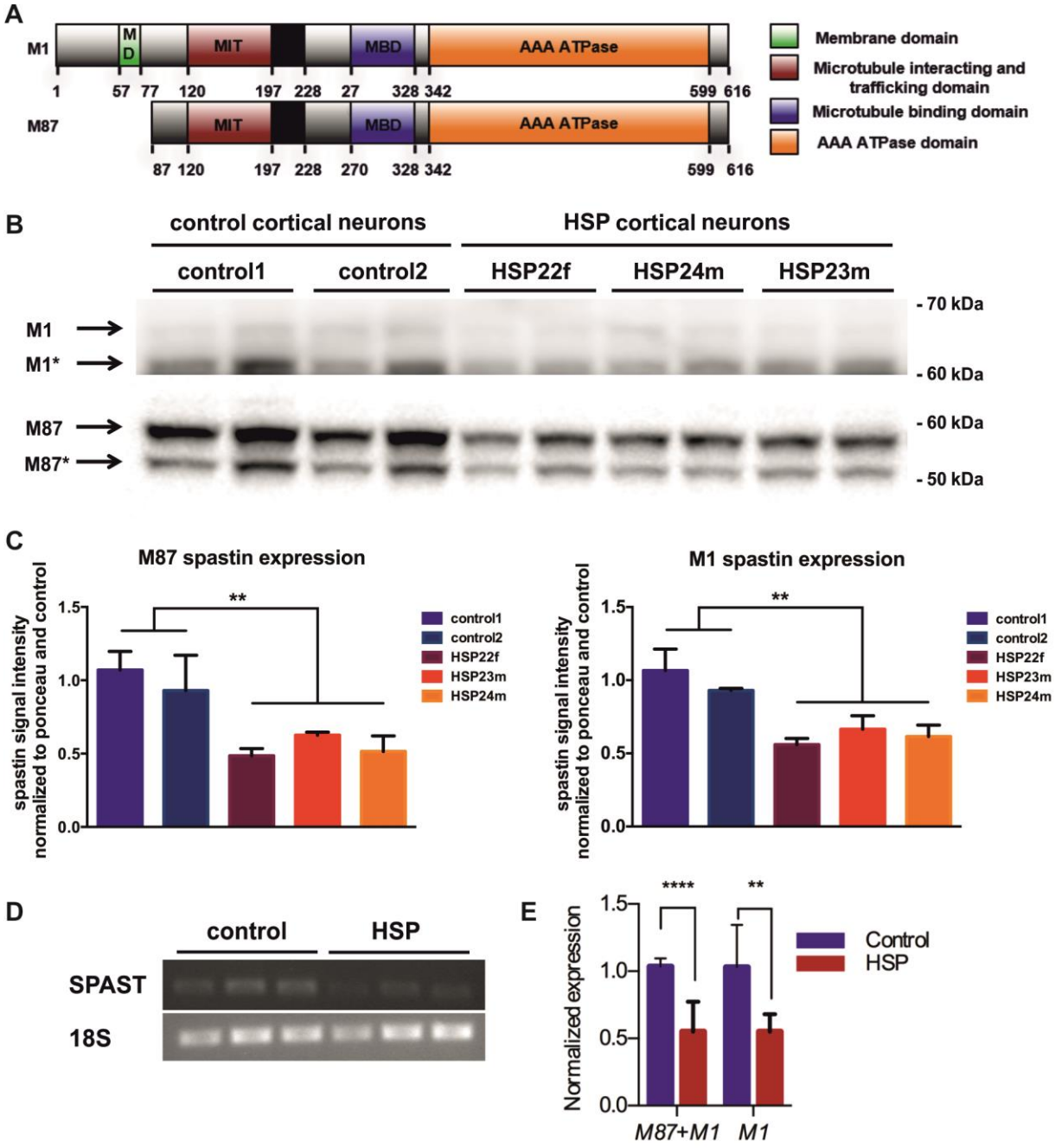

Figure 3.16 Assessment of spastin expression

Spastin expression in control and SPG4 neurons. (A) Spastin is expressed as two major isoforms resulting from alternative translational start sites (M1 and M87) and two splice variants, in which exon 4 is missing (M1* and M87*, exon 4 is shaded in black). (B) The spastin isoforms M87 and M87* can be visualized via western blot after a short exposure time, whereas the M1 and M1* isoforms are only visible after prolonged exposure and are therefore analyzed separately to compare spastin expression levels between neurons from SPG4 patients and controls. (C) Quantification of isoforms M1 and M87 confirmed that spastin expression is reduced by about 50 % in SPG4 neurons compared to controls. Unpaired t-test, **: $p < 0.01$. Error bars show SD. (D) Semiquantitative RT-PCR generated with primers binding at the 5' end of the respective mRNA transcript, visualizes a reduction of *SPAST* RNA in SPG4 neurons compared to control. (E) Q-PCR of the M87+M1 and M1 isoform of *SPAST* normalized to 18S levels and control (control: n=6, HSP: n=6). 2way Anova, **: $p < 0.01$, ***: $p < 0.001$. Error bars show SD.

3.4 Assessment of disease-specific early phenotypes in cortical SPG4 neurons

3.4.1 Cortical SPG4 neurons display an impaired neurite outgrowth

Spastin is a microtubule severing enzyme, thus a difference on the neurite level can be expected between SHP-SPG4 and control neurons. Concentrating on early phenotypic analysis, neurite outgrowth was investigated after 24 hours on day 58, after replating the neurons at single cell density on day 57. (Figure 3.17A). After staining against TUBB3, short patient neurites were already evident (Figure 3.17B). Quantification revealed that the neurite outgrowth within 24 hours ranged from 39µm to 75µm in control neurons and from 17µm to 39µm in patient neurons, depending on the experiment (Figure 3.17C). In general, the mean length of patient neurites clustered very closely together, whereas there was more variation in controls. Overall, neurite length in patient neurons was drastically decreased by 51%. In numbers, the mean neurite length of control neurons was 61µm and that of HSP neurons 29µm, respectively (Figure 3.17D).

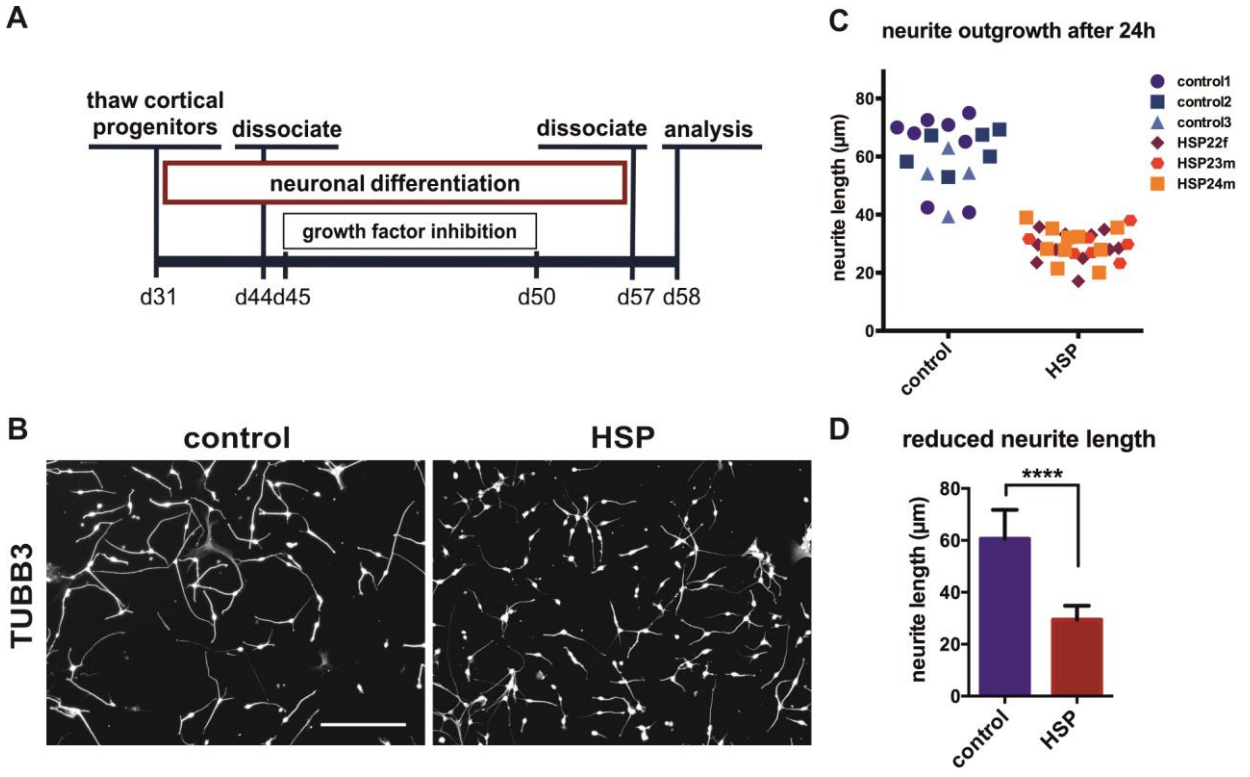

Figure 3.17 Neurite outgrowth assay
(A) Cortical cultures were triturated to single cells and replated at single cell density on day 57. (B) Cells were fixed and stained for TUBB3 after 24 hours on day 58. Scale bar: 100µm. (C) Neurite outgrowth was quantified using at least ten images with 200-2000 neurons. Analysis was performed with ImageJ and the NeuronJ plugin or the INCell Developer software. (D) Overall, SPG4 neurons exhibit a highly significant reduction in neurite length after 24 hours compared to controls (control: n=18, mean HSP: n=28). Unpaired t-test, ****: $p < 0.0001$. Error bars show SD.

3.4.2 Growth cones of cortical SPG4 neurons are significantly enlarged

After observing such a striking phenotype early on, the question arose whether other cytoskeletal compartments were affected as well. Therefore, the focus was on the actin cytoskeleton, which is closely connected to the microtubules. Thus, neurons were treated analogue to the neurite assay and stained against TUBB3 and actin with ActinRed 555 after 24 hours (Figure 3.18A). In neurons, ActinRed 555 stains specifically the growth cones: extensions of growing neurites filled with actin filaments, which provide shape and support. Morphologically, it was already noticeable that some of the growth cones of patient neurons were enlarged compared to those of controls (Figure 3.18B). Quantification revealed that the average growth cone area after 24 hours ranged from 3.9µm^2 to 17.1µm^2 in control neurons and from 20.0µm^2 to 37.2µm^2 in patient neurons (Figure 3.18C). The overall growth cone area of patient neurons was dramatically enlarged. The mean growth cone area of controls was 11.2µm^2 and of the SPG4 neurons 27.9µm^2, respectively (Figure 3.18D).

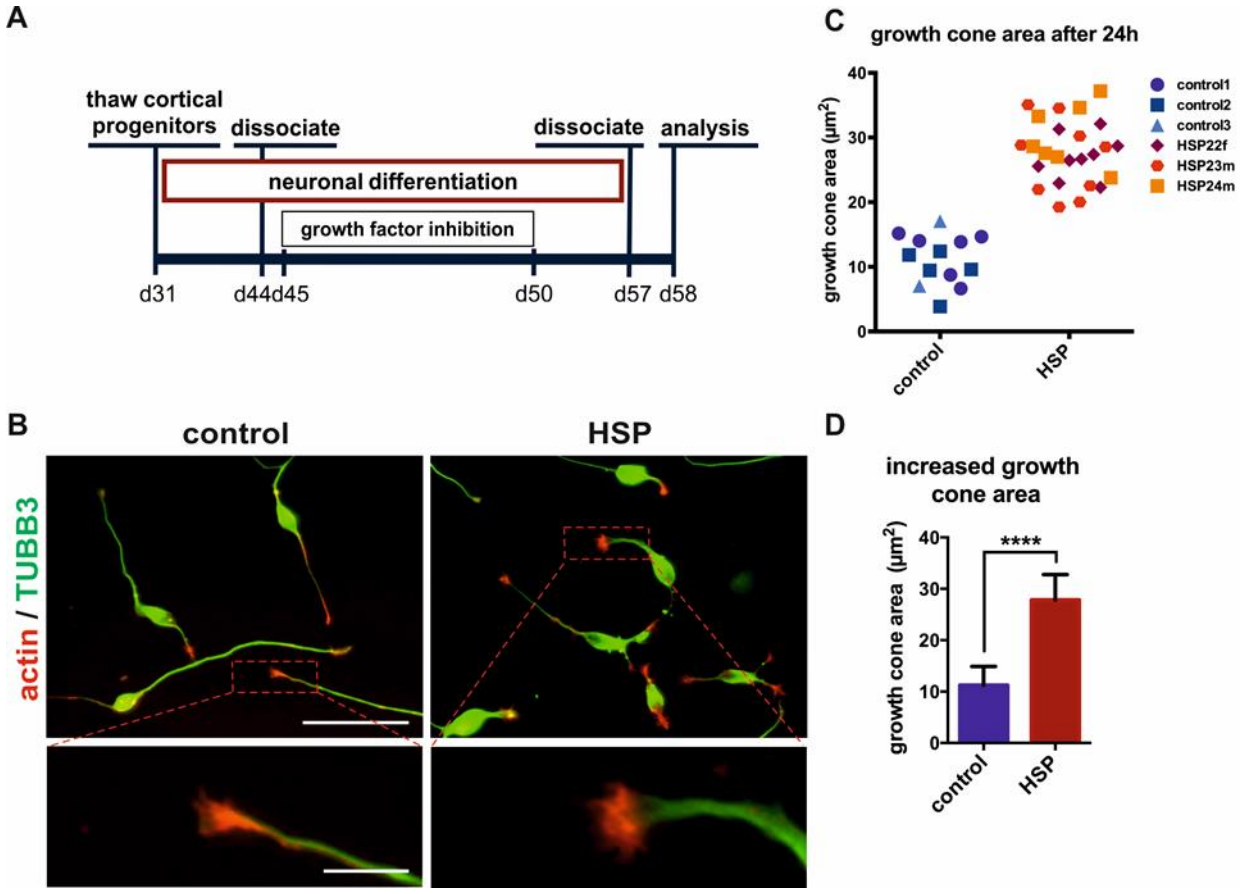

Figure 3.18 Growth cone area of SPG4 neurons
(A) Cortical cultures were singularized and replated on day 57. (B) After 24 hours cells were fixed and stained for TUBB3 and incubated with ActinRed 555 on day 58. Scale bar: 50µm. Insets show magnifications of typical growth cones. Scale bar: 10µm. (C) Quantification of actin positive growth cone area in SPG4 and control neurons. (D) SPG4 neurons exhibit a significant increase in growth cone area after 24 hours (control: n=15, mean HSP: n=25). Unpaired t-test, ****: $p < 0.0001$. Error bars show SD.

3.4.3 Taxol treatment leads to rapid induction of TAU1-positive axons

Since retrograde degeneration of the corticospinal neurons is the main symptom of SPG4, it can be classified as an axonopathy. Consequently, the axonal marker TAU1 was chosen to investigate axonal integrity in SPG4 and control neurons. However, on day 50 no TAU1 positive axonal structures could be detected in the generated neuronal cultures. After prolonged maturation until day 75, a large number of TAU1-positive axons and MAP2-positive dendrites were present and formed very dense neuronal networks (Figure 3.19A). Unfortunately, these networks were so dense, that single axons were hardly distinguishable and were thus not suited for quantitative analysis.

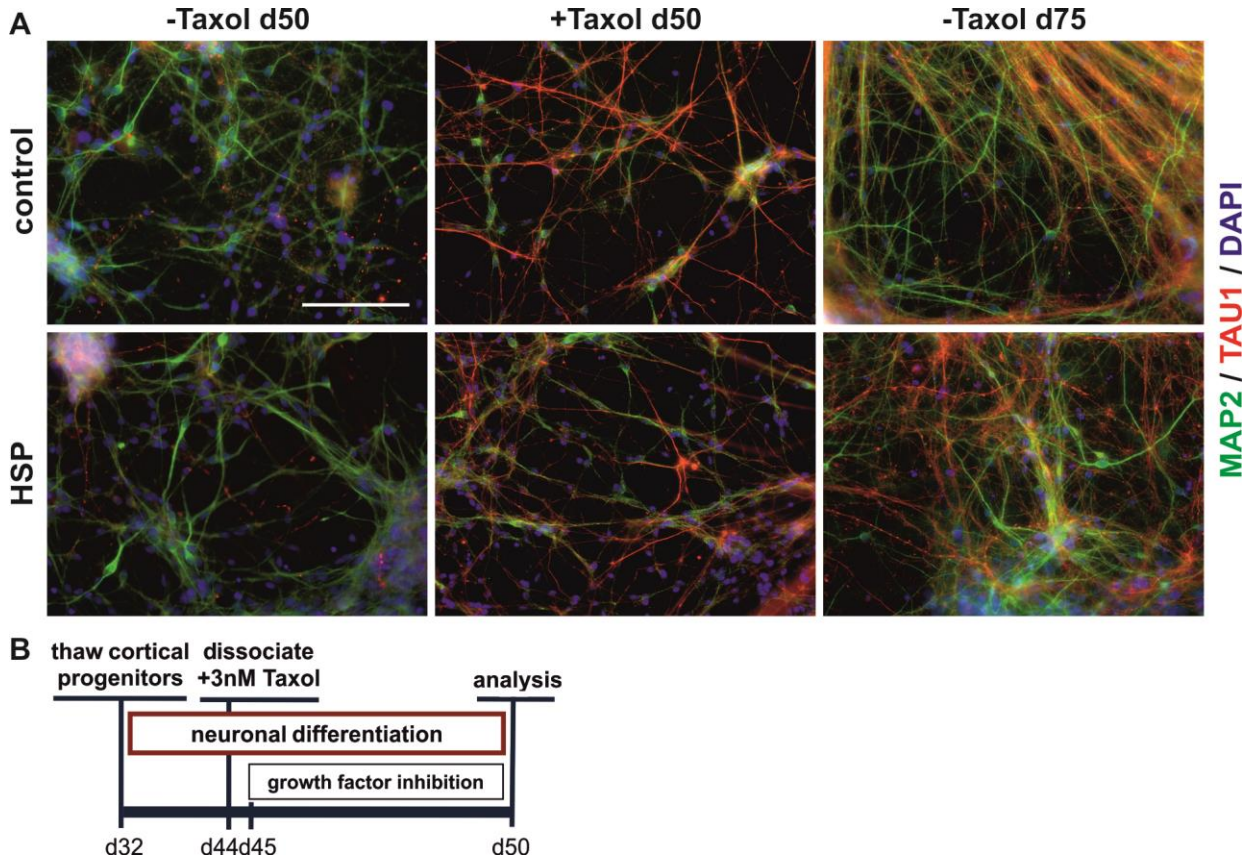

Figure 3.19 Taxol induces Tau1-positive axonal structures
(A) Immunofluorescence staining against TAU1 (red) in day 50 cortical neurons demonstrates a lack of TAU1 positive structures, only dendritic MAP2 positive (green) structures are present. By day 75, TAU1 positive axons have been formed by control and SPG4 for neurons and built a very dense neuronal network. To be able to analyze cultures of less density earlier, Taxol was used on day 44 to induce TAU1 positive axonal structures within one week. (B) For Taxol treatment, cortical progenitors were dissociated on day 44, followed by overnight treatment with 3nM Taxol. Scale bar: 100µm.

This was resolved by inducing axonal structures early on by using low concentrations of Taxol, while the network was still thin enough to be analyzed. Treatment with low doses of the microtubule stabilizing drug Taxol, also known as Paclitaxel, was reported to lead to a four-fold increase of the axonal marker TAU1 in mouse hippocampal neurons compared with control neurons (Witte et al. 2008). Remarkably, overnight treatment of our cultures with 3nM Taxol on

day 44 led to induction of TAU1 positive axons within five days (Figure 3.19). Two beneficial side effects for the readout assay were that the analysis could be performed very early on and that the neurons are faced with the challenge of producing a lot of axons within a short time span, leading to an early visible phenotype.

3.4.4 Cortical SPG4 neurons show axonal swellings

Neurons were treated with Taxol on day 44 to form a complex but low-density neuronal network containing MAP2 positive dendrites and TAU1 positive axons by day 50. Those cultures were used as basis to investigate an axonal phenotype in the SPG4 cortical neuronal cultures (Figure 3.20B). Indeed, in patient neurons but not in control neurons, axonal swellings, a hallmark of SPG4 pathology, which has been previously found in *SPAST*-deficient patients and mouse models, were visible (Figure 3.20A). These swellings in patient axons varied in diameter from 1 to 7 µm and were mostly located at the very distal end of the axon. The swellings counted in control neurons only reached a diameter of 1 to 2 µm and were located throughout the axon. Only swellings in otherwise intact axons were considered. Defragmentation of axons, a normal side effect of *in vitro* cell culture, was likewise present in patient and control neurons and was not included in this analysis. For standardization purposes, every axon thickening was counted as swelling and normalized to the total length of TAU1-positive axons, which was determined using ImageJ. A minimum of 10 pictures per data point were analyzed. The number of TAU1 positive axonal swellings in patient neurons was significantly higher (1.54 /mm) compared to that of control neurons (0.07 /mm). Interestingly, more swellings were detected in neurons of patients HSP23m and HSP24m: 1.65 /mm and 2.06 /mm, respectively – compared to neurons of patient HSP22f, where 0.96 swellings /mm were observed (Figure 3.20C).

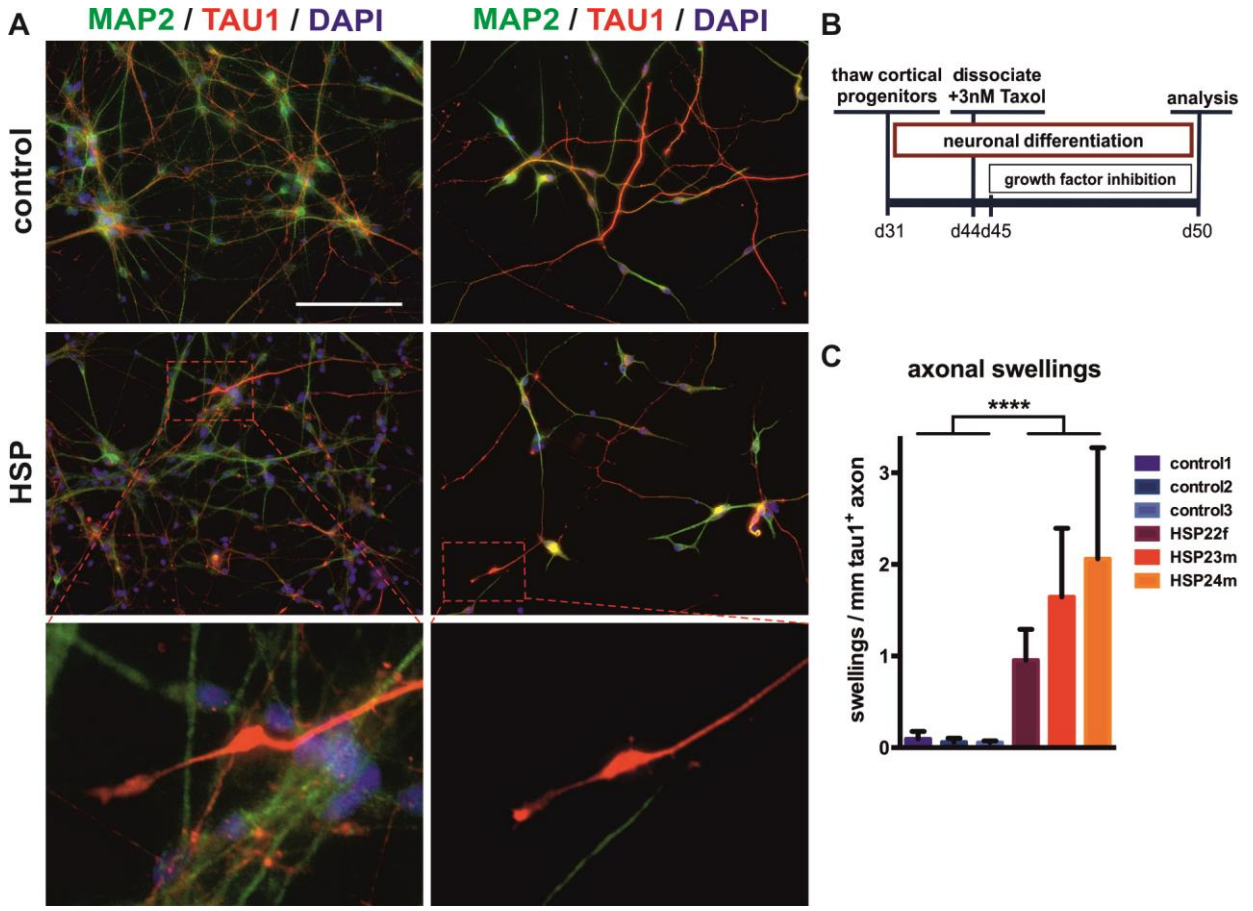

Figure 3.20 Analysis of axonal swellings in cortical HSP and control neurons
(A) Cortical neurons were fixed and stained for the dendrite marker MAP2 and the axon marker TAU1. SPG4 neurons exhibit prominent TAU1 positive axonal swellings. Scale bar: 100µm. (B) Timeline of differentiation and stimulation: Neurons were stimulated with 3nM Taxol on day 44 and cultivated until day 50. (C) Quantification of TAU1 positive axonal swellings (control1: n=7, control2: n=7, control3: n=4, HSP22f: n=10, HSP23m: n=7, HSP24m: n=9). Unpaired t-test, ****: $p < 0.0001$. Error bars show SD.

3.5 Generation and validation of GABAergic neurons

So far SPG4 specific phenotypes were investigated in glutamatergic cortical deep layer projection neurons, a cell type that is also affected in patients. To address the questions, whether the phenotypes are subtype specific or if they are also present in other *in vitro* cell types and only masked *in vivo*, an alternative neuronal population was employed. To this end, the neuronal differentiation protocol was modified to yield mostly GABAergic forebrain neurons, which was achieved by using different dual smad inhibitor concentrations and shortening the proliferation phase (Figure 3.21A). In analogy to the glutamatergic protocol, late precursors were frozen down as one batch to ensure comparability. Due to the shortened proliferation phase, this was done on day 20 instead of day 31. Furthermore, late precursors did not keep on proliferating as extensively as the cortical precursors did after thawing, they started to generate neurons already after one week. Therefore, late precursors were dissociated and prepared for complete neuronal differentiation using FGF and Notch signaling inhibition with 10µM PD0325901 and 10µM DAPT on day 27. A complete neuronal network, comparable in age to d57 glutamatergic neuronal

cultures, was formed by day 37, consisting of almost 100% TUBB3 positive neurons. These neurons were TBR1 negative, mostly GABAergic and positive for the forebrain marker FOXG1 and for CTIP2, which is also expressed in other brain regions besides the cortex, for example the striatum (Figure 3.21B). The cellular identity was further illuminated using Affymetrix expression data obtained from control GABAergic neurons. The expression data is presented log2 transformed and is usually interpreted as follows: 0-4: not expressed, 4-8: medium expression, >8: highly expressed. The Affymetrix expression data confirmed the expression of GABA producing enzymes *GAD1* and *GAD2* and the absence of *vGLUT1*. The generated GABAergic neurons expressed the GABAergic subtype marker somatostatin (*SST*), but did not express Calbindin2 (*CALB2*), Parvalbumin (*PVALB*) or vasoactive intestinal peptide (*VIP*) (Kelsom and Lu 2013; Darmanis et al. 2015), which might be due to the early time point of differentiation (Figure 3.21C). Among other expressed markers were the forebrain marker *FOXG1*, the striatal markers distal-less homeobox 1 (*DLX1*), *DLX2*, *DLX5*, LIM homeobox 6 (*LHX6*), the migration markers aristaless related homeobox (*ARX*) and roundabout homolog 1 (*ROBO1*) and the transcription factor *CTIP2*, which can be present in the cortex in glutamatergic or GABAergic neurons as well as in the striatum (Leid et al. 2004; Nikouei, Muñoz-Manchado, and Hjerling-Leffler 2016). Two typical makers of glutamatergic cortical progenitors and neurons, *TBR1* and Eomesodermin/TBR2 (*EOMES*), were not expressed (Figure 3.21D). In conclusion, this alternative neuronal population consists of forebrain interneurons, displaying a marker profile, which overlaps with classical cortical glutamatergic neurons and is thus an excellent neuronal population for comparison of disease phenotype expression.

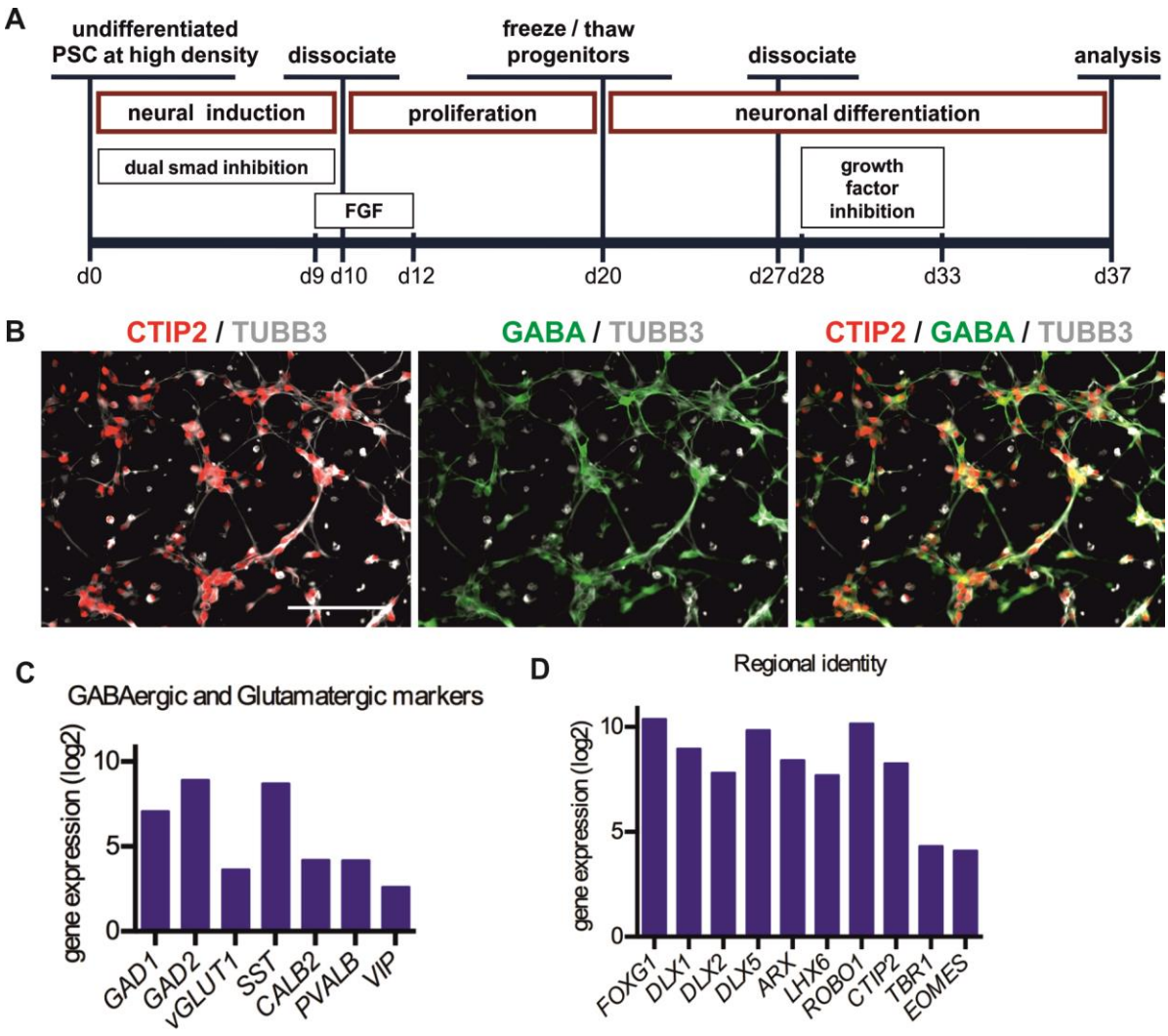

Figure 3.21 Derivation of GABAergic neurons
(A) Upon shortening of the proliferation phase of the neuronal differentiation, neural progenitors start to generate neurons from day 20 onwards. The cultures are completely neuronal after 30 days, upon addition of FGF and Notch inhibitors. (B) The generated TUBB3 positive neurons are almost exclusively GABAergic and mostly co-stain for CTIP2. Scale bar: 100µm. (C, D) Affymetrix expression data (log2) of two control GABAergic differentiations on day 37, confirms the expression of the GABA producing enzymes *GAD1* and *GAD2* and the absence of the vesicular glutamate transporter *vGLUT1*. Of the GABA subtype markers, only Somatostatin (*SST*) is expressed at this time point. (D) The GABAergic cultures express the forebrain marker *FOXG1*, the striatal markers *DLX1, DLX2, DLX5, ARX* and *LHX6*, the migration marker *ROBO1* and the transcription factor *CTIP2*, which is both present in the cortex and the striatum. The forebrain markers *TBR1* and *EOMES* are not expressed.

In order to assess the functionality, GABAergic neurons were matured for three months on mouse astrocytes to evaluate the electrophysiological activity. At this time point, both the control and the SPG4 neurons fired repetitive action potentials in response to 500ms depolarizing current interaction and exhibited fast inactivating inward current and sustained outward current in response to depolarizing voltage. In addition, spontaneous pre-synaptic currents could be measured, which is a sign of an active neuronal network (the electrophysiology data was obtained by Dr. Jaideep Kesavan) (Figure 3.22).

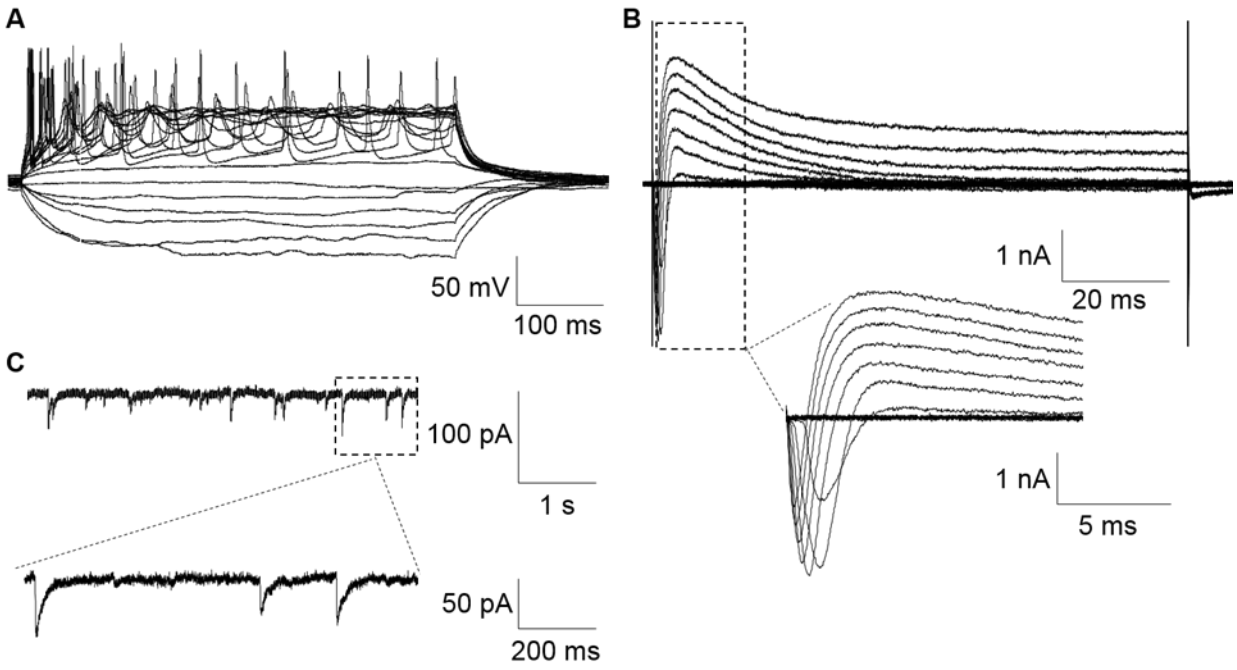

Figure 3.22 Electrophysiological properties of GABAergic neurons
GABAergic neurons were cultured on mouse astrocytes for three months to mature *in vitro*. (A) Repetitive traces of action potentials recorded from GABAergic neurons in response to 500ms depolarizing current injection. (B) Representative trace of fast inactivating inward current and sustained outward current in response to depolarizing voltage steps. Inset shows magnified view of the boxed area. (C) Representative trace of spontaneous postsynaptic currents. Expanded view of the boxed region is shown in the inset.

3.6 GABAergic SPG4 neurons do not show disease-associated phenotypes

These generated forebrain GABAergic neurons, which represent a population with an alternative neurotransmitter type, were used to investigate whether GABAergic SPG4 neurons also exhibit disease-associated phenotypes such as shorter neurites, enlarged growth cones and axonal swellings.

First, we set out to investigate the neurite outgrowth and the growth cone phenotypes in GABAergic forebrain neurons. The GABAergic neuronal network was grown for 10 days before dissociation on day 37. The dissociated neurons were plated at single cell density and plated for 24 hours (Figure 3.23A). Subsequently, control and SPG4 neurons were stained for TUBB3 and actin, via ActinRed 555 (Figure 3.23B). Surprisingly the mean neurite length of control neurons was 53.3 µm and the mean neurite length of patient neurons 64.4µm after 24h (Figure 3.23C). Thus, GABAergic SPG4 neurites were slightly longer than GABAergic control neurons. Especially neurites of patient HSP22f were significantly prolonged compared to control2. To confirm this finding, the neurite length was investigated again after 48 hours. The mean neurite length of control (59.8µm) and patient (75.6µm) neurons was slightly longer after 48 hours and neurites of SPG4 neurons were still significantly longer than those of controls.

Next, the growth cones of GABAergic neurons were stained using ActinRed 555 and quantified with the INCell Developer toolbox (Figure 3.23D). The mean growth cone area of control neurons

was 17.6µm^2 compared to 19.5µm^2 of patient growth cones after 24 hours. Even though growth cones of patient neurons were slightly larger, the difference was not significant. To confirm this finding, the growth cone area was investigated again after 48 hours. The mean area of control (19µm^2) and patient (20µm^2) growth cones was slightly larger after 48 hours but did not significantly differ between patient and control neurons.

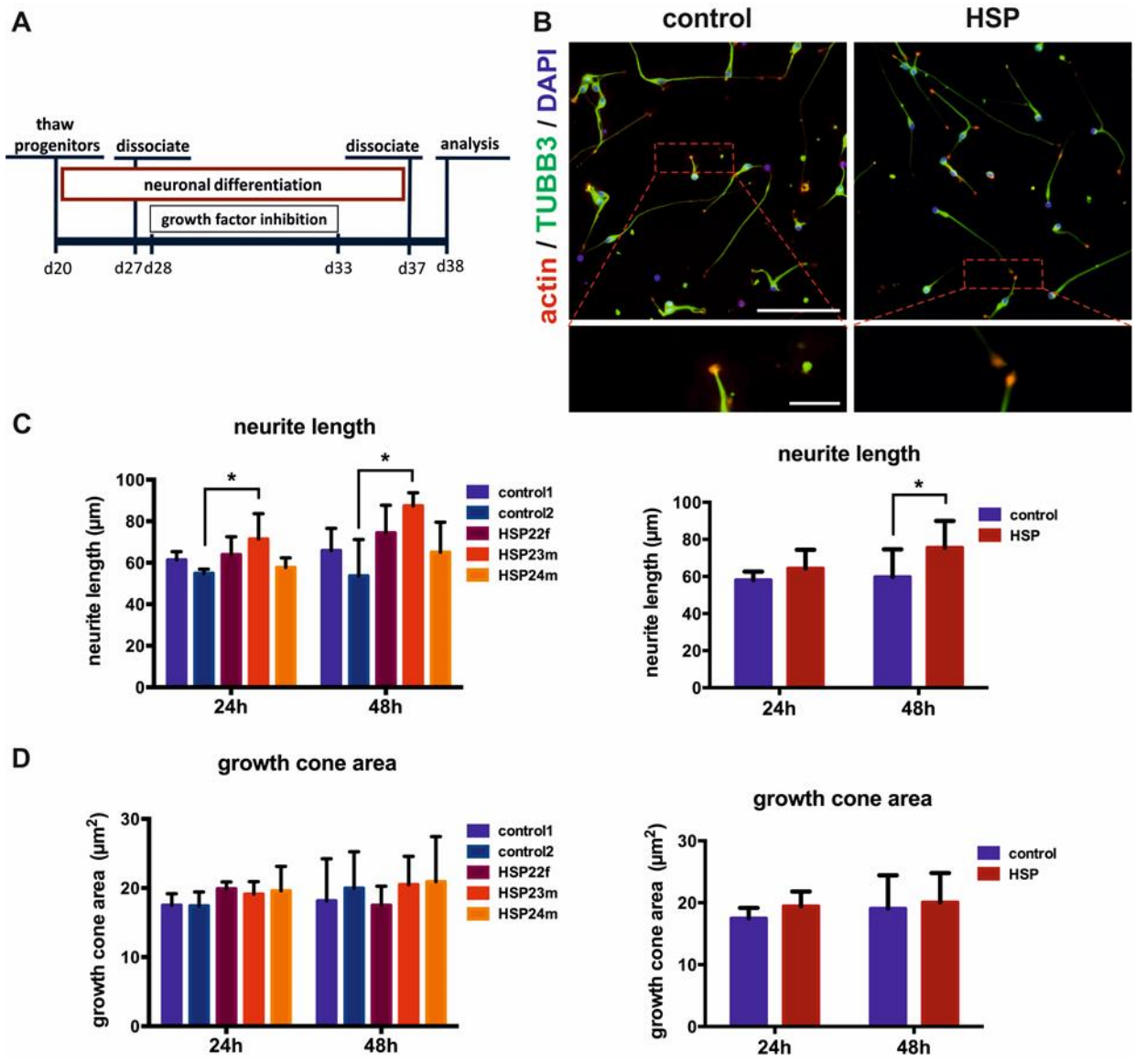

Figure 3.23 Analysis of neurite outgrowth and growth cone area in GABAergic neurons
(A) GABAergic cultures were triturated to single cells and replated on day 37. (B) After 24 hours and 48 hours cells were fixed, stained for TUBB3 and incubated with ActinRed 555. Scale bar: 50µm. Insets show magnifications of typical growth cones. Scale bar: 10 µm. (C) Neurite outgrowth was quantified using at least ten TUBB3 images. Analysis was performed with the INCell Developer software (control: n=8, HSP: n=12). Neurite length after 24 hours and 48 hours was not reduced in SPG4 neurons, but instead enhanced in one patient. (D) Actin positive growth cone area was quantified with the INCell Developer Software. Growth cone area of SPG4 GABAergic neurons did not differ after 24 hours or 48 hours (control: n=8, HSP: n=10). 2way ANOVA, *: $p < 0.05$. Error bars show SD.

For fast induction of axonal structures, cultures were treated with 3nM Taxol overnight on day 27 (Figure 3.24B). However, although the neurons stained positive for MAP2, no TAU1 positive

axons could be detected in the cultures after 10 days. This was surprising, since the glutamatergic cultures expressed TAU1 positive axons already 5 days after Taxol treatment. Since the quantification of axonal swellings was not possible, the neurons were stained against normal TAU and acetylated tubulin, a more stable form of tubulin associated with axons (Figure 3.24). Indeed, the cultures expressed TAU and acetylated tubulin and displayed occasional thickenings in the otherwise smooth neurites. After quantification of the swellings and normalization against the total filament length no difference between control and SPG4 cultures could be detected (Figure 3.24C). The mean number of TAU positive swellings in controls was 0.2/mm, compared to patient cultures, which exhibited 0.1 swellings/mm TAU filament. Consistently, the mean numbers of acetylated tubulin positive swellings were only slightly higher with 0.3/mm in controls and 0.2 swellings /mm in patient cultures.

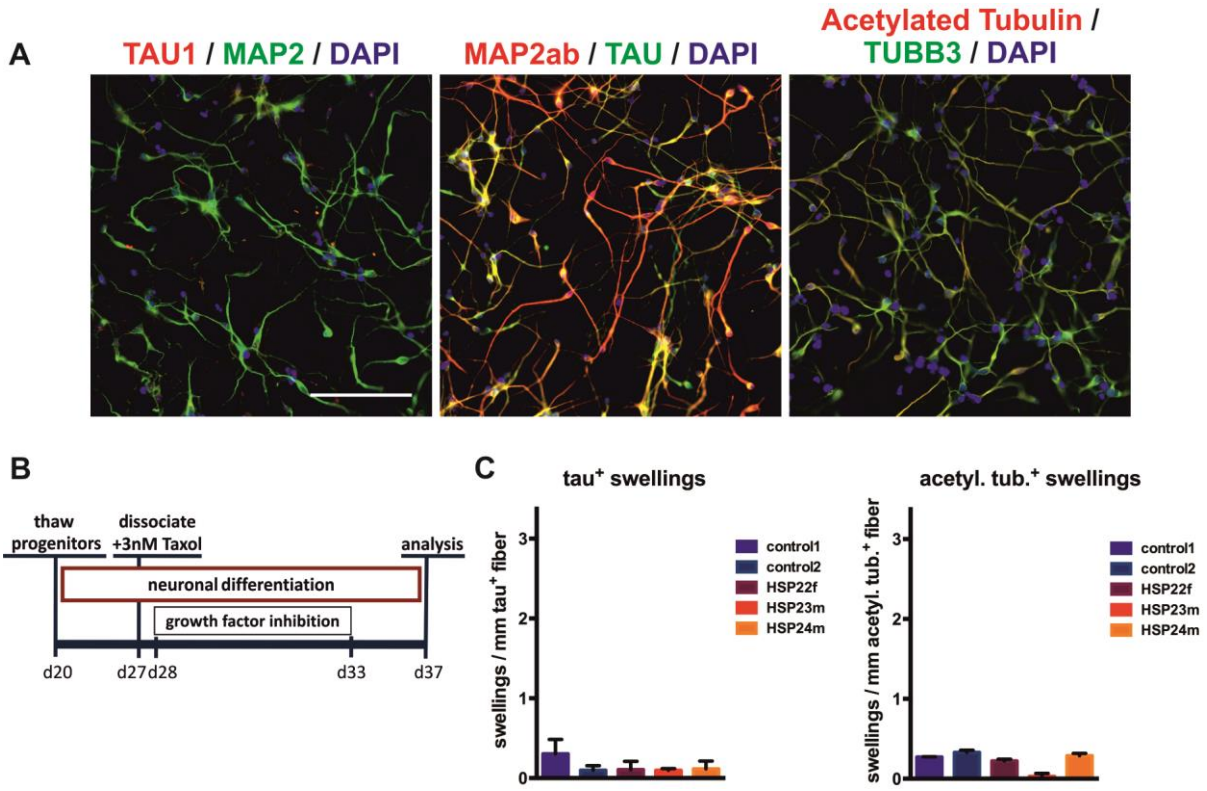

Figure 3.24 Assessment of swellings in GABAergic neurons
(A) GABAergic cultures were fixed and analyzed on day 37. Despite Taxol treatment on day 27, GABAergic cultures are devoid of TAU1 positive structures 10 days later. However, normal TAU, acetylated tubulin, a stable form of tubulin and dendritic MAP2 are expressed. (B) Timeline of differentiation and stimulation. (C) Both control and SPG4 neurons are nearly devoid of TAU positive and acetylated tubulin positive swellings (control: n=4, HSP: n=6). Scale bar: 100µm. Error bars show SD.

In conclusion, disease specific phenotypes that were present in glutamatergic neurons could not be confirmed in SPG4 GABAergic forebrain neurons.

3.7 GABAergic neurons display elevated M1 *SPAST* levels

Considering the different results obtained in the phenotypic assays with glutamatergic or GABAergic neurons, we set out to compare the populations further to find an explanation. The cDNA of different differentiations of two control lines and all three patient lines were used to analyze differences in expression levels of *SPAST* between glutamatergic and GABAergic cultures on day 57 or day 37, respectively. As expected, control and patient GABAergic cultures express the GABA producing enzymes glutamate decarboxylase (*GAD*) *1* and *GAD2*, which were nearly absent in glutamatergic cultures, whereas the vesicular glutamate transporter *vGLUT1* is only expressed in glutamatergic cultures (Figure 3.25A). Since the basis of SPG4 in our patients is a haploinsufficiency of spastin, the levels of M87 and M1 *SPAST* in the glutamatergic and GABAergic cultures were investigated. QPCR of the highly expressed M87 isoform confirmed the expected reduction of *SPAST* in glutamatergic and GABAergic patient cultures compared to control. Since the M87 *SPAST* isoform shares 100 % identity with the M1 isoform, when targeting M87 in qPCR, M1 is always detected as well. However, the M87 *SPAST* isoform is more abundant and therefore contributes the majority of the signal.

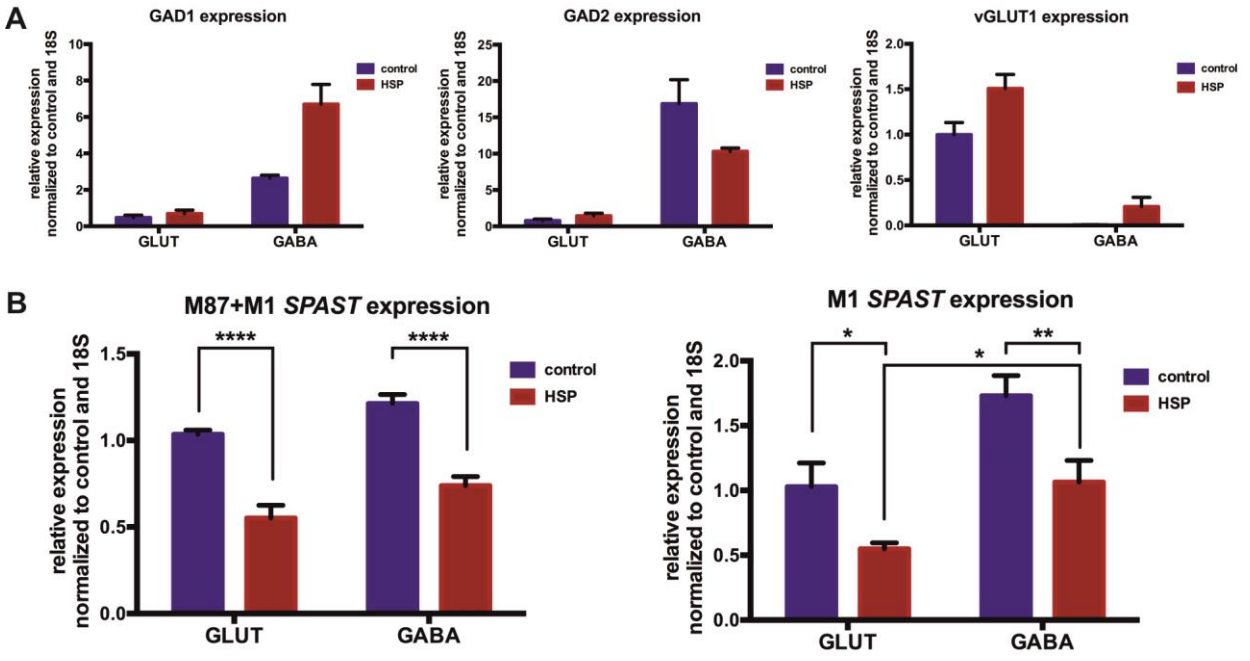

Figure 3.25 Comparative qPCR analysis of cortical and GABAergic neurons
QPCR of cortical glutamatergic cultures and GABAergic cultures was performed to identify differences in expression levels. (A) Control and SPG4 GABAergic cultures display higher levels of GABA synthesizing enzymes *GAD1* and *GAD2*, whereas control and SPG4 glutamatergic cultures exhibit *VGLUT1* expression. (B) The M 87 isoform of *SPAST* is significantly reduced in both glutamatergic and GABAergic SPG4 neurons. Glutamatergic vs. GABAergic cultures however exhibit no difference. Expression of the longer M1 *SPAST* isoform on the other hand is significantly increased in GABAergic SPG4 neurons compared to glutamatergic SPG4 neurons. Indeed, there is no difference in M1 *SPAST* expression between glutamatergic control neurons and GABAergic SPG4 neurons. 2way ANOVA, *: $p < 0.05$, **: $p < 0.01$, ****: $p < 0.0001$. Error bars show SEM of triplicates.

The M87+M1 *SPAST* levels in GABAergic cultures of both patient and control were slightly, but not significantly higher compared to glutamatergic cultures. Analysis of the membrane-bound M1 isoform revealed drastically elevated *SPAST* levels in patient and control GABAergic cultures compared to glutamatergic cultures. Especially the *SPAST* M1 level is significantly increased in GABAergic compared to glutamatergic patient cultures; its expression level is in fact comparable to glutamatergic control cultures (Figure 3.25B). An elevated level of M1 *SPAST* in GABAergic patient cultures might explain the missing phenotype in GABAergic patient cultures and would point towards a central role of M1 spastin rather than M87 spastin in SPG4.

3.8 Compound evaluation in cortical SPG4 neurons

3.8.1 Read-through molecules fail to upregulate spastin levels

The reduced spastin expression level in patient neurons seems to be crucial for the development of a disease phenotype *in vivo* and *in vitro*. To counteract phenotypes in cortical patient neurons, an upregulation of spastin in glutamatergic patient cultures should be beneficial. Since all three patients are carrying nonsense mutations in the SPAST gene, a read-through of the premature stop codon might be a promising strategy.

The aminoglycoside Gentamycin is an antibiotic that mediates translational read-through by binding to the small ribosomal subunit. It induces a conformational change that leads to incorporation of a random amino-acid at the premature termination codon position (Malik et al. 2010). PTC-124 acts through the same mechanism but is more specific (Welch et al. 2007). The usual working concentrations of Gentamycin are 1mg /ml (2.1mM), whereas 10µM PTC-124 are sufficient. In a disease model of retinitis pigmentosa, PTC-124 restored up to 20% of endogenous, full length RP2 protein (Schwarz et al. 2015). Amlexanox has been reported to induce the synthesis of full-length proteins by stabilizing mRNAs containing nonsense mutations (Gonzalez et al. 2012). Specifically for spastin, it has been reported that FGF and IGF influence its expression due to an unknown mechanism (Qiang et al. 2010; Korulu and Karabay 2011).

To test the above-mentioned small molecules for their ability of spastin upregulation, neuronal cultures of two patients and two controls were treated daily for 7 days with either 1mg/ml Gentamycin, 10µM PTC-124, 10µM Amlexanox, 10µM PTC-124 and Amlexanox or 100ng/ml FGF2 and IGF1. Subsequently, proteins were harvested and analyzed via western blotting. However, no upregulation of spastin in drug treated patient cultures compared to untreated controls could be detected.

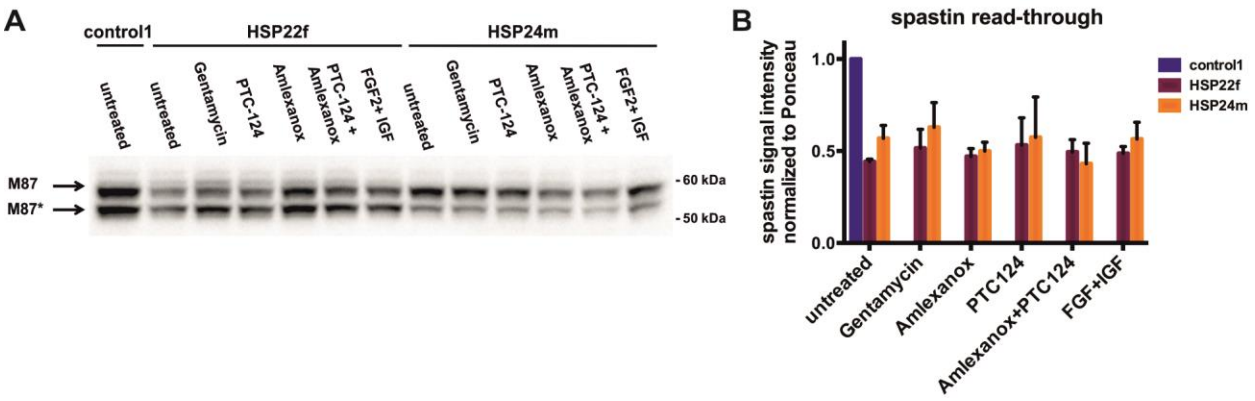

Figure 3.26 The effect of read-through molecules on spastin expression
Evaluation of the effect of the read-through molecules Gentamycin, PTC-124, Amlexanox and the growth factors FGF and IGF on spastin level in SPG4 neurons carrying a nonsense mutation. (A) SPG4 neurons were treated daily for one week followed by western blot analysis of spastin isoform M87 and M87*. (B) Quantification of spastin levels shows no upregulated of spastin upon drug treatment. Error bars show SD.

3.8.2 Automated analysis and selection of candidate compounds

All three described phenotypic assays described show a good separation between control and patient populations, which makes them amenable for drug testing. The advantage of testing drugs on three disease specific early phenotypes is the possibility to exclude drugs which might have a random non-disease-related mechanism. Another strength of this iPSC disease model is the possibility to test drugs on cells of three different patients with different genetic backgrounds. The testing was performed on 96-well plates, making sure that the same conditions of all three patient and all three control lines were on the same plate, in order to reduce experimental variability. The plates were fixed and stained manually, followed by automated image acquisition with the INCell Analyzer 2200 and automated or semi-automated image analysis with the INCell Developer and the CellProfiler software.

Promising substances were selected for drug testing based on literature inquiry, choosing substance classes that have been implicated in SPG4 or other neurodegenerative diseases (Table 3.2). The microtubule targeting drugs Vinblastine and Taxol have been successfully used to counteract axonal swellings, for instance in a mouse model of SPG4 and were thus chosen for this drug testing (Fassier et al. 2013). Taxol is a microtubule binding reagent used as a chemotherapeutic for cancer treatment. It stabilizes microtubules by binding to the incorporated β-tubulin subunits and therefore prevents depolymerization (Gornstein et al. 2014). While high concentrations of Taxol interfere with microtubule disassembly during cell division and lead to cell cycle arrest and cell death (Zhang et al. 2014), low doses of Taxol induce the formation of multiple axons in neurons (Witte et al. 2008). Like Taxol, Vinblastine is an anticancer drug inhibiting mitosis by binding to microtubules. But contrary to Taxol, Vinblastine inhibits the assembly of microtubules, leading to destabilization. Low concentrations of Vinblastine suppress microtubule

dynamics while high concentrations lead to a reduction in microtubule polymer mass (Jordan et al. 2004).

In a disease model using patient olfactory mucosa cells, marginally slower moving peroxisomes could be rescued by Noscapine, a drug that acts similar to Vinblastine, but is able to cross the blood-brain barrier (Ye et al. 1998; Fan et al. 2014).

Since we discovered a novel phenotype in patient neurons, i.e. the enlargement of growth cones and thus revealed a so far unknown dysregulation of actin in SPG4, we included actin modulating drugs in this drug test. Jasplakinolide is an actin modulating drug, that stabilizes F-actin by polymerization of actin filaments (Holzinger 2009). On the contrary, the actin destabilizing drugs Cytochalasin B and Latrunculin B inhibit actin polymerization mainly by blocking monomer addition at the fast-growing end of F-actin filaments (MacLean-Fletcher et al. 1980; Wakatsuki et al. 2001). In addition, Latrunculin B has been reported to promote neurite elongation (Bradke et al. 1999).

Spastin is an inhibitor of BMP signaling, therefore a BMP inhibitor might rescue the lack of BMP inhibition and the associated phenotypes caused by reduction of spastin. We decided to test the small molecule BMP inhibitor Dorsomorphine and its highly selective, small molecule analogue DMH1 (Hao et al. 2010; Neely et al. 2012).

Lipid homeostasis and insufficient lipid droplet formation have been implicated in the disease formation of SPG4 (Papadopoulos et al. 2015). The Liver X Receptor (LXR) agonist GW3965 induces and expands lipid droplets and is able to cross the blood-brain barrier and was therefore chosen for this testing (Donkin et al. 2010; Lei et al. 2013). Furthermore, GW3965 showed neuroprotective properties in ischemia models (Cui et al. 2013), where it improved functional outcome by increasing synaptic protein expression and axonal density, possibly by blockade of nuclear factor-kappaB activation and the subsequent suppression of Cyclooxygenase-2 (COX-2) in the post-ischemic brain (Cheng et al. 2010). Moreover, GW3965 improved memory and reduced β-Amyloid levels in mouse models of Alzheimer's disease (AD) and improved cognitive recovery and suppressed axonal damage after traumatic brain injury by upregulation of Apolipoprotein E (ApoE) and ATP-binding cassette transporter (ABCA1) (Donkin et al. 2010; Namjoshi et al. 2013). In addition, LXRs regulate cholesterol metabolism and transport, lipogenesis and protect from cholesterol overload (Prüfer et al. 2007).

Another common theme in HSP besides lipid metabolism are mitochondria. TRO19622, also known as Olesoxime, has a cholesterol-like structure and acts as inhibitor of the mitochondrial permeability pore (mPTP) preventing a response to oxidative stress (Bordet et al. 2010). It has been proven to be neuroprotective in several disease models and is currently tested in phase III clinical trials for the treatment of spinal muscular atrophy, a disease affecting the spinal motor neurons and amyotrophic lateral sclerosis (ALS), a disorder disturbing both the upper and lower

motor neurons, which is somewhat similar but more severe than HSP (Martin et al. 2010; Zanetta et al. 2014).

The histone deacetylase inhibitor Scriptaid has neuroprotective properties and has been proven to be beneficial in models of ALS and models of the most common neurodegenerative diseases: Parkinson disease and Alzheimer's disease (Corcoran, Mitchison, and Liu 2004; Traynor et al. 2006). Furthermore Scriptaid provides protection of motor and cognitive functions in a mouse model of traumatic brain injury (Wang et al. 2013).

Substance class	Mode of action	Name	Concentrations
Microtubule modulation	Microtubule stabilization	Taxol	3nM
	Microtubule destabilization	Vinblastine	10nM
	Microtubule destabilization	Noscapine	10µM
Actin modulation	Actin stabilization	Jasplakinolide	1nM, 3nM, 10nM
	Actin destabilization	Cytochalasin B	1nM, 3nM, 10nM
	Actin destabilization	Latrunculin B	1nM, 3nM, 10nM
BMP signaling	BMP inhibition	DMH1	1µM
	BMP inhibition	Dorsomorphin	1µM
Lipid homeostasis	Liver X receptor agonist	GW3965	5µM, 10µM
Mitochondria	Mitochondrial pore inhibitor	TRO19622	3µM, 10µM
Histone modification	Histone deacetylase inhibition	Scriptaid	1µM

Table 3.2 Overview of tested small molecules

3.8.3 Modulation of neurite outgrowth and growth cone area with small molecules

The effect of the selected drugs on neurite outgrowth and growth cone area was tested simultaneously on 96-well plates. Neuronal cultures of three patients and three controls were dissociated on day 57 and seeded in single cell density on 96-well plates, preloaded with the drugs of interest, obtaining duplicates of each condition (Figure 3.27). Each plate was fixed and stained against TUBB3, actin and DAPI after 24 hours.

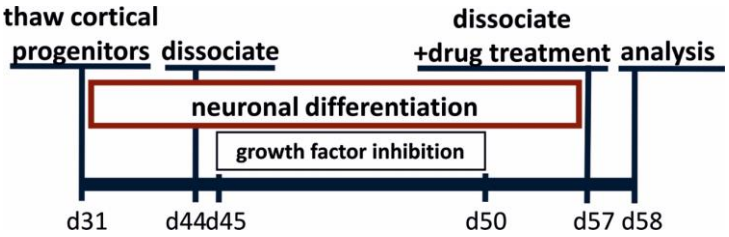

Figure 3.27 Timeline for drug treatment in the neurite outgrowth and growth cone assay
Cortical neurons were dissociated and singularized on d57 and seeded on 96-well plates preloaded with drugs. After 24 hours, plates were fixed and stained against TUBB3, actin and DAPI.

In this drug test, the neurite length was quantified automatically employing the INCell Developer software. The mean neurite length of all control samples (n=10) was used as positive control, whereas the mean neurite length of all patient samples (n=14) was used as negative control. The reference neurite lengths of untreated neurons in numbers were 63.9µm and 36µm, respectively. The actin destabilizing drug Latrunculin B led to a significant increase in patient neurite length, which reached a length of 48.9µm after treatment with 1nM, 50.6µm after treatment with 3nM and 50.2µm after treatment with 10nM Latrunculin B. 5µM of the LXR agonist GW3965 also caused a significant increase in patient neurite length, it reached 50.01µm. The drugs Taxol, low doses of Jasplakinolide, low doses of Cytochalasin B, 1µM DMH1, 1µM Dorsomorphin, 10µM GW3965 and 3µM TRO19622 had no significant effect on the neurite length of either patient or control neurons. However, 10nM Vinblastine, 10nM Jasplakinolide, 10nM Cytochalasin B and 1µM Scriptaid led to decrease of neurite length in controls and are thus unsuitable due to neurotoxicity (Figure 3.28).

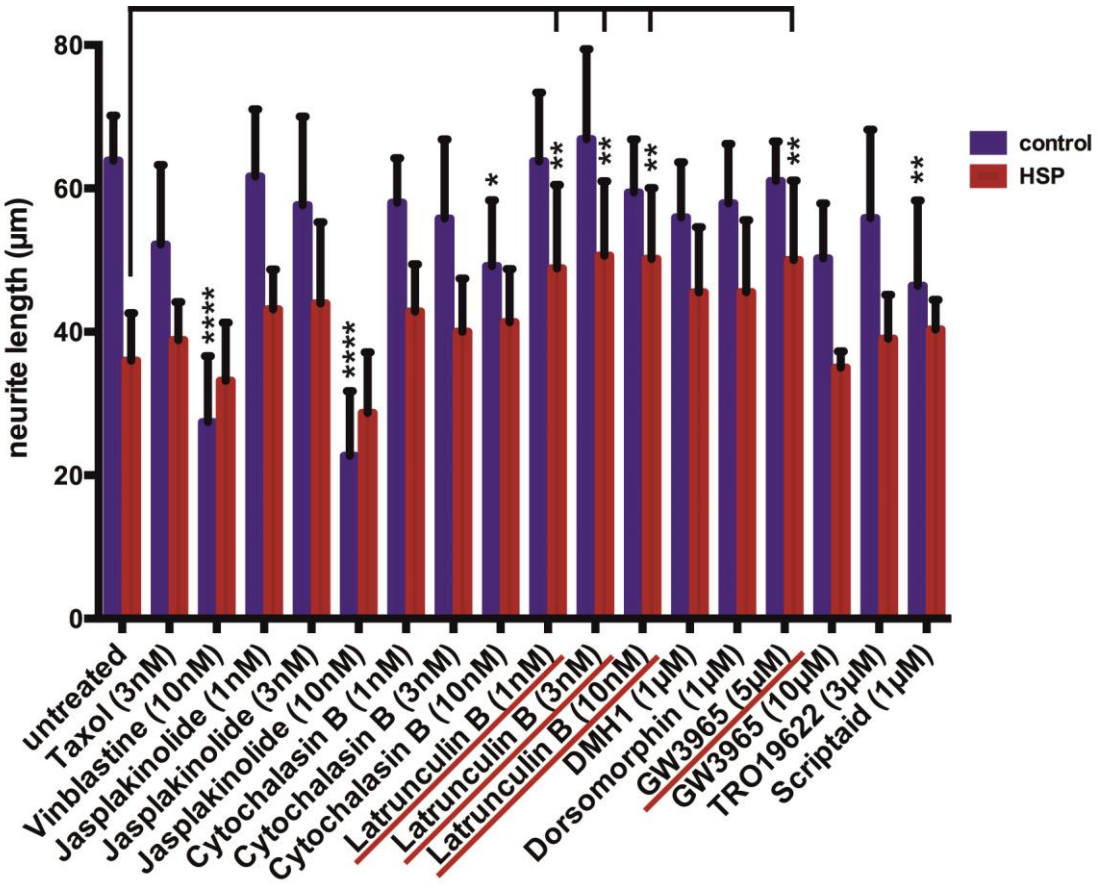

Figure 3.28 Neurite outgrowth modulation in SPG4 neurons
Neurite length of control (control1, control2, control3) and SPG4 (HSP22f, HSP23m, HSP24m) neurons and the effects of drug treatments after 24 hours were quantified using the INCell Developer software. Drugs that significantly increase neurite length of SGP4 neurons were underlined. Neurotoxicity can be identified by a decrease of neurite length in control neurons. 2way ANOVA, *: $p < 0.05$, **: $p < 0.01$, ****: $p < 0.0001$. Error bars show SD. Control: n=10, HSP: n=14.

For the analysis of the growth cone areas after drug treatment, a semi-automated approach was chosen in order to yield high accuracy and an unbiased analysis. With the CellProfiler software, randomly acquired actin images were converted to binary images followed by automated area quantification of the signal. Due to some residual actin-positive astrocytes and staining artifacts, which had to be excluded from analysis, the data of growth cone areas was picked out of the total pool of quantifications manually. For this purpose, merged images of TUBB3, DAPI, actin and the automatically generated quantification data were generated.

The obtained quantification data showed a good separation between populations in all experiments. However, the overall growth cone area differed between experiments. Thus, the growth cone area was normalized to the mean of the untreated controls to determine the relative differences between SPG4-, control- and drug-treated-growth cones.

As a result of analysis and normalization, the relative mean of the growth cone area in controls representing the positive control was 1, whereas the relative mean of the growth cone area in patients, the negative control and reference was 2.76.

Several of the tested drugs achieved a significant reduction of patient growth cone areas. 3nM Taxol reduced the relative patient growth cone area to 2.04, 1nM Jasplakinolide to 1,78, 3nM Jasplakinolide to 0.87, 3nM Latrunculin B to 2.03, 1µM DMH1 to 1.89, 1µM Dorsomorphin to 1.9, 5µM GW3965 to 1.83, 3µM TRO19622 to 1.98, and 1µM Scriptaid to 1.65. The strongest reduction of patient growth cone area could be observed after treatment with 3nM Jasplakinolide. However, it also caused a disorganization of actin in control neurons, which developed actin positive spots in the cell body (Figure 3.30). The higher concentration of 10nM Jasplakinolide completely diminished all growth cones in control and patient neurons. Vinblastine had no significant effect on the growth cone area of neither patient nor control neurons. On the contrary, 10nM Cytochalasin B led to a significant increase in growth cone area of control neurons, which could also be observed as a trend in lower concentrations of Cytochalasin B and Taxol (Figure 3.29).

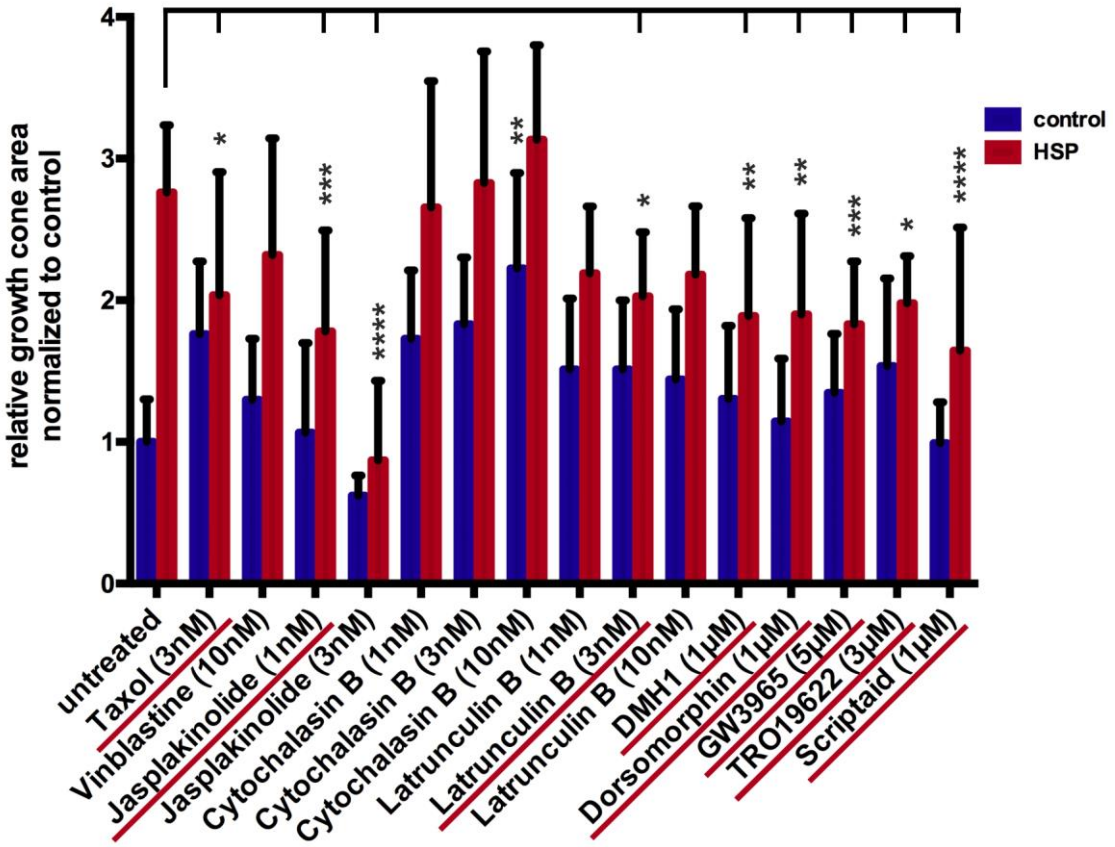

Figure 3.29 Growth cone area modulation in SPG4 neurons
Growth cone area in control (control1, control2, control3) and HSP (HSP22f, HSP23m, HSP24m) neurons and the effects of drug treatments after 24 hours. Drugs that significantly reduce growth cone area of SGP4 neurons were underlined. 2way ANOVA, *: $p < 0.05$, **: $p < 0.01$, ***: $p < 0.001$, ****: $p < 0.0001$. Error bars show SD. Control: n=10, HSP: n=14.

Summarizing the results of the drug testing on neurite outgrowth assay and the growth cone assay, only two drugs achieved a phenotype improvement in both assays. 3M Latrunculin B and 5µM GW3965 were both able to induce an increase of neurite length and a reduction of growth cone area in patient neurons, while maintaining normal neuronal morphology in patient and control neurons. (Figure 3.30).

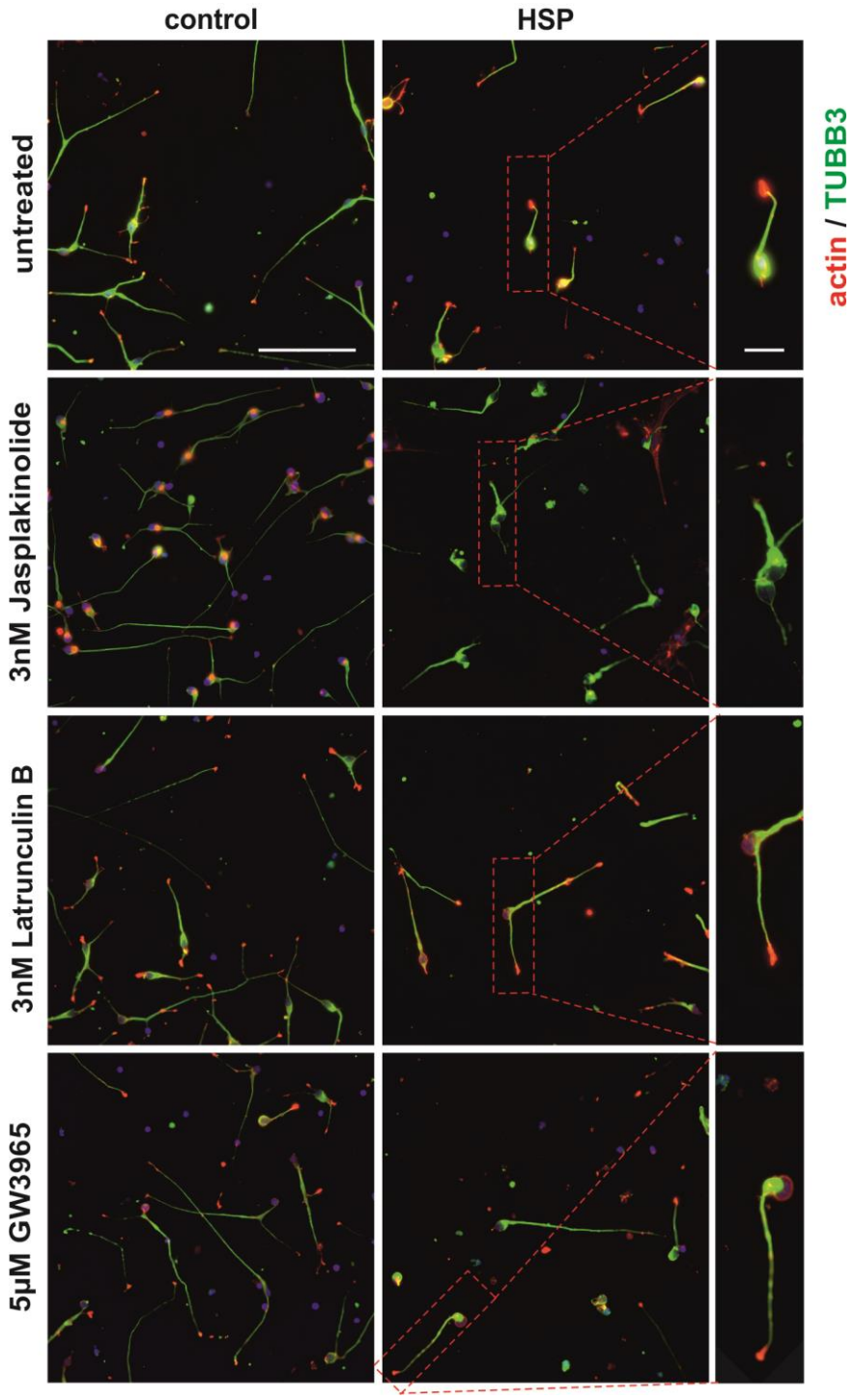

Figure 3.30 Examples for successful neurite outgrowth and growth cone area modulation
Representative immunofluorescence images of TUBB3 (green), actin (red) and DAPI (blue) stainings of cortical control and SPG4 neurons after the drug testing on day 58. Scale bar: 50µm. Insets show magnifications of typical neurites and growth cones. Scale bar: 10 µm.

3.8.4 Modulation of axonal swellings using small molecules

For the axonal swelling assay, TAU1 was induced on day 44 with 3nM Taxol, leaving the swellings six days to form, before fixation on day 50. For the drug testing the timeline was kept and the drug treatment was applied daily from day 45 to day 50 (Figure 3.31). Only Vinblastine and Noscapine were applied for 24 hours from day 49 to day 50, according to published reports (Denton et al. 2014).

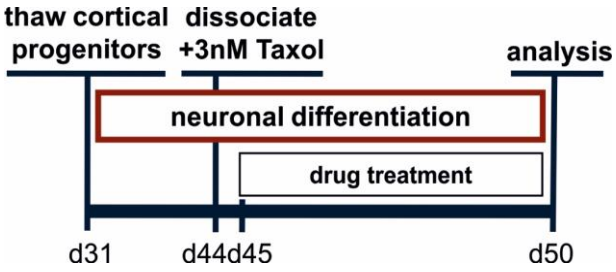

Figure 3.31 Timeline for drug treatment in the axonal swelling assay

On day 50 cortical cultures were fixed and stained for the axonal marker TAU1 and the dendritic marker MAP2. TAU1 positive axonal swellings were counted manually, whereas the total length of TAU1 positive filament which was used for normalization, was quantified automatically using the INCell Developer software.

The mean number of swellings per mm TAU1 positive axon of all control samples (n=9) was used as positive control and the mean number of swellings per mm TAU1 positive axon of all patient samples (n=14) was used as negative control. The swelling numbers of untreated neurons control and patient neurons used as reference were 0.066/mm axon and 1.127/mm axon, respectively.

All tested drugs led to a significant reduction of axonal swellings in SPG4 cultures. However, some led to an only moderate reduction of axonal swelling frequency: 1µM Dorsomorphin reduced swellings to 0.451/mm, 3µM TRO19622 to 0.438 /mm and 1µM Scriptaid to 0.708/mm. Other drugs almost completely eliminated axonal swellings: 1µM DMH1 reduced the frequency of axonal swellings in SPG4 neurons to 0.16 /mm, 5µM GW3965 to 0.105/mm and 10µM TRO19622 to 0.202/mm. Noscapine and Vinblastine treatment for 24 hours decreased axonal swellings in SPG4 neurons moderately to 0.407/mm and 0.45/mm, respectively (Figure 3.32). However, treatment with Vinblastine for 5 days showed neurotoxic effects and diminished, along with the axonal swellings, nearly all neuronal structures.

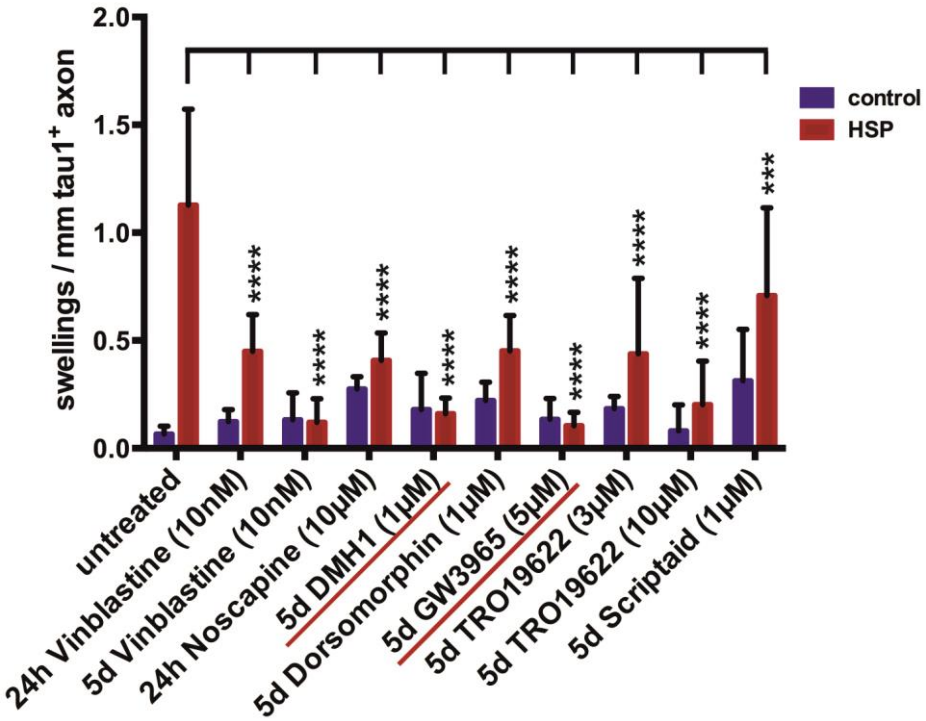

Figure 3.32 Overview of axonal swelling modulation in SPG4 neurons
Axonal swellings in control (control1, control2, control3) and SPG4 (HSP22f, HSP23m, HSP24m) neurons and the effects of drug treatments after five days or 24 hours, respectively. All tested drugs reduced axonal swellings significantly in SPG4 neurons. However, the drugs with the best effect, combined with normal neuronal morphology are underlined. 2way ANOVA, ***: $p < 0.001$, ****: $p < 0.0001$. Error bars show SD.

Hence, the most effective reduction, accompanied by normal neuronal morphology was achieved by 1µM DMH1 and 5µM GW3965 treatment (Figure 3.33).

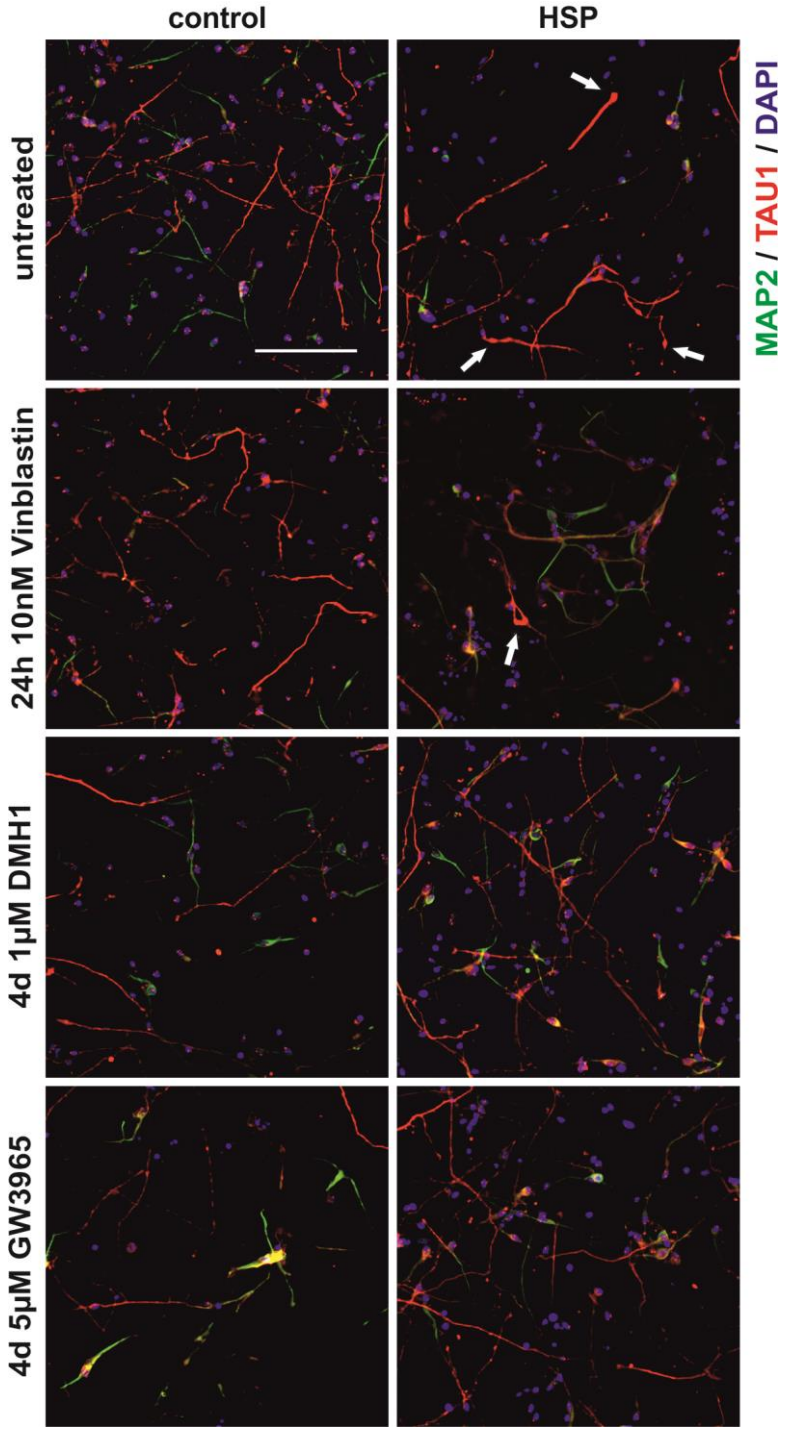

Figure 3.33 Examples of axonal swelling modulation in SPG4 neurons
Representative immunofluorescence images of TAU1 (red), MAP2 (green) and DAPI (blue) stainings of cortical control and SPG4 neurons after the drug testing on day 50. White arrows mark axonal swellings. Scale bar: 50µm.

In summary, the LXR agonist GW3965 was able to rescue all three phenotypes of SPG4 neurons. It induced an increase of neurite outgrowth, a decrease of growth cone area and a reduction of axonal swellings. Importantly, GW3965 had no effect on control neurons, but acted specifically on pathophenotypes (Table 3.3).

Tested small molecule	Concentrations	Neurite outgrowth	Growth cone area	Axonal swellings
Taxol	3nM	0.9952	0.0138	n.d.
Vinblastine	10nM	0.9953	0.3379	<0.0001
Noscapine	10µM	n.d.	n.d.	<0.0001
Jasplakinolide	1nM	0.4392	0.0002	n.d.
	3nM	0.2471	<0.0001	n.d.
	10nM	0.3052	n.d.	n.d.
Cytochalasin B	1nM	0.4641	0.9993	n.d.
	3nM	0.9611	0.9996	n.d.
	10nM	0.7768	0.5652	n.d.
Latrunculin B	1nM	0.0080	0.0991	n.d.
	3nM	0.0010	0.0122	n.d.
	10nM	0.0017	0.0877	n.d.
DMH1	1µM	0.0964	0.0013	<0.0001
Dorsomorphin	1µM	0.0933	0.0016	<0.0001
GW3965	5µM	0.0038	0.0005	<0.0001
	10µM	0.9997	n.d.	n.d.
TRO19622	3µM	0.9989	0.0440	<0.0001
	10µM	n.d.	n.d.	<0.0001
Scriptaid	1µM	0.9209	<0.0001	0.0005

Table 3.3 Overview of tested small molecules and p-values obtained for SPG4 neurons
Shown p-values for treated SPG4 neurons against untreated SPG4 neurons were obtained with Dunnett's multiple comparisons test after ANOVA. Positive effects were shaded green, effects on the control neurons were shaded in red. Data points that were not determined (n.d.) were labeled with: n.d.

3.8.5 Cryopreservation of the SPG4 neurite phenotype

For high-throughput drug screening, a large batch of readily available neurons would be most feasible. This was achieved by investigating whether the neurons are amenable for freezing and can be used for to the neurite outgrowth assay after cryopreservation. Control and SPG4 neurons were dissociated on day 57 in analogue to the described neurite outgrowth assay and frozen down as single cells in a specially developed neuronal freezing medium containing Trehalose in addition to DMSO. Trehalose is a natural disaccharide that prevents protein denaturation and crystallization (Traynor et al. 2006). After a few days of storage at -150°C, the frozen neurons were thawed and cultured for 24 hours before fixation and TUBB3 staining. The separation after thawing needs to be further optimized to prevent cell clumps, but in concurrence with previous experiments, automated analysis revealed significantly reduced neurite outgrowth in SPG4 neurons. The mean neurite length of control neurons was 61.3µm, whereas the mean neurite length of patient neurons was only 32.7µm (Figure 3.34).

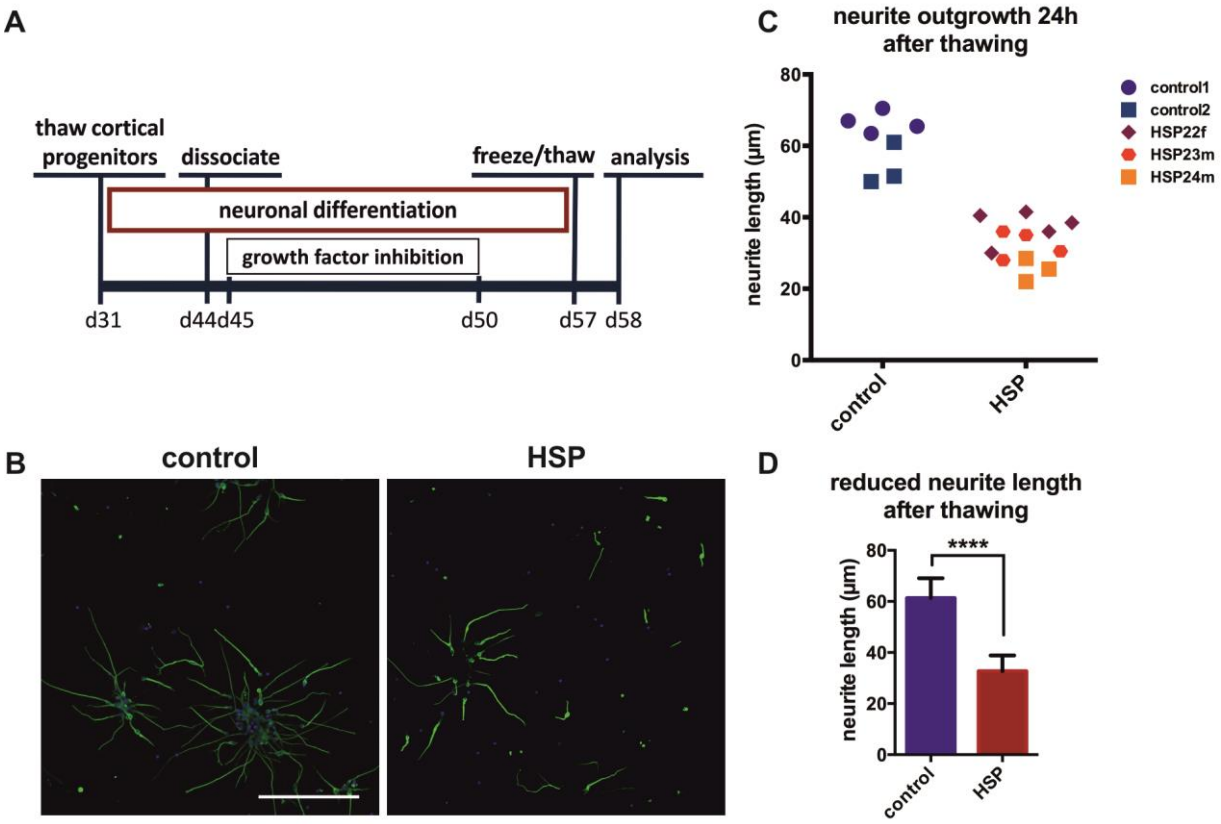

Figure 3.34 Neurite outgrowth assay using cryopreserved neurons
(A) Cortical cultures were singularized and frozen in neuronal freezing medium. (B) Cells were thawed, seeded at single cell density and grown for 24 hours. They were fixed and stained for TUBB3 after the next day. Scale bar: 100µm. (C) Neurite outgrowth was quantified based on at least ten images. Analysis was performed with the INCell Developer software. (D) Overall, HSP neurons exhibit 46% reduction in neurite length 24 hours after thawing compared to controls. Unpaired t-test, ****: $p < 0.0001$. Error bars show SD.

4 DISCUSSION

SPG4 is the most common form of HSP however, the disease mechanism is still unknown and a treatment has not yet been developed. Furthermore, research is hampered by limited access to the affected cell type, cortical neurons. IPSCs provide the possibility of *in vitro* differentiation into all somatic cell types and have thus opened up new possibilities for disease modeling, especially of neuronal diseases, where human samples are hard to obtain. The aim of this thesis was the generation of an iPSC-based disease model for SPG4 to analyze disease specific phenotypes *in vitro* and to develop assays that provide a platform for drug discovery. To this end, a human iPSC-based SPG4 model was developed and very early phenotypes, which emerged within a few days could be identified. Cortical SPG4 neurons exhibited reduced neurite outgrowth, enlarged growth cones and axonal swellings, a hallmark of the HSP pathology. All three fast phenotypic assays were transferred to an automated or semi-automated 96-well-setup and potentially therapeutic compounds counteracting SPG4-associated neuronal phenotypes were identified.

4.1 Generation and quality control of iPSCs

While generating an iPSC disease model, it is important to ensure the suitability of the generated iPSC lines. To this end, iPSC clones were extensively validated regarding their genomic integrity, pluripotency, differentiation potential and absence of virus transcript.

The genome integrity is of utter importance, since additional mutations can be acquired during reprogramming or the reprogramming process can select for pre-existing mutations in the parental fibroblasts pool (Hussein et al. 2011; Abyzov et al. 2012). These newly acquired or pre-existing somatic mutations might mask the initial disease-causing point mutation and thus need to be excluded to draw disease relevant conclusions. To detect these additional genomic aberrations, single nucleotide polymorphisms (SNP) analysis was performed. Every individual has unique SNPs within the genome, which can be analyzed with microarray chips. On the basis of missing or duplicated SNPs, copy number variations (CNVs) can be detected (Spits et al. 2008). In contrast to classical karyotyping such as G-banding, SNP analysis has a much higher resolution and can detect duplications and deletions as small as 300kb in comparison to 10Mb in karyotyping (Bickmore 2001; Shaffer and Bejjani 2004). The disadvantage is that whole balanced chromosomal translocations cannot be identified. However, major aberrations lead most likely to changes in growth rate and morphology, which are closely monitored during cell culture. Thus, newly generated iPSC clones, which display abnormalities during cell culture are immediately discarded. For this project fourteen iPSC clones of patient HSP23m and HSP24m had to be analyzed to identify three lines with an intact genome. Thus over 70% of the picked iPSC clones carried additional mutations, which is more than expected. This was most likely due to pre-existing mutations already present in a subset of fibroblasts, since SNP analysis of HSP23m and HSP24m

fibroblasts already revealed partial duplications or deletions on several chromosomes. These somatic mosaics are fairly common within primary fibroblasts and can be accelerated by extensive culturing time *in vitro* (Abyzov et al. 2012; Rouhani et al. 2016), which applies to the fibroblasts used in this study. Primary fibroblast with a high passage number usually show signs of senescence and are more difficult to reprogram. Therefore, an efficient reprogramming method had to be employed.

The fibroblasts of the first patient (HSP22f-1) were reprogrammed by the means of integrating FLAG-tagged retroviruses (Aasen et al. 2008). Integrating viruses like retro-viruses have a high reprogramming efficiency and the transgene expression was silenced within the first passages of the generated iPSC line. However, integration into the genome can lead to insertional mutagenesis and the silencing can be incomplete, leading to a defect in differentiation potential. These disadvantages can be overcome by the use of non-integrating Sendai viruses (Fusaki et al. 2009), which were used to reprogram fibroblasts of patients HSP23m and HSP24m.

To exclude any remaining clone specific effects interfering with disease-associated phenotypes, two clones of every patient were used in this study. Unfortunately, although two clones of patient HSP23m passed the validation process, one of them showed no neurogenic potential but was only able to generate glial cells and thus could not be included in the study. This reduced differentiation potential was likely due to one or several small mutations below the resolution of SNP analysis or epigenetic changes.

To confirm the identity of the patient iPSC lines after reprogramming, the mutated area of the SPAST gene was sequenced. All patient lines did indeed contain a point mutation, leading to a premature stop codon at position 577 of the SPAST gene. The three patients selected for this study are relatives and thus carry the same point mutation. Remarkably, on a clinical level they have disease onsets that vary between age 18, 32 and 40. This variation might either be caused by a different level of awareness of the patient and the physician or by other factors within the genome that might modulate the disease onset. Thus, it is of great interest to evaluate whether the severity of *in vitro* phenotypes differs between patient lines.

Pluripotency of the iPSC lines was determined on immunofluorescence level by visualizing the enzyme alkaline phosphatase and staining with the antibodies TRA-1-60 and TRA-1-81 which detect two proteoglycans specifically present on human pluripotent stem cells. Whereas alkaline phosphatase is a rather unspecific marker, TRA-1-60 and TRA-1-80 identify fully reprogrammed iPSCs (Chan et al. 2009).

Besides the expression of pluripotency markers, pluripotent stem cells have the potential to give rise to all three germ layers. Teratoma analysis, an assay in which cells differentiate *in vivo* after transplantation into the testis of immunocompromised mice, used to be the gold standard to determine the differentiation potential of human PSCs. However, the drawbacks are the need of test animals and the long differentiation time of ten weeks *in vivo*. The complementary *in vitro*

assay is the undirected differentiation of EBs for three weeks with subsequent immunofluorescence staining for germ layer markers. This method is faster but for feasibility reasons restricted to very few markers, giving a highly biased picture of the differentiation potential. To overcome these restrictions, the suitability of a novel pluripotency test, the Scorecard assay was evaluated using two iPSC lines that were already successfully validated with an *in vivo* teratoma analysis and an *in vitro* EB assay. Initially, iPSCs were subjected to undirected EB differentiation for two weeks followed by TaqMan analysis of several markers of the three germ layers. However, for the first clone the ectodermal- and for the second clone the mesodermal- and endodermal markers did not overcome the threshold, even though the clones were clearly able to generate all three germ layers in the classical teratoma and EB assays. Since each germ layer differentiates best under certain conditions, I established short directed differentiation protocols for each germ layer. After five days of directed differentiations, the iPSC lines showed a robust marker expression of all three germ layers in the Scorecard assay. Employing this fast assay to evaluate the differentiation potential and to explore the suitability of a certain line for directed *in vitro* differentiation, the other generated iPSC lines were validated. All tested lines showed an upregulation of all three germ layers upon differentiation. In the meantime a similar protocol has been published by the originators of the Scorecard assay (Tsankov et al. 2015). In addition, the scorecard panel contains primers to detect transcripts of Sendai origin. Sendai virus is a replication incompetent, non-integrating RNA virus, which is usually eliminated from iPSCs within a few passages, however persistence of Sendai virus transcripts has been reported (Ban et al. 2011). Thus, it is important to confirm the absence of virus transcripts after reprogramming. Since no Sendai signal could be detected in the Scorecard, the virus has been fully eliminated. Furthermore, the epigenetic silencing of the transgenes transduced with retroviruses was confirmed by qPCR against the endogenous and the total expression of the used reprogramming factors. We observed minor variability between the signal of total and endogenous primers which was already observed in the publication originally describing this method (Yu et al. 2007). However, the total expression level of the reprogramming factors was not elevated compared to endogenous levels, indicating absence of transgene expression.

In conclusion, all selected iPSC lines met the quality control criteria, including an intact genome, expression of pluripotency markers, differentiation potential and absence of transgene expression and can be considered as high-quality iPSC lines.

4.2 Derivation of highly enriched neuronal cultures with cortical identity

In hereditary spastic paraplegia, upper motor neurons, which reside in the motor cortex, degenerate, leading to spastic motor deficits. In order to model SPG4 successfully, iPSCs had to be differentiated into a disease relevant cell type, i.e. cortical projection neurons. Since no protocol for the generation of upper motor neurons exists so far, a published protocol was adapted

to generate cortical neurons highly enriched for layers V and VI, the layers where cortical projection neurons are localized.

The differentiation procedure into cortical neurons was based on a protocol published in 2012 (Shi et al. 2012). Complete neural induction was achieved by dual SMAD inhibition using the small molecules SB431542 to inhibit the TGFβ pathway and Dorsomorphin to inhibit the BMP pathway (Chambers et al. 2009). At a later stage of this project, the BMP inhibitor Dorsomorphin was replaced with the more specific inhibitor LDN-193189 (Cuny et al. 2008), to ensure a complete neural induction across different cell lines and to avoid non-neural cells in the cultures.

After neural induction, the precursors were kept under proliferative conditions by addition of FGF2. Cortical precursors were frozen down as one batch on day 31 in order to have a standardized starting point for final neuronal differentiation. To avoid continuing proliferation of cortical progenitors upon growth factor withdrawal and thus the generation of higher cortical layers, the FGF and Notch pathways - which drive proliferation of cortical progenitors (Lui et al. 2011; Rash et al. 2011) – were blocked using the inhibitory small molecules PD0325901 and DAPT, respectively (Borghese et al. 2010). To ensure cell identity and comparability between cell lines, the cultures were extensively validated and only used if a very high percentage of deep layer projection neurons (>80%) and only very few contaminating cells were present, which was almost always the case.

Deep layer projection neurons reside in the layer V and VI of the cortex, are glutamatergic and usually express either the layer V marker CTIP2 or the layer VI marker TBR1. Most of the neurons generated here express both markers CTIP2 and TBR1, which is most likely due to the fact that the differentiation was forced at a time point were the development was on the verge between layer V and VI. Co-expression of both of those markers has also been observed during human development *in vivo* (Ip et al. 2011; Aevermann et al. 2017). In addition, both markers are typical for cortical deep layer projection neurons and the *in vitro* expression remains stable over a prolonged differentiation time of at least three months. The generated cells are very homogeneous and thus suitable for the single cell assay that were performed in this study. In addition to the expression of CTIP2 and TBR1, the neurons expressed the glutamatergic marker vGlut1, the forebrain marker FOXG1 and the projection neuron marker FEZF2. General neuronal identity itself is characterized by the typical neuronal morphology with a small cell body, multiple dendrites and one long axon and a positive staining against TUBB3. However, the most important quality of a mature neuron is the functionality, such as synaptic transmission and the ability to fire action potentials. Since the neurons were generated from pluripotent stem cells, they are comparable to embryonic to fetal stage neurons and thus are initially immature. To promote maturation, the generated deep layer projection neurons were co-cultured with astrocytes for three months (Johnson et al. 2007; Prè et al. 2014). Indeed, after this time span, the analyzed neurons were electrophysiological active and fired action potentials. However, for the anticipated

screening assays, a maturation time of three months in addition to two months differentiation is not feasible, especially since a re-plating after maturation, would lead to stress responses and massive cell death. The presence of the astrocytes layer would further complicate read-outs and introduce variability. Therefore, all following experiments were performed between days 50 and 60, after confirmation of the cortical projection neuron cell fate. In conclusion, high-quality cortical cultures with at least 80% deep layer projection neurons were generated for disease modeling and drug screening purposes.

4.3 Spastin loss of function in SPG4 neurons

Due to the premature stop codon in the SPAST gene, cortical neurons of SPG4 patients have a lower expression level of the spastin protein. Since no truncated protein could be detected, haploinsufficiency is the most likely disease mechanism of the patients included in this study. Only very few SPAST mutations have been associated with a dominant negative mode of action (Pantakani et al. 2008; Solowska et al. 2010; Solowska et al. 2014). In this study, the *SPAST* reduction can already be seen on mRNA level indicating that the truncated mRNA is degraded via nonsense-mediated mRNA decay. Interestingly, patient HSP22f appears to have a slightly lower expression level of spastin, which correlates with an earlier age of onset. This might be a causative correlation or a coincidence caused by other modifying factors.

Two major spastin isoforms exist, a shorter M87 isoform and a longer M1 isoform, which holds an additional N-terminal membrane domain. The M87 isoform is ubiquitously expressed and has the most abundant expression. This does not necessarily mean that this isoform is more important, since the enzyme functions as a hexamer, which could consist of various combinations of M87 and M1 isoforms. However, only the membrane domain of the M1 isoform can localize the hexamer to the ER membrane. Furthermore, expression of the M1 isoform is elevated within the corticospinal pathway of rats and has thus been reported to be the more disease relevant isoform (Solowska et al. 2008). Since the M87 isoform is more abundantly expressed, the M1 isoform might be the limiting factor, which is not easily compensated. Overall, the level of spastin protein seems to be most critical for the development of disease phenotypes. For this study, patients with nonsense mutations were chosen, providing the opportunity to test a possible read-through of the premature stop codon in the SPAST gene. However, a seven-day treatment with read-through inducing molecules did not lead to an up regulation of spastin. For this assay five different conditions were tested and evaluated on protein level. Although this readout is informative, it is also very time-consuming and laborious and thus not suitable to test a larger number of conditions or small molecules.

4.4 Identification of early, rapid phenotypes in SPG4 neurons

SPG4 patient iPSC-derived neurons were analyzed via immunocytochemical stainings and three very early phenotypes could be identified. Within two weeks, SPG4 neurons exhibited a neurite outgrowth deficit, enlarged growth cones and axonal swellings.

In this study, SPG4 neurite outgrowth was reduced by 51% after 24 hours. In a previously published iPSC disease model, a decrease in neurite length of 40% could only be detected after 6 weeks in culture (Havlicek et al. 2014). The observation of such a strong phenotype after just 24 hours at this early stage in development is quite unexpected, since it takes decades until HSP patients develop clinical symptoms. However, the emergence of early phenotypes might be explained by the fact that the neurons were cultured in a reduced environment lacking the endogenous niche, which is composed of different cell types such as astroglia, which provide trophic support and nutrients to the neurons. This lack of support and the comparably high oxygen level might render the neurons stressed during *in vitro* cultivation. Thus, phenotypes like the neurite outgrowth deficit that might never develop *in vivo* can emerge *in vitro* due to the absence of compensating factors and supporting cells. The neurite outgrowth deficit itself can be explained by overly stabilized microtubule, due to spastin haploinsufficiency. However spastin also plays a role in lipid metabolism and BPM inhibition and both of these mechanisms are very important for neurite outgrowth (Ko et al. 2005; Bond et al. 2012; Hegarty et al. 2014).

The enlarged growth cone phenotype described here has so far not been reported in any other disease model of HSP. And there might even be a connection between the neurite outgrowth deficit and the enlarged growth cones. Overly stabilized growth cones might inhibit microtubule protrusion leading to shorter neurites or *vice versa*, overly stabilized microtubule might not be able to push the growth cones forward, which, in consequence, grow larger.

The neurite outgrowth deficit and enlarged growth cones identified here for the first time *in vitro*, have so far not been described *in vivo*. However, they might also be present in patients without generating a noticeable phenotype or might be compensated by other cell types in the more supportive *in vivo* environment. An *in vitro* neurite outgrowth deficit is often found in neurodegenerative iPSC disease models and it might be a phenotype linked to many neurodegenerative diseases (Ozeki et al. 2003; Sánchez-Danés et al. 2012; Reinhardt et al. 2013a).

Axonal swellings on the other hand are also found in HSP patients *post mortem* (Kasher et al. 2009). To analyze axonal swellings in iPSC-derived HSP neurons *in vitro*, axons had to be specifically visualized. For this, TAU1, an antibody detecting only axonal TAU, was used, as it is more specific than the commonly used acetylated tubulin, which is found in all stabilized neurites. To induce axonal TAU1 expression early on, low doses of Taxol were used, which stabilizes β-tubulin and thus accelerates axon formation (Amos and Löwe 1999; Witte et al. 2008). In the

SPG4 disease model presented here, axonal swellings, an authentic HSP phenotype can be seen after five days *in vitro.* In two other previously published iPSC disease models, swellings could also be detected, however only acetylated tubulin positive swellings, which emerged at a late time point after several weeks in culture (Denton et al. 2014; Havlicek et al. 2014). The emergence of axonal swellings is most likely due to the missing microtubule severing caused by spastin haploinsufficiency, which might lead to an abundance of disorganized microtubule. These disorganized microtubule in swellings were previously demonstrated using electron microscopy (Havlicek et al. 2014).

Interestingly, the data presented here shows that the neurons from patient HSP22f exhibited slightly less swellings compared to neurons from other patients, even though this patient has the earliest age of onset. This *in vitro* finding might be explained by higher culture densities in the swelling assay, which were caused by an increased proliferation rate of HSP22f neuronal progenitors. Another explanation could be the contribution of other cell types present *in vivo*, which might contribute to a more severe phenotype in the patient.

The combination of all three phenotypes builds a strong disease model suitable for the identification of therapeutic substances. The *in vitro* phenotypes observed here aim at several possible disease mechanisms, i.e. stabilized and disorganized microtubule, an overly stabilized actin skeleton, lack of BMP inhibition or a lipid imbalance due to dysregulation at the smooth ER.

4.5 Subtype specificity of described phenotypes

The protein spastin is ubiquitously expressed, but the patient phenotype is caused by degeneration of a very distinct set of neurons, i.e. cortical deep layer projection neurons. This points towards a subtype specificity regarding phenotype development in neurons. To test whether this is also the case *in vitro* and whether the neurotransmitter subtype has an influence, we generated a distinctly different but related neuronal population to analyze disease related phenotypes. Inhibitory forebrain neurons were generated by slightly alternating the differentiation protocol, in particularly by shortening the proliferation phase. These GABAergic neurons expressed the forebrain marker FOXG1 and the marker CTIP2 but not the layer VI marker TBR1 and were electrophysiological active after three months of maturation on astrocytes. The combination of CTIP2, FOXG1 and GABA expression *in vivo* is found in interneurons of the cortex and the striatum, which is adjacent to the cortex during development (Arlotta et al. 2008; Ma et al. 2013). The expression of other striatal markers like *DLX1* and *DLX2* points towards a striatal localization of these GABAergic forebrain neurons. This neuronal population is distinctly different due to GABAergic neurotransmitter expression, but has an overlapping marker profile, which is optimal to proof cell-type specificity of the observed phenotypes. Thus, this population is a useful tool to investigate whether cortical deep layer projection neurons are the only cell type affected by the lack of spastin or if this population is just most severely affected.

Since the GABAergic neurons were post-mitotic weeks before the glutamatergic neurons during differentiation, GABAergic neurons on day 37 were comparable in age to glutamatergic neurons on day 57. Interestingly, GABAergic patient neurons did not show shorter neurites, enlarged growth cones or swellings in the established assays. Thus, the observed phenotypes are specific to glutamatergic cortical neurons, which is in line with a predominant degeneration of corticospinal neurons in SPG4 patients.

One hypothesis of SPG4 disease development is that only the longest axons are affected, e.g. corticospinal neurons. In our neurite assay, the neurite length of control glutamatergic and GABAergic neurons after 24 hours was comparable. The GABAergic SPG4 neurites were able to grow more than 60µm within 24 hours, whereas the glutamatergic SPG4 neurons only achieved 30µm compared to 60µm in controls. GABAergic neurites of one patient grew even significantly longer compared to one control. And GABAergic SPG4 neurites were even longer than glutamatergic control neurites.

In GABAergic neurons, the growth cone area did not differ between SPG4 and control growth cones. The area of GABAergic growth cones was intermediate between the area of control and patient glutamatergic growth cones. Thus, the importance of axon length alone does not explain the reduced outgrowth.

Surprisingly, Taxol treatment of GABAergic cultures was not able to induce TAU1 positive axons. Interestingly, so far axon induction with Taxol has only been reported for glutamatergic neurons of either cortical or hippocampal origin (Witte, Neukirchen, and Bradke 2008). This indicates fundamental differences in TAU sorting and axon generation between glutamatergic and GABAergic neurons. Since the quantification of swellings in TAU1 positive axons of GABAergic neurons was not possible at a time point where glutamatergic neurons were analyzed, alternative markers for stabilized neurites were used to quantify swellings, such as TAU and acetylated microtubule. In these structures there was no difference between patient and control cultures in the overall swelling frequency. Comparing glutamatergic and GABAergic control cultures, the amount of TAU-positive swellings in control neurites was with 0.2/mm much higher in GABAergic neurons in contrast to glutamatergic control neurons, which had a swelling frequency of 0.07/mm TAU1-positive axon.

One explanation of the selectivity of the observed phenotypes to glutamatergic cortical neurons, might be the total level of *SPAST* expression in these neuronal subtypes. We found increased levels of M1 *SPAST* in GABAergic SPG4 cultures, comparable to levels found in glutamatergic control cultures. This dosage phenomenon might explain the absence of a phenotype in GABAergic patient cultures and points toward a critical role of M1 spastin in SPG4 pathology.

4.6 Assay automation for compound screening

With this SPG4 iPSC disease model at hand, it is now possible to test compounds on authentic patient neurons. To establish a successful high-throughput screening, fast, reliable phenotypes, with a good separation between control and patient population, a small experimental variability and a fast, automated analysis are needed. Multiparametric assays, with more than one phenotype, are especially useful to elucidate complex diseases where multiple pathways could be involved. These multiparametric assays increase the chance of discovering disease relevant molecules.

The three very early phenotypes presented here, are a good start and could represent the basis of an even larger multiparametric screening platform. Due to the single cell density of the cultures during the neurite outgrowth and growth cone assay, these assays were especially amenable to automation. Immunocytochemical stainings can be performed on multiwell plates followed by (semi-) automated image acquisition and analysis. Furthermore, due to the short timeframe of just twenty-four hours a large number of molecules can be tested within a short amount of time. Even though the swellings themselves could not be analyzed automatically, the overall axon length, which was used for normalization was detected automatically.

Before switching the neurite outgrowth assay and the growth cone assay to an automated setup, both assays displayed little experimental variability and good separation between populations, which calculated to a z-factors above 0.5, qualifying them for high-throughput screening. During the screening process however, the assays showed a relatively high experimental variability, which led to a z-factor below 0.5. This is probably due to manual handling of 96-well plates and should be avoidable with a robotic handling system. Nevertheless, the assays showed a good separation between populations and were therefore suitable for screening of selected small molecules.

4.7 Identification of hit compounds rescuing SPG4 pathophenotypes

Different cellular mechanisms have been proposed to be associated with HSP pathology. Thus, small molecules were tested that modulate potentially HSP-associated disease pathways or that have been shown to act against neurodegeneration in general.

Within the substance class of microtubule modulation, Taxol was chosen as prominent microtubule stabilizer and Vinblastine and Noscapine as microtubule destabilizers, since they have been shown to counteract HSP phenotypes such as swellings and reduced peroxisome velocity (Denton et al. 2014; Fan et al. 2014). Taxol was only tested in the neurite assay and the growth cone assay and not tested as treatment against axonal swellings, since it was used for induction of TAU1 and therefore enabled the formation of swellings. Taxol did lead to a significant reduction of growth cone area in SPG4 neurons but had no significant effect on neurite outgrowth.

Vinblastine in comparison, significantly reduced axonal swellings, but had a toxic effect on control neurites in the neurite outgrowth assay.

For actin modulation, Jasplakinolide acts as a stabilizer, whereas Cytochalasin B and Latrunculin B destabilize actin. Furthermore Latrunculin B has been reported to increase neurite outgrowth in mouse neurons (Bradke et al. 1999). Jasplakinolide reduced the growth cone area of SPG4 neurons, but did not have an effect on neurite outgrowth, whereas Latrunculin B had a positive effect on both, neurite outgrowth and growth cone area. This leaves Latrunculin B as a promising drug candidate, which should be tested further in the axonal swelling assay.

Data obtained in HeLa cells suggested that spastin acts as BMP inhibitor, however this finding has not yet been confirmed. Nevertheless, treatment with the BMP inhibitors DMH1 and Dorsomorphin led to a decrease in growth cone area and a reduction of axonal swellings in SPG4 neurons but were not able to rescue the neurite outgrowth phenotype. It would be interesting to follow up on role of spastin as a BMP inhibitor in human neurons, even though, the disease manifestation is probably not caused by missing BMP inhibition alone.

The small molecule GW3965, the only molecule tested that rescued all three phenotypes, is a liver X receptor (LXR) agonist and regulates lipid homeostasis. Two LXR receptors are known, LXR-alpha and LXR-beta, of which LXR-alpha is restricted to tissues rich in lipid metabolism, like the liver (Lu et al. 2001; Collins et al. 2002), whereas LXR-beta is expressed ubiquitary and thus also in the brain. GW3965 is especially suitable as drug candidate, since it has a higher affinity to the ubiquitously LXR-beta compared to the LXR-alpha. The function of LXRs includes the regulation of reverse cholesterol transport, which leads to a raise in HDL cholesterol levels. However, LXR agonists can also cause increased hepatic triglyceride synthesis, hypertriglyceridemia, and hepatic steatosis in by the stimulation of lipogenesis the liver. Due to its selectivity of the LXR-beta however, GW3965 is a very weak LXR activator in human hepatoma and only induces minor lipogenesis (Miao et al. 2004). In cells, activation of LXR leads to upregulation of pathways involved in cholesterol synthesis, and to an even higher extend to cholesterol efflux out of the cells (Hong et al. 2014). Thus, LXR activation might be required to drain excess sterols and lipids from the central nervous system to prevent an overload.

The identification of GW3965 as small molecule, that rescues all three phenotypes, may point towards a central role of cholesterol metabolism in SPG4. This is remarkable, since Hydroxycholesterol-27 accumulates in SPG5, a related disease, which is a phenocopy of SPG4, and causes neurotoxicity of corticospinal neurons. The accumulation of Hydroxycholesterol-27 in SPG5 is caused by mutations in CYP7B1 and is predominantly found in the cerebrospinal fluid (Schüle et al. 2010). Hydroxycholesterol-27 itself, is a weak LXR agonist and only its derivate, 24-Hydroxycholesterol can be transported over the blood brain barrier for clearing (Wójcicka et al. 2007). Within the brain, the spinal cord seems to be a specialized compartment regarding cholesterol homeostasis. Only in the spinal cord, a different cholesterol excretion pathways

besides 24-Hydroxycholesterol plays a role, which functions through the ABC binding cassettes G5 and G8, located at various cellular membranes (Yu et al. 2003). Possibly, spastin's roles in lipid droplet formation and endosomal transport interfere with an efficient cholesterol regulation in the spinal cord, based on this pathway.

Several lines of evidence suggest an important role for cholesterol homeostasis in the cortex and the spinal cord. First of all, it has been reported that the spinal cord exhibits a higher cholesterol concentration compared to residual CNS. Secondly, mice with inactivated LXR-beta exhibit lipid accumulation in the spinal cord accompanied by motor neuron degeneration, mimicking ALS (Andersson et al. 2005). Moreover, it has been shown, that cortical neurons have less cholesterol and also tolerate only low levels of cholesterol fluctuation. Higher or lower cholesterol levels lead to decreased neurite outgrowth in mouse cortical neurons. This effect is specific to cortical neurons and was not found to be true for hippocampal neurons (Ko et al. 2005). Furthermore, growth cones also represent a specialized compartment and are sensitive to cholesterol concentrations, they contain less cholesterol than the normal plasma membrane (Sbaschnig-Agler et al. 1988). Mechanistically, in SPG4 patients, accumulation of cholesterol derivatives in the spinal cord could damage the axons of the particularly sensitive corticospinal neurons, leading to retrograde degeneration.

4.8 Outlook

During this thesis, a very promising drug candidate for the treatment of SPG4 has been identified. The liver X receptor agonist GW3965 represents a suitable lead substance for further drug testing and can be used as basis for a more detailed evaluation of the molecular mechanism of SPG4.

To be certain of the specificity of GW3965, different other LXR agonists should be tested. The LXR agonist BMS-779788 would be a good candidate, since it has already completed a phase I clinical trial for safety evaluation for the treatment of atherosclerosis (Hong and Tontonoz 2014). To exclude another mode of action of GW3965 besides LXR activation, the effect of a LXR antagonist, e.g. Geranylgeranylpyrophosphate (GGPP) on neurite outgrowth, growth cone area, axonal swellings of healthy control neurons could be investigated (Wójcicka et al. 2007). In case of specificity of the inhibitors, a mimic of SPG4 phenotypes in control neurons would be expected. One possibility of an alternative mode of actin for GW3965, besides lipid homeostasis and cholesterol metabolism, is an upregulation of spastin upon GW3965 treatment, which is worth investigating. However, a mechanism involving upregulation of cholesterol synthesis and efflux acting on SPG4 disease formation is more probable. To illuminate the connection between spastin haploinsufficiency, lipid homeostasis and cholesterol metabolism, lipidomics analysis in neuronal control and patient cultures with and without GW3965 treatment should be performed.

Furthermore, additional cellular mechanisms, like endosomal trafficking in which spastin is involved should be evaluated. Especially, since vesicle trafficking might be a common pathway connecting motor neuron diseases like ALS, SMA and HSP (Ikenaka et al. 2012). ALS2 is caused

by mutations in the protein alsin, which controls endosomal dynamics (Otomo et al. 2003), whereas mutations in the synaptobrevin-associated membrane protein B (VAPB), which plays a role in ER to Golgi trafficking lead to ALS8 or SMA (Nishimura et al. 2004). ALS17 however, is caused by mutations in CHMP2B, a component of the vesicular trafficking complex ESCRTIII, which also interacts with spastin (Reid et al. 2005; Parkinson et al. 2006; Cox et al. 2010).

To further improve the screening assays, like the neurite assay, it would be beneficial to include more parameters. Quantification of the number of neurite branches is one option, since spastin is reported to have an impact on branching (Riano et al. 2009). An upscaling from 96-well to 384-well format would further increase the throughput. Furthermore, to lower the experimental variability, a liquid handling system should be employed. To become completely independent of the neural differentiation timeline, freezing of neurons that are readily available for screening should be optimized to prevent clumping and enable single cell analysis.

In this study, three unrelated, healthy controls and three patients were used for compound screening. This has the advantage of testing the effect of drugs on six different genetic backgrounds. However, constantly using 12 cell lines including two clones of each individual, is not compatible with a high-throughput approach. To advance the setup further, isogenic controls are needed. Due to new developments, these can be generated by using the clustered regularly interspaced short palindromic repeats (CRISPR)-Cas9 technology, which consists of two components, the guide RNA (gRNA) and the CRISPR-associated endonuclease Cas9. The gRNA guides the Cas9 endonuclease to a specific genomic target and enables a double strand break (Jinek et al. 2012). This technology can be used to efficiently knock-out genes in human pluripotent stem cells or to correct diseased cells via homologous recombination (Cong et al. 2013; Mali et al. 2013). To avoid off-target effects, a Cas9 nickase can be used instead of a Cas9 endonuclease (Ran et al. 2014). Generating knock-outs in control cell lines is easier than repairing a mutation, however, the influence of the genomic background on disease formation would be unpredictable. Thus, a repair of the disease mutation would be preferable, especially in this case, where the disease is caused by a point mutation, which can be more easily repaired than larger mutations. However, two or more isogenic pairs are optimal, to control for differences in the genetic background (Musunuru 2013). Due to time limitations, the generation of isogenic controls could not be realized in this thesis but should be performed to develop the screening further. Nevertheless, the SPG4 disease model and the fast phenotypic assays, proved to be applicable for drug screening and the identification of a lead substance.

5 REFERENCES

Aasen, Trond, Angel Raya, Maria J Barrero, Elena Garreta, Antonella Consiglio, Federico Gonzalez, Rita Vassena, et al. 2008. “Efficient and Rapid Generation of Induced Pluripotent Stem Cells from Human Keratinocytes.” *Nature Biotechnology* 26 (11). Nature Publishing Group: 1276–84. doi:10.1038/nbt.1503.

Abrahamsen, Greger, Yongjun Fan, Nicholas Matigian, Gautam Wali, Bernadette Bellette, Ratneswary Sutharsan, Jyothy Raju, et al. 2013. “A Patient-Derived Stem Cell Model of Hereditary Spastic Paraplegia with SPAST Mutations.” *Disease Models & Mechanisms* 6 (2): 489–502. doi:10.1242/dmm.010884.

Abyzov, Alexej, Jessica Mariani, Dean Palejev, Ying Zhang, Michael Seamus Haney, Livia Tomasini, Anthony F Ferrandino, et al. 2012. “Somatic Copy Number Mosaicism in Human Skin Revealed by Induced Pluripotent Stem Cells.” *Nature* 492 (7429). Nature Publishing Group: 438–42. doi:10.1038/nature11629.

Aevermann, Brian, Jamison McCorrison, Pratap Venepally, Rebecca Hodge, Trygve Bakken, Jeremy Miller, Mark Novotny, et al. 2017. “Production of a Preliminary Quality Control Pipeline for Single Nuclei RNA- Seq and Its Application in the Analysis of Cell Type Diversity of Post-Mortem Human Brain Neocortex.” *Pacific Symposium on Biocomputing. Pacific Symposium on Biocomputing* 22. NIH Public Access: 564–75. doi:10.1142/9789813207813_0052.

Allison, Rachel, Jennifer H Lumb, Coralie Fassier, James W Connell, Daniel Ten Martin, Matthew N J Seaman, Jamilé Hazan, and Evan Reid. 2013. “An ESCRT-Spastin Interaction Promotes Fission of Recycling Tubules from the Endosome.” *The Journal of Cell Biology* 202 (3): 527–43. doi:10.1083/jcb.201211045.

Amos, Linda A., and Jan Löwe. 1999. “How Taxol® Stabilises Microtubule Structure.” *Chemistry and Biology*. doi:10.1016/S1074-5521(99)89002-4.

Andersson, Sandra, Nina Gustafsson, Margaret Warner, and Jan-Ake Gustafsson. 2005. “Inactivation of Liver X Receptor Beta Leads to Adult-Onset Motor Neuron Degeneration in Male Mice.” *Proceedings of the National Academy of Sciences of the United States of America* 102 (10): 3857–62. doi:10.1073/pnas.0500634102.

Andrews, P W, G Banting, I Damjanov, D Arnaud, and P Avner. 1984. “Three Monoclonal Antibodies Defining Distinct Differentiation Antigens Associated with Different High Molecular Weight Polypeptides on the Surface of Human Embryonal Carcinoma Cells.” *Hybridoma* 3 (4): 347–61. http://www.ncbi.nlm.nih.gov/pubmed/6396197.

Arlotta, Paola, Bradley J. Molyneaux, Denis Jabaudon, Yutaka Yoshida, and Jeffrey D. Macklis. 2008. “Ctip2 Controls the Differentiation of Medium Spiny Neurons and the Establishment of the Cellular Architecture of the Striatum.” *Journal of Neuroscience* 28 (3): 622–32. doi:10.1523/JNEUROSCI.2986-07.2008.

Bakowska, Joanna C, Henri Jupille, Parvin Fatheddin, Rosa Puertollano, and Craig Blackstone. 2007. “Troyer Syndrome Protein Spartin Is Mono-Ubiquitinated and Functions in EGF Receptor Trafficking.” *Molecular Biology of the Cell* 18 (5): 1683–92. doi:10.1091/mbc.E06-09-0833.

Ban, Hiroshi, Naoki Nishishita, Noemi Fusaki, Toshiaki Tabata, Koichi Saeki, Masayuki Shikamura, Nozomi Takada, et al. 2011. “Efficient Generation of Transgene-Free Human Induced Pluripotent Stem Cells (IPSCs) by Temperature-Sensitive Sendai Virus Vectors.” *Proceedings of the National Academy of Sciences of the United States of America* 108 (34). National Academy of Sciences: 14234–39. doi:10.1073/pnas.1103509108.

Baxter, Sally L, Denise E Allard, Christopher Crowl, and Nina Tang Sherwood. 2014. “Cold Temperature Improves Mobility and Survival in Drosophila Models of Autosomal-Dominant Hereditary Spastic Paraplegia (AD-HSP).” *Disease Models & Mechanisms* 7 (8): 1005–12. doi:10.1242/dmm.013987.

Bear, Mark F., Barry W. Connors, and Michael A. Paradiso. 2007. *Neuroscience Exploring the Brain*. 3rd ed.

Beers, Jeanette, Daniel R Gulbranson, Nicole George, Lauren I Siniscalchi, Jeffrey Jones, James a

Thomson, and Guokai Chen. 2012. “Passaging and Colony Expansion of Human Pluripotent Stem Cells by Enzyme-Free Dissociation in Chemically Defined Culture Conditions.” *Nature Protocols* 7 (11): 2029–40. doi:10.1038/nprot.2012.130.

Bickmore, Wendy A. 2001. “Karyotype Analysis and Chromosome Banding.” http://onlinelibrary.wiley.com/doi/10.1038/npg.els.0001160/abstract.

Blackstone, Craig. 2012. “Cellular Pathways of Hereditary Spastic Paraplegia.” *Annual Review of Neuroscience* 35 (March): 25–47. doi:10.1146/annurev-neuro-062111-150400.

Blackstone. 2018. “Hereditary Spastic Paraplegia.” In *Handbook of Clinical Neurology*, 148:633–52. doi:10.1016/B978-0-444-64076-5.00041-7.

Bock, Christoph, Evangelos Kiskinis, Griet Verstappen, Hongcang Gu, Gabriella Boulting, Zachary D Smith, Michael Ziller, et al. 2011. “Reference Maps of Human ES and IPS Cell Variation Enable High-Throughput Characterization of Pluripotent Cell Lines.” *Cell* 144 (3): 439–52. doi:10.1016/j.cell.2010.12.032.

Bond, Allison M, Oneil G Bhalala, and John a Kessler. 2012. “The Dynamic Role of Bone Morphogenetic Proteins in Neural Stem Cell Fate and Maturation.” *Developmental Neurobiology* 72 (7): 1068–84. doi:10.1002/dneu.22022.

Bordet, Thierry, Patrick Berna, Jean-Louis Abitbol, and Rebecca M. Pruss. 2010. “Olesoxime (TRO19622): A Novel Mitochondrial-Targeted Neuroprotective Compound.” *Pharmaceuticals* 3 (2): 345–68. doi:10.3390/ph3020345.

Borghese, Lodovica, Dasa Dolezalova, Thoralf Opitz, Simone Haupt, Anke Leinhaas, Barbara Steinfarz, Philipp Koch, Frank Edenhofer, Ales Hampl, and Oliver Brüstle. 2010. “Inhibition of Notch Signaling in Human Embryonic Stem Cell-Derived Neural Stem Cells Delays G1/S Phase Transition and Accelerates Neuronal Differentiation in Vitro and in Vivo.” *Stem Cells* 28 (5): 955–64. doi:10.1002/stem.408.

Boukhris, Amir, Rebecca Schule, José L Loureiro, Charles Marques Lourenço, Emeline Mundwiller, Michael A Gonzalez, Perrine Charles, et al. 2013. “Alteration of Ganglioside Biosynthesis Responsible for Complex Hereditary Spastic Paraplegia.” *American Journal of Human Genetics* 93 (1). Elsevier: 118–23. doi:10.1016/j.ajhg.2013.05.006.

Boyer, Laurie A, Tong Ihn Lee, Megan F Cole, Sarah E Johnstone, Stuart S Levine, Jacob P Zucker, Matthew G Guenther, et al. 2005. “Core Transcriptional Regulatory Circuitry in Human Embryonic Stem Cells.” *Cell* 122 (6): 947–56. doi:10.1016/j.cell.2005.08.020.

Bradke, F., and C. Dotti. 1999. “The Role of Local Actin Instability in Axon Formation.” *Science* 283 (5409): 1931–34. doi:10.1126/science.283.5409.1931.

Bray, Mark-anthony, and Anne E. Carpenter. 2013. “Advanced Assay Development Guidelines for Image-Based High Content Screening and Analysis Assay Guidance Manual.” *Assay Guidance Manual*.

Briscoe, James, and Bennett G Novitch. 2008. “Regulatory Pathways Linking Progenitor Patterning, Cell Fates and Neurogenesis in the Ventral Neural Tube.” *Philosophical Transactions of the Royal Society B: Biological Sciences* 363 (1489): 57–70. doi:10.1098/rstb.2006.2012.

Burke, Robert E., and Karen O’Malley. 2013. “Axon Degeneration in Parkinson’s Disease.” *Experimental Neurology* 246 (August): 72–83. doi:10.1016/j.expneurol.2012.01.011.

Butler, Richard, Jonathan D Wood, Jennifer a Landers, and Vincent T Cunliffe. 2010. “Genetic and Chemical Modulation of Spastin-Dependent Axon Outgrowth in Zebrafish Embryos Indicates a Role for Impaired Microtubule Dynamics in Hereditary Spastic Paraplegia.” *Disease Models & Mechanisms* 3 (11–12): 743–51. doi:10.1242/dmm.004002.

Casari, G, M De Fusco, S Ciarmatori, M Zeviani, M Mora, P Fernandez, G De Michele, et al. 1998. “Spastic Paraplegia and OXPHOS Impairment Caused by Mutations in Paraplegin, a Nuclear-Encoded Mitochondrial Metalloprotease.” *Cell* 93 (6): 973–83.

Chambers, Stuart M, Christopher a Fasano, Eirini P Papapetrou, Mark Tomishima, Michel Sadelain, and Lorenz Studer. 2009. “Highly Efficient Neural Conversion of Human ES and IPS Cells by Dual Inhibition of SMAD Signaling.” *Nature Biotechnology* 27 (3): 275–80. doi:10.1038/nbt.1529.

Chan, Elayne M, Sutheera Ratanasirintrawoot, In-Hyun Park, Philip D Manos, Yuin-Han Loh, Hongguang

REFERENCES

Huo, Justine D Miller, et al. 2009. “Live Cell Imaging Distinguishes Bona Fide Human IPS Cells from Partially Reprogrammed Cells.” *Nature Biotechnology* 27 (11): 1033–37. doi:10.1038/nbt.1580.

Chang, Jaerak, Seongju Lee, and Craig Blackstone. 2014. “Spastic Paraplegia Proteins Spastizin and Spatacsin Mediate Autophagic Lysosome Reformation.” *The Journal of Clinical Investigation* 124 (12): 5249–62. doi:10.1172/JCI77598.

Chen, Guokai, Daniel R Gulbranson, Zhonggang Hou, Jennifer M Bolin, Victor Ruotti, Mitchell D Probasco, Kimberly Smuga-Otto, et al. 2011. “Chemically Defined Conditions for Human IPSC Derivation and Culture.” *Nature Methods* 8 (5): 424–29. doi:10.1038/nmeth.1593.

Cheng, Oumei, Robert P Ostrowski, Wenwu Liu, and John H Zhang. 2010. “Activation of Liver X Receptor Reduces Global Ischemia Brain Injury by Reduction of Nuclear Factor-KB.” *Neuroscience* 166 (4): 1101–9. doi:10.1016/j.neuroscience.2010.01.024.Activation.

Ciccarelli, Francesca D, Christos Proukakis, Heema Patel, Harold Cross, Shakil Azam, Michael A Patton, Peer Bork, and Andrew H Crosby. 2003. “The Identification of a Conserved Domain in Both Spartin and Spastin, Mutated in Hereditary Spastic Paraplegia.” *Genomics* 81 (4): 437–41. doi:10.1016/S0888-7543(03)00011-9.

Claudiani, Pamela, Elena Riano, Alessia Errico, Gennaro Andolfi, and Elena I. Rugarli. 2005. “Spastin Subcellular Localization Is Regulated through Usage of Different Translation Start Sites and Active Export from the Nucleus.” *Experimental Cell Research* 309 (2): 358–69. doi:10.1016/j.yexcr.2005.06.009.

Cong, L., F. A. Ran, D. Cox, S. Lin, R. Barretto, N. Habib, P. D. Hsu, et al. 2013. “Multiplex Genome Engineering Using CRISPR/Cas Systems.” *Science* 339 (6121): 819–23. doi:10.1126/science.1231143.

Connell, James W., Catherine Lindon, J. Paul Luzio, and Evan Reid. 2009. “Spastin Couples Microtubule Severing to Membrane Traffic in Completion of Cytokinesis and Secretion.” *Traffic* 10 (1): 42–56. doi:10.1111/j.1600-0854.2008.00847.x.

Corcoran, Lisa J, Timothy J Mitchison, and Qing Liu. 2004. “A Novel Action of Histone Deacetylase Inhibitors in a Protein Aggresome Disease Model.” *Current Biology* 14 (6): 488–92. doi:10.1016/j.

Cox, Laura E., Laura Ferraiuolo, Emily F. Goodall, Paul R. Heath, Adrian Higginbottom, Heather Mortiboys, Hannah C. Hollinger, et al. 2010. “Mutations in CHMP2B in Lower Motor Neuron Predominant Amyotrophic Lateral Sclerosis (ALS).” Edited by Mark R. Cookson. *PLoS ONE* 5 (3): e9872. doi:10.1371/journal.pone.0009872.

Cui, Xu, Michael Chopp, Alex Zacharek, Yisheng Cui, Cynthia Roberts, and Jieli Chen. 2013. “The Neurorestorative Benefit of GW3965 Treatment of Stroke in Mice.” *Stroke* 44 (1): 153–61. doi:10.1016/j.surg.2006.10.010.Use.

Cuny, Gregory D, Paul B Yu, Joydev K Laha, Xuechao Xing, Ji-Feng Liu, Carol S Lai, Donna Y Deng, Chetana Sachidanandan, Kenneth D Bloch, and Randall T Peterson. 2008. “Structure-Activity Relationship Study of Bone Morphogenetic Protein (BMP) Signaling Inhibitors.” *Bioorganic & Medicinal Chemistry Letters* 18 (15). NIH Public Access: 4388–92. doi:10.1016/j.bmcl.2008.06.052.

Darmanis, Spyros, Steven A. Sloan, Ye Zhang, Martin Enge, Christine Caneda, Lawrence M. Shuer, Melanie G. Hayden Gephart, Ben A. Barres, and Stephen R. Quake. 2015. “A Survey of Human Brain Transcriptome Diversity at the Single Cell Level.” *Proceedings of the National Academy of Sciences* 112 (23): 7285–90. doi:10.1073/pnas.1507125112.

Darr, Henia, and Nissim Benvenisty. 2006. “Human Embryonic Stem Cells: The Battle between Self-Renewal and Differentiation.” *Regenerative Medicine* 1 (3): 317–25. doi:10.2217/17460751.1.3.317.

De Los Angeles, Alejandro, Francesco Ferrari, Ruibin Xi, Yuko Fujiwara, Nissim Benvenisty, Hongkui Deng, Konrad Hochedlinger, et al. 2015. “Hallmarks of Pluripotency.” *Nature* 525 (7570). Nature Research: 469–78. doi:10.1038/nature15515.

Denton, KR, L Lei, J Grenier, Vladimir Rodionov, Craig Blackstone, and Xue-Jun Li. 2014. “Loss of Spastin Function Results in Disease-Specific Axonal Defects in Human Pluripotent Stem Cell-Based Models of Hereditary Spastic Paraplegia.” *Stem Cells* 32 (2): 414–23.

Denton, Kyle R., Ling Lei, Jeremy Grenier, Vladimir Rodionov, Craig Blackstone, and Xue-Jun Jun Li. 2014. “Loss of Spastin Function Results in Disease-Specific Axonal Defects in Human Pluripotent Stem

Cell-Based Models of Hereditary Spastic Paraplegia." *Stem Cells (Dayton, Ohio)* 32 (2): 414–23. doi:10.1002/stem.1569.

Dick, Katherine J, Matthias Eckhardt, Coro Paisán-Ruiz, Aisha Alkhayat Alshehhi, Christos Proukakis, Naomi A Sibtain, Helena Maier, et al. 2010. "Mutation of FA2H Underlies a Complicated Form of Hereditary Spastic Paraplegia (SPG35)." *Human Mutation* 31 (4): E1251-60. doi:10.1002/humu.21205.

Donkin, James J., Sophie Stukas, Veronica Hirsch-Reinshagen, Dhananjay Namjoshi, Anna Wilkinson, Sharon May, Jeniffer Chan, Jianjia Fan, Jon Collins, and Cheryl L. Wellington. 2010. "ATP-Binding Cassette Transporter A1 Mediates the Beneficial Effects of the Liver X Receptor Agonist GW3965 on Object Recognition Memory and Amyloid Burden in Amyloid Precursor Protein/Presenilin 1 Mice." *Journal of Biological Chemistry* 285 (44): 34144–54. doi:10.1074/jbc.M110.108100.

Du, Fang, Emily F Ozdowski, Ingrid K Kotowski, Douglas a Marchuk, and Nina Tang Sherwood. 2010. "Functional Conservation of Human Spastin in a Drosophila Model of Autosomal Dominant-Hereditary Spastic Paraplegia." *Human Molecular Genetics* 19 (10): 1883–96. doi:10.1093/hmg/ddq064.

Dürr, Alexandra, Chantal Tallaksen, and Christel Depienne. 2012. "Spastic Paraplegia 4." University of Washington, Seattle. http://www.ncbi.nlm.nih.gov/books/NBK1160/.

Eastman, Scott W., Mina Yassaee, and Paul D. Bieniasz. 2009. "A Role for Ubiquitin Ligases and Spartin/SPG20 in Lipid Droplet Turnover." *Journal of Cell Biology* 184 (6): 881–94. doi:10.1083/jcb.200808041.

Edwards, Thomas L, Virginia E Clowes, Hilda T H Tsang, James W Connell, Christopher M Sanderson, J Paul Luzio, and Evan Reid. 2009. "Endogenous Spartin (SPG20) Is Recruited to Endosomes and Lipid Droplets and Interacts with the Ubiquitin E3 Ligases AIP4 and AIP5." *The Biochemical Journal* 423 (1): 31–39. doi:10.1042/BJ20082398.

Elkabetz, Yechiel, Georgia Panagiotakos, George Al Shamy, Nicholas D. Socci, Viviane Tabar, and Lorenz Studer. 2008. "Human ES Cell-Derived Neural Rosettes Reveal a Functionally Distinct Early Neural Stem Cell Stage." *Genes & Development* 22 (2): 152–65. doi:10.1101/gad.1616208.

Erlich, Y., S. Edvardson, E. Hodges, S. Zenvirt, P. Thekkat, A. Shaag, T. Dor, G. J. Hannon, and O. Elpeleg. 2011. "Exome Sequencing and Disease-Network Analysis of a Single Family Implicate a Mutation in KIF1A in Hereditary Spastic Paraparesis." *Genome Research* 21 (5): 658–64. doi:10.1101/gr.117143.110.

Estrada-Cuzcano, Alejandro, Shaun Martin, Teodora Chamova, Matthis Synofzik, Dagmar Timmann, Tine Holemans, Albena Andreeva, et al. 2017. "Loss-of-Function Mutations in the *ATP13A2/* PARK9 Gene Cause Complicated Hereditary Spastic Paraplegia (SPG78)." *Brain* 140 (2). Oxford University Press: 287–305. doi:10.1093/brain/aww307.

Evans, Katia J., Edgar R. Gomes, Steven M. Reisenweber, Gregg G. Gundersen, and Brett P. Lauring. 2005. "Linking Axonal Degeneration to Microtubule Remodeling by Spastin-Mediated Microtubule Severing." *The Journal of Cell Biology* 168 (4): 599–606. doi:10.1083/jcb.200409058.

Evans, M J, and M H Kaufman. 1981. "Establishment in Culture of Pluripotential Cells from Mouse Embryos." *Nature* 292 (5819): 154–56.

Falk, Julia, Magdalena Rohde, Mohamed M Bekhite, Sophie Neugebauer, Peter Hemmerich, Michael Kiehntopf, Thomas Deufel, Christian A Hübner, and Christian Beetz. 2014. "Functional Mutation Analysis Provides Evidence for a Role of REEP1 in Lipid Droplet Biology." *Human Mutation* 35 (4): 497–504. doi:10.1002/humu.22521.

Fan, Yongjun, Gautam Wali, Ratneswary Sutharsan, Bernadette Bellette, Denis I Crane, Carolyn M Sue, and Alan Mackay-Sim. 2014. "Low Dose Tubulin-Binding Drugs Rescue Peroxisome Trafficking Deficit in Patient-Derived Stem Cells in Hereditary Spastic Paraplegia." *Biology Open* 3 (6): 1–9. doi:10.1242/bio.20147641.

Fassier, Coralie, Anne Tarrade, Leticia Peris, Sabrina Courageot, Philippe Mailly, Cécile Dalard, Stéphanie Delga, et al. 2013. "Microtubule-Targeting Drugs Rescue Axonal Swellings in Cortical Neurons from Spastin Knockout Mice." *Disease Models & Mechanisms* 6 (1): 72–83. doi:10.1242/dmm.008946.

Ferrari, R, D Kapogiannis, E D Huey, and P Momeni. 2011. "FTD and ALS: A Tale of Two Diseases." *Current Alzheimer Research* 8 (3). NIH Public Access: 273–94.

http://www.ncbi.nlm.nih.gov/pubmed/21222600.

Finsterer, Josef, Wolfgang Löscher, Stefan Quasthoff, Julia Wanschitz, Michaela Auer-Grumbach, and Giovanni Stevanin. 2012. "Hereditary Spastic Paraplegias with Autosomal Dominant, Recessive, X-Linked, or Maternal Trait of Inheritance." *Journal of the Neurological Sciences* 318 (1–2). Elsevier B.V.: 1–18. doi:10.1016/j.jns.2012.03.025.

Fischer-Hayes, Lindsey R., Terrell Brotherton, and Jonathan D. Glass. 2013. "Axonal Degeneration in the Peripheral Nervous System: Implications for the Pathogenesis of Amyotrophic Lateral Sclerosis." *Experimental Neurology* 246 (August): 6–13. doi:10.1016/j.expneurol.2013.05.001.

Freeman, Caroline, Matthew N J Seaman, and Evan Reid. 2013. "The Hereditary Spastic Paraplegia Protein Strumpellin: Characterisation in Neurons and of the Effect of Disease Mutations on WASH Complex Assembly and Function." *Biochimica et Biophysica Acta* 1832 (1): 160–73. doi:10.1016/j.bbadis.2012.10.011.

Fuerst, Julia C, Andreas W Henkel, Armin Stroebel, Oliver Welzel, Teja W Groemer, Johannes Kornhuber, and Dominikus Bönsch. 2011. "Distinct Intracellular Vesicle Transport Mechanisms Are Selectively Modified by Spastin and Spastin Mutations." *Journal of Cellular Physiology* 226 (2): 362–68. doi:10.1002/jcp.22341.

Fusaki, Noemi, Hiroshi Ban, Akiyo Nishiyama, Koichi Saeki, and Mamoru Hasegawa. 2009. "Efficient Induction of Transgene-Free Human Pluripotent Stem Cells Using a Vector Based on Sendai Virus, an RNA Virus That Does Not Integrate into the Host Genome." *Proceedings of the Japan Academy, Series B* 85 (8): 348–62. doi:10.2183/pjab.85.348.

Gonzalez, Sara, Terence Beghyn, Jieshuang Jia, Nadège Debreuck, Gonzague Berte, Kamel Mamchaoui, Vincent Mouly, et al. 2012. "Rescue of Nonsense Mutations by Amlexanox in Human Cells." *Orphanet Journal of Rare Diseases* 7 (1): 58. doi:10.1186/1750-1172-7-58.

Gornstein, Erica, and Thomas L. Schwarz. 2014. "The Paradox of Paclitaxel Neurotoxicity: Mechanisms and Unanswered Questions." *Neuropharmacology* 76. Elsevier: 175–83. doi:10.1016/j.neuropharm.2013.08.016.

Goyal, Uma, and Craig Blackstone. 2013. "Untangling the Web: Mechanisms Underlying ER Network Formation." *Biochimica et Biophysica Acta - Molecular Cell Research* 1833 (11). Elsevier B.V.: 2492–98. doi:10.1016/j.bbamcr.2013.04.009.

Guyton, Arthur C., and Hall John E. 2006. *Textbook of Medical Physiology*.

Haines, Jeffery D, Matilde Inglese, and Patrizia Casaccia. 2011. "Axonal Damage in Multiple Sclerosis." *The Mount Sinai Journal of Medicine, New York* 78 (2). NIH Public Access: 231–43. doi:10.1002/msj.20246.

Hanein, Sylvain, Elodie Martin, Amir Boukhris, Paula Byrne, Cyril Goizet, Abdelmadjid Hamri, Ali Benomar, et al. 2008. "Identification of the SPG15 Gene, Encoding Spastizin, as a Frequent Cause of Complicated Autosomal-Recessive Spastic Paraplegia, Including Kjellin Syndrome." *The American Journal of Human Genetics* 82 (4): 992–1002. doi:10.1016/j.ajhg.2008.03.004.

Hansen, Jens Jacob, Alexandra Dürr, Isabelle Cournu-Rebeix, Costa Georgopoulos, Debbie Ang, Marit Nyholm Nielsen, Claire-Sophie Davoine, et al. 2002. "Hereditary Spastic Paraplegia SPG13 Is Associated with a Mutation in the Gene Encoding the Mitochondrial Chaperonin Hsp60." *American Journal of Human Genetics* 70 (5): 1328–32. doi:10.1086/339935.

Hansen, David V. V., John L.R. L R Rubenstein, and Arnold R. R. Kriegstein. 2011. "Deriving Excitatory Neurons of the Neocortex from Pluripotent Stem Cells." *Neuron* 70 (4). Elsevier Inc.: 645–60. doi:10.1016/j.neuron.2011.05.006.

Hao, Jijun, Joshua N Ho, Jana a Lewis, Kaleh a Karim, R Nathan Daniels, Patrick R, Corey R Hopkins, Craig W Lindsley, and Charles C Hong. 2010. "In Vivo Structure Activity Relationship Study of Dorsomorphin Analogs Identifies Selective VEGF and BMP Inhibitors." *ACS Chemical Biology* 5 (2): 245–53. doi:10.1021/cb9002865.In.

Hashimoto, Yutaka, Michiko Shirane, Fumiko Matsuzaki, Shotaro Saita, Takafumi Ohnishi, and Keiichi I. Nakayama. 2014. "Protrudin Regulates Endoplasmic Reticulum Morphology and Function Associated with the Pathogenesis of Hereditary Spastic Paraplegia." *Journal of Biological Chemistry* 289 (19): 12946–61. doi:10.1074/jbc.M113.528687.

Havlicek, Steven, Zacharias Kohl, Himanshu K. Mishra, Iryna Prots, Esther Eberhardt, Naime Denguir, Holger Wend, et al. 2014. “Gene Dosage-Dependent Rescue of HSP Neurite Defects in SPG4 Patients’ Neurons.” *Human Molecular Genetics* 23 (10): 2527–41. doi:10.1093/hmg/ddt644.

Hazan, J, N Fonknechten, D Mavel, C Paternotte, D Samson, F Artiguenave, C S Davoine, et al. 1999. “Spastin, a New AAA Protein, Is Altered in the Most Frequent Form of Autosomal Dominant Spastic Paraplegia.” *Nature Genetics* 23 (3): 296–303. doi:10.1038/15472.

Heesen, Ludwig, Michael Peitz, Laura Torres-Benito, Irmgard Hölker, Kristina Hupperich, Kristina Dobrindt, Johannes Jungverdorben, et al. 2016. “Plastin 3 Is Upregulated in IPSC-Derived Motoneurons from Asymptomatic SMN1-Deleted Individuals.” *Cellular and Molecular Life Sciences* 73 (10): 2089–2104. doi:10.1007/s00018-015-2084-y.

Hegarty, Shane V., Louise M. Collins, Aisling M. Gavin, Sarah L. Roche, Sean L. Wyatt, Aideen M. Sullivan, and Gerard W. O’Keeffe. 2014. “Canonical BMP-Smad Signalling Promotes Neurite Growth in Rat Midbrain Dopaminergic Neurons.” *NeuroMolecular Medicine* 16 (2): 473–89. doi:10.1007/s12017-014-8299-5.

Heilker, Ralf, Stefanie Traub, Peter Reinhardt, Hans R. Schöler, and Jared Sterneckert. 2014. “IPS Cell Derived Neuronal Cells for Drug Discovery.” *Trends in Pharmacological Sciences* 35 (10). doi:10.1016/j.tips.2014.07.003.

Ho, Shinn-Ying, Chih-Yuan Chao, Hui-Ling Huang, Tzai-Wen Chiu, Phasit Charoenkwan, and Eric Hwang. 2011. “NeurphologyJ: An Automatic Neuronal Morphology Quantification Method and Its Application in Pharmacological Discovery.” *BMC Bioinformatics* 12 (1). BioMed Central Ltd: 230. doi:10.1186/1471-2105-12-230.

Holzinger, Andreas. 2009. “Jasplakinolide: An Actin-Specific Reagent That Promotes Actin Polymerization.” *Methods in Molecular Biology (Clifton, N.J.)* 586 (January): 71–87. doi:10.1007/978-1-60761-376-3_4.

Hong, Cynthia, and Peter Tontonoz. 2014. “Liver X Receptors in Lipid Metabolism: Opportunities for Drug Discovery.” *Nature Reviews. Drug Discovery* 13 (6). Nature Publishing Group: 433–44. doi:10.1038/nrd4280.

Hotta, Akitsu, and James Ellis. 2008. “Retroviral Vector Silencing During IPS Cell Induction: An Epigenetic Beacon That Signals Distinct Pluripotent States Akitsu.” *Journal of Cellular Biochemistry* 105 (4): 940–48. doi:10.1002/jcb21912.

Hoyle, J Chad, Michael C Isfort, Jennifer Roggenbuck, and W David Arnold. 2015. “The Genetics of Charcot-Marie-Tooth Disease: Current Trends and Future Implications for Diagnosis and Management.” *The Application of Clinical Genetics* 8. Dove Press: 235–43. doi:10.2147/TACG.S69969.

Hughes, JP P., S. S. Rees, SB B. Kalindjian, and K. L. KL Philpott. 2011. “Principles of Early Drug Discovery.” *British Journal of Pharmacology* 162 (6): 1239–49. doi:10.1111/j.1476-5381.2010.01127.x.

Hussein, Samer M., Nizar N. Batada, Sanna Vuoristo, Reagan W. Ching, Reija Autio, Elisa Närvä, Siemon Ng, et al. 2011. “Copy Number Variation and Selection during Reprogramming to Pluripotency.” *Nature* 471 (7336): 58–62. doi:10.1038/nature09871.

Ikenaka, Kensuke, Masahisa Katsuno, Kaori Kawai, Shinsuke Ishigaki, Fumiaki Tanaka, and Gen Sobue. 2012. “Disruption of Axonal Transport in Motor Neuron Diseases.” *Int. J. Mol. Sci. Int. J. Mol. Sci* 13: 1225–38. doi:10.3390/ijms13011225.

Ip, Bui Kar, Nadhim Bayatti, Nicholas J. Howard, Susan Lindsay, and Gavin J. Clowry. 2011. “The Corticofugal Neuron-Associated Genes ROBO1, SRGAP1, and CTIP2 Exhibit an Anterior to Posterior Gradient of Expression in Early Fetal Human Neocortex Development.” *Cerebral Cortex (New York, N.Y. : 1991)* 21 (6): 1395–1407. doi:10.1093/cercor/bhq219.

Jinek, Martin, Krzysztof Chylinski, Ines Fonfara, Michael Hauer, Jennifer A Doudna, and Emmanuelle Charpentier. 2012. “A Programmable Dual-RNA – Guided DNA Endonuclease in Adaptive Bacterial Immunity.” *Science* 337 (August): 816–22. doi:10.1126/science.1225829.

Johnson, M. Austin, Jason P. Weick, Robert A. Pearce, and Su-Chun Zhang. 2007. “Functional Neural Development from Human Embryonic Stem Cells: Accelerated Synaptic Activity via Astrocyte Coculture.” *Journal of Neuroscience* 27 (12).

REFERENCES

Johnson, B V, N Shindo, P D Rathjen, J Rathjen, and R A Keough. 2008. “Understanding Pluripotency--How Embryonic Stem Cells Keep Their Options Open.” *Molecular Human Reproduction* 14 (9): 513–20. doi:10.1093/molehr/gan048.

Jordan, Mary Ann, and Leslie Wilson. 2004. “Microtubules as a Target for Anticancer Drugs.” *Nat. Rev. Cancer* 4 (4): 253–65. doi:10.1038/nr1317.

Jouet, M, A Rosenthal, G Armstrong, J MacFarlane, R Stevenson, J Paterson, A Metzenberg, V Ionasescu, K Temple, and S Kenwrick. 1994. “X-Linked Spastic Paraplegia (SPG1), MASA Syndrome and X-Linked Hydrocephalus Result from Mutations in the L1 Gene.” *Nature Genetics* 7 (3): 402–7. doi:10.1038/ng0794-402.

Kanaan, Nicholas M., Gustavo F. Pigino, Scott T. Brady, Orly Lazarov, Lester I. Binder, and Gerardo A. Morfini. 2013. “Axonal Degeneration in Alzheimer’s Disease: When Signaling Abnormalities Meet the Axonal Transport System.” *Experimental Neurology* 246 (August): 44–53. doi:10.1016/j.expneurol.2012.06.003.

Kasher, Paul R, Kurt J De Vos, Stephen B Wharton, Catherine Manser, Ellen J Bennett, Megan Bingley, Jonathan D Wood, et al. 2009. “Direct Evidence for Axonal Transport Defects in a Novel Mouse Model of Mutant Spastin-Induced Hereditary Spastic Paraplegia (HSP) and Human HSP Patients.” *Journal of Neurochemistry* 110 (1): 34–44. doi:10.1111/j.1471-4159.2009.06104.x.

Kashyap, Vasundhra, Naira C Rezende, Kymora B Scotland, Sebastian M Shaffer, Jenny Liao Persson, Lorraine J Gudas, and Nigel P Mongan. 2009. “Regulation of Stem Cell Pluripotency and Differentiation Involves a Mutual Regulatory Circuit of the NANOG, OCT4, and SOX2 Pluripotency Transcription Factors with Polycomb Repressive Complexes and Stem Cell MicroRNAs.” *Stem Cells and Development* 18 (7): 1093–1108. doi:10.1089/scd.2009.0113.

Kelsom, Corey, and Wange Lu. 2013. “Development and Specification of GABAergic Cortical Interneurons.” *Cell & Bioscience* 3 (1). Cell & Bioscience: 19. doi:10.1186/2045-3701-3-19.

Kim, Dae-Sung, Jae Souk Lee, Joong Woo Leem, Yong Jun Huh, Ji Young Kim, Han-Soo Kim, In-Hyun Park, George Q Daley, Dong-Youn Hwang, and Dong-Wook Kim. 2010. “Robust Enhancement of Neural Differentiation from Human ES and IPS Cells Regardless of Their Innate Difference in Differentiation Propensity.” *Stem Cell Reviews* 6 (2): 270–81. doi:10.1007/s12015-010-9138-1.

Kleinsmith, L J, and G B Pierce. 1964. “Multipotentiality of Single Embryonal Carcinoma Cells.” *Cancer Research* 24 (October): 1544–51.

Kneynsberg, Andrew, Benjamin Combs, Kyle Christensen, Gerardo Morfini, and Nicholas M Kanaan. 2017. “Axonal Degeneration in Tauopathies: Disease Relevance and Underlying Mechanisms.” *Frontiers in Neuroscience* 11. Frontiers Media SA: 572. doi:10.3389/fnins.2017.00572.

Ko, Mihee, Kun Zou, Hirohisa Minagawa, Wenxin Yu, Jian-Sheng Gong, Katsuhiko Yanagisawa, and Makoto Michikawa. 2005. “Cholesterol-Mediated Neurite Outgrowth Is Differently Regulated between Cortical and Hippocampal Neurons.” *The Journal of Biological Chemistry* 280 (52): 42759–65. doi:10.1074/jbc.M509164200.

Korulu, Sirin, and Arzu Karabay. 2011. “IGF-1 Participates Differently in Regulation of Severing Activity of Katanin and Spastin.” *Cellular and Molecular Neurobiology* 31 (4): 497–501. doi:10.1007/s10571-011-9654-9.

Krajewski, K M, R A Lewis, D R Fuerst, C Turansky, S R Hinderer, J Garbern, J Kamholz, and M E Shy. 2000. “Neurological Dysfunction and Axonal Degeneration in Charcot-Marie-Tooth Disease Type 1A.” *Brain : A Journal of Neurology* 123 (Pt 7) (July): 1516–27. http://www.ncbi.nlm.nih.gov/pubmed/10869062.

Lacroix, Benjamin, Juliette van Dijk, Nicholas D. Gold, Julien Guizetti, Gudrun Aldrian-Herrada, Krzysztof Rogowski, Daniel W. Gerlich, and Carsten Janke. 2010. “Tubulin Polyglutamylation Stimulates Spastin-Mediated Microtubule Severing.” *The Journal of Cell Biology* 189 (6): 945–54. doi:10.1083/jcb.201001024.

Laurent, Louise C, Igor Ulitsky, Ileana Slavin, Ha Tran, Andrew Schork, Robert Morey, Candace Lynch, et al. 2011. “Dynamic Changes in the Copy Number of Pluripotency and Cell Proliferation Genes in Human ESCs and IPSCs during Reprogramming and Time in Culture.” *Cell Stem Cell* 8 (1). Elsevier: 106–18. doi:10.1016/j.stem.2010.12.003.

Lee, Hyojin, George Al Shamy, Yechiel Elkabetz, Claude M Schofield, Neil L Harrsion, Georgia Panagiotakos, Nicholas D Socci, Viviane Tabar, and Lorenz Studer. 2007. “Directed Differentiation and Transplantation of Human Embryonic Stem Cell-Derived Motoneurons.” *Stem Cells* 25 (8): 1931–39. doi:10.1634/stemcells.2007-0097.

Lei, Peng, Anton Baysa, Hilde Irene Nebb, Guro Valen, Tor Skomedal, Jan Bj??rn Osnes, Zaiqing Yang, and Fred Haugen. 2013. “Activation of Liver X Receptors in the Heart Leads to Accumulation of Intracellular Lipids and Attenuation of Ischemia-Reperfusion Injury.” *Basic Research in Cardiology* 108 (1). doi:10.1007/s00395-012-0323-z.

Leid, Mark, Jane E. Ishmael, Dorina Avram, David Shepherd, Valérie Fraulob, and Pascal Dollé. 2004. “CTIP1 and CTIP2 Are Differentially Expressed during Mouse Embryogenesis.” *Gene Expression Patterns* 4 (6): 733–39. doi:10.1016/j.modgep.2004.03.009.

Lin, Pengfei, Jianwei Li, Qiji Liu, Fei Mao, Jisheng Li, Rongfang Qiu, Huili Hu, et al. 2008. “A Missense Mutation in SLC33A1, Which Encodes the Acetyl-CoA Transporter, Causes Autosomal-Dominant Spastic Paraplegia (SPG42).” *American Journal of Human Genetics* 83 (6). Elsevier: 752–59. doi:10.1016/j.ajhg.2008.11.003.

Liu, Aimin, and Lee A. Niswander. 2005. “Bone Morphogenetic Protein Signalling and Vertebrate Nervous System Development.” *Nature Reviews. Neuroscience* 6 (12): 945–54. doi:10.1038/nrn1805.

Lo Giudice, Temistocle, Federica Lombardi, Filippo Maria Santorelli, Toshitaka Kawarai, and Antonio Orlacchio. 2014. “Hereditary Spastic Paraplegia: Clinical-Genetic Characteristics and Evolving Molecular Mechanisms.” *Experimental Neurology* 261 (November). Elsevier B.V.: 518–39. doi:10.1016/j.expneurol.2014.06.011.

Lodato, Simona, Bradley J Molyneaux, Emanuela Zuccaro, Loyal a Goff, Hsu-Hsin Chen, Wen Yuan, Alyssa Meleski, et al. 2014. “Gene Co-Regulation by Fezf2 Selects Neurotransmitter Identity and Connectivity of Corticospinal Neurons.” *Nature Neuroscience* 17 (8). Nature Publishing Group: 1046–54. doi:10.1038/nn.3757.

Ludwig, Tenneille E, Veit Bergendahl, Mark E Levenstein, Junying Yu, Mitchell D Probasco, and James a Thomson. 2006. “Feeder-Independent Culture of Human Embryonic Stem Cells.” *Nature Methods* 3 (8): 637–46. doi:10.1038/nmeth902.

Ludwig, Tenneille E, Mark E Levenstein, Jeffrey M Jones, W Travis Berggren, Erika R Mitchen, Jennifer L Frane, Leann J Crandall, et al. 2006. “Derivation of Human Embryonic Stem Cells in Defined Conditions.” *Nature Biotechnology* 24 (2): 185–87. doi:10.1038/nbt1177.

Lui, Jan H. H., David V. V. Hansen, and Arnold R. R. Kriegstein. 2011. “Development and Evolution of the Human Neocortex.” *Cell* 146 (1). Elsevier Inc.: 18–36. doi:10.1016/j.cell.2011.06.030.

Ma, Tong, Congmin Wang, Lei Wang, Xing Zhou, Miao Tian, Qiangqiang Zhang, Yue Zhang, et al. 2013. “Subcortical Origins of Human and Monkey Neocortical Interneurons.” *Nature Neuroscience* 16 (11). Nature Publishing Group: 1588–97. doi:10.1038/nn.3536.

MacLean-Fletcher, Susan, and Thomas D. Pollard. 1980. “Mechanism of Action of Cytochalasin B on Actin.” *Cell* 20 (0): 329–41. doi:10.1101/SQB.1973.037.01.069.

Maherali, Nimet, and Konrad Hochedlinger. 2008. “Guidelines and Techniques for the Generation of Induced Pluripotent Stem Cells.” *Cell Stem Cell* 3 (6): 595–605. doi:10.1016/j.stem.2008.11.008.

Mali, Prashant, Luhan Yang, Kevin M Esvelt, John Aach, Marc Guell, James E DiCarlo, Julie E Norville, and George M Church. 2013. “RNA-Guided Human Genome Engineering via Cas9.” *Science* 339 (6121): 823–26. doi:10.1126/science.1232033.

Malik, Vinod, Louise R Rodino-Klapac, Laurence Viollet, and Jerry R Mendell. 2010. “Aminoglycoside-Induced Mutation Suppression (Stop Codon Readthrough) as a Therapeutic Strategy for Duchenne Muscular Dystrophy.” *Therapeutic Advances in Neurological Disorders* 3 (6): 379–89. doi:10.1177/1756285610388693.

Mannan, Ashraf U., Philip Krawen, Simone M. Sauter, Johann Boehm, Agnieszka Chronowska, Walter Paulus, Juergen Neesen, and Wolfgang Engel. 2006. “ZFYVE27 (SPG33), a Novel Spastin-Binding Protein , Is Mutated in Hereditary Spastic Paraplegia.” *The American Journal of Human Genetics* 79 (8): 351–57. doi:10.1086/504927.

Mannan, Ashraf U, Johann Boehm, Simone M Sauter, Anne Rauber, Paula C Byrne, Juergen Neesen, and

Wolfgang Engel. 2006. “Spastin, the Most Commonly Mutated Protein in Hereditary Spastic Paraplegia Interacts with Reticulon 1 an Endoplasmic Reticulum Protein.” *Neurogenetics* 7 (2): 93–103. doi:10.1007/s10048-006-0034-4.

Martin, Elodie, Rebecca Schüle, Katrien Smets, Agnès Rastetter, Amir Boukhris, José L Loureiro, Michael A Gonzalez, et al. 2013. “Loss of Function of Glucocerebrosidase GBA2 Is Responsible for Motor Neuron Defects in Hereditary Spastic Paraplegia.” *American Journal of Human Genetics* 92 (2). Elsevier: 238–44. doi:10.1016/j.ajhg.2012.11.021.

Martin, G R. 1981. “Isolation of a Pluripotent Cell Line from Early Mouse Embryos Cultured in Medium Conditioned by Teratocarcinoma Stem Cells.” *Proceedings of the National Academy of Sciences of the United States of America* 78 (12): 7634–38.

Martin, Lee J. 2010. “Olesoxime, a Cholesterol-like Neuroprotectant for the Potential Treatment of Amyotrophic Lateral Sclerosis.” *IDrugs* 13 (8): 568–80. doi:10.1016/j.micinf.2011.07.011.Innate.

Martínez Murillo, F, H Kobayashi, E Pegoraro, G Galluzzi, G Creel, C Mariani, E Farina, et al. 1999. “Genetic Localization of a New Locus for Recessive Familial Spastic Paraparesis to 15q13-15.” *Neurology* 53 (1): 50–56. http://www.ncbi.nlm.nih.gov/pubmed/10408536.

Mertens, Jerome, Kathrin Stüber, Daniel Poppe, Jonas Doerr, Julia Ladewig, Oliver Brüstle, and Philipp Koch. 2013. “Embryonic Stem Cell-Based Modeling of Tau Pathology in Human Neurons.” *The American Journal of Pathology* 182 (5). American Society for Investigative Pathology: 1769–79. doi:10.1016/j.ajpath.2013.01.043.

Moloney, Elizabeth B, Fred de Winter, and Joost Verhaagen. 2014. “ALS as a Distal Axonopathy: Molecular Mechanisms Affecting Neuromuscular Junction Stability in the Presymptomatic Stages of the Disease.” *Frontiers in Neuroscience* 8. Frontiers Media SA: 252. doi:10.3389/fnins.2014.00252.

Montenegro, Gladys, Adriana P. Rebelo, James Connell, Rachel Allison, Carla Babalini, Michela D Aloia, Pasqua Montieri, et al. 2012. “Mutations in the ER-Shaping Protein Reticulon 2 Cause the Axon-Degenerative Disorder Hereditary Spastic Paraplegia Type 12.” *The Journal of Clinical Investigation* 122 (2): 538–44. doi:10.1172/JCI60560.

Musunuru, Kiran. 2013. “Genome Editing of Human Pluripotent Stem Cells to Generate Human Cellular Disease Models.” *Disease Models & Mechanisms* 6 (4).

Namjoshi, Dhananjay R, Georgina Martin, James Donkin, Anna Wilkinson, Sophie Stukas, Jianjia Fan, Michael Carr, et al. 2013. “The Liver X Receptor Agonist GW3965 Improves Recovery from Mild Repetitive Traumatic Brain Injury in Mice Partly through Apolipoprotein E.” *PloS One* 8 (1): e53529. doi:10.1371/journal.pone.0053529.

Närvä, Elisa, Reija Autio, Nelly Rahkonen, Lingjia Kong, Neil Harrison, Danny Kitsberg, Lodovica Borghese, et al. 2010. “High-Resolution DNA Analysis of Human Embryonic Stem Cell Lines Reveals Culture-Induced Copy Number Changes and Loss of Heterozygosity.” *Nature Biotechnology* 28 (4): 371–77. doi:10.1038/nbt.1615.

Neely, M Diana, Michael J Litt, Andrew M Tidball, Gary G Li, Asad a Aboud, Corey R Hopkins, Reed Chamberlin, Charles C Hong, Kevin C Ess, and Aaron B Bowman. 2012. “DMH1, a Highly Selective Small Molecule BMP Inhibitor Promotes Neurogenesis of HiPSCs: Comparison of PAX6 and SOX1 Expression during Neural Induction.” *ACS Chemical Neuroscience* 3 (6): 482–91. doi:10.1021/cn300029t.

Nichols, Jennifer, and Austin Smith. 2009. “Naive and Primed Pluripotent States.” *Cell Stem Cell* 4 (6). Elsevier Inc.: 487–92. doi:10.1016/j.stem.2009.05.015.

Nikouei, Kasra, Ana B. Muñoz-Manchado, and Jens Hjerling-Leffler. 2016. “BCL11B/CTIP2 Is Highly Expressed in GABAergic Interneurons of the Mouse Somatosensory Cortex.” *Journal of Chemical Neuroanatomy* 71 (January): 1–5. doi:10.1016/j.jchemneu.2015.12.004.

Nishimura, Agnes L., Miguel Mitne-Neto, Helga C.A. Silva, Antônio Richieri-Costa, Susan Middleton, Duilio Cascio, Fernando Kok, et al. 2004. “A Mutation in the Vesicle-Trafficking Protein VAPB Causes Late-Onset Spinal Muscular Atrophy and Amyotrophic Lateral Sclerosis.” *The American Journal of Human Genetics* 75 (5): 822–31. doi:10.1086/425287.

Novarino, Gaia, Ali G Fenstermaker, Maha S Zaki, Matan Hofree, Jennifer L Silhavy, Andrew D Heiberg, Mostafa Abdellateef, et al. 2014. “Exome Sequencing Links Corticospinal Motor Neuron Disease to

Common Neurodegenerative Disorders." *Science* 343 (6170): 506–11. doi:10.1126/science.1247363.

Okita, Keisuke, Masato Nakagawa, Hong Hyenjong, Tomoko Ichisaka, and Shinya Yamanaka. 2008. "Generation of Mouse Induced Pluripotent Stem Cells Without Viral Vectors." *Science* 322 (5903): 949–53. doi:10.1126/science.1164270.

Orso, Genny, Andrea Martinuzzi, Maria Giovanna Rossetto, Elena Sartori, Mel Feany, and Andrea Daga. 2005. "Disease-Related Phenotypes in a Drosophila Model of Hereditary Spastic Paraplegia Are Ameliorated by Treatment with Vinblastine." *The Journal of Clinical Investigation* 115 (11): 3026–34. doi:10.1172/JCI24694.3026.

Orthmann-Murphy, Jennifer L, Ettore Salsano, Charles K Abrams, Alberto Bizzi, Graziella Uziel, Mona M Freidin, Eleonora Lamantea, Massimo Zeviani, Steven S Scherer, and Davide Pareyson. 2009. "Hereditary Spastic Paraplegia Is a Novel Phenotype for GJA12/GJC2 Mutations." *Brain : A Journal of Neurology* 132 (Pt 2): 426–38. doi:10.1093/brain/awn328.

Otomo, Asako, Shinji Hadano, Takeya Okada, Hikaru Mizumura, Ryota Kunita, Hitoshi Nishijima, Junko Showguchi-Miyata, et al. 2003. "ALS2, a Novel Guanine Nucleotide Exchange Factor for the Small GTPase Rab5, Is Implicated in Endosomal Dynamics." *Human Molecular Genetics* 12 (14): 1671–87. http://www.ncbi.nlm.nih.gov/pubmed/12837691.

Oz-Levi, Danit, Bruria Ben-Zeev, Elizabeth K Ruzzo, Yuki Hitomi, Amir Gelman, Kimberly Pelak, Yair Anikster, et al. 2012. "Mutation in TECPR2 Reveals a Role for Autophagy in Hereditary Spastic Paraparesis." *American Journal of Human Genetics* 91 (6): 1065–72. doi:10.1016/j.ajhg.2012.09.015.

Ozeki, Y., T. Tomoda, J. Kleiderlein, A. Kamiya, L. Bord, K. Fujii, M. Okawa, et al. 2003. "Disrupted-in-Schizophrenia-1 (DISC-1): Mutant Truncation Prevents Binding to NudE-like (NUDEL) and Inhibits Neurite Outgrowth." *Proceedings of the National Academy of Sciences* 100 (1). National Academy of Sciences: 289–94. doi:10.1073/pnas.0136913100.

Pantakani, D. V Krishna, Lakshmipuram S. Swapna, Narayanaswamy Srinivasan, and Ashraf U. Mannan. 2008. "Spastin Oligomerizes into a Hexamer and the Mutant Spastin (E442Q) Redistribute the Wild-Type Spastin into Filamentous Microtubule." *Journal of Neurochemistry* 106 (2): 613–24. doi:10.1111/j.1471-4159.2008.05414.x.

Papadopoulos, Chrisovalantis, Genny Orso, Giuseppe Mancuso, Marija Herholz, Sentiljana Gumeni, Nimesha Tadepalle, Christian Jüngst, et al. 2015. "Spastin Binds to Lipid Droplets and Affects Lipid Metabolism." *PLOS Genetics* 11 (4): e1005149. doi:10.1371/journal.pgen.1005149.

Park, In-Hyun, and George Q Daley. 2009. "Human IPS Cell Derivation/Reprogramming." *Current Protocols in Stem Cell Biology* Chapter 4 (January): Unit 4A.1. doi:10.1002/9780470151808.sc04a01s8.

Park, S.H. Seong H, Peng-peng P.P. Zhu, Rell L Parker, and Craig Blackstone. 2010. "Hereditary Spastic Paraplegia Proteins REEP1, Spastin, and Atlastin-1 Coordinate Microtubule Interactions with the Tubular ER Network." *The Journal of Clinical Investigation* 120 (4). American Society for Clinical Investigation: 1097–1110. doi:10.1172/JCI40979DS1.

Parkinson, N., P. G. Ince, M. O. Smith, R. Highley, G. Skibinski, P. M. Andersen, K. E. Morrison, et al. 2006. "ALS Phenotypes with Mutations in CHMP2B (Charged Multivesicular Body Protein 2B)." *Neurology* 67 (6): 1074–77. doi:10.1212/01.wnl.0000231510.89311.8b.

Patel, Heema, Harold Cross, Christos Proukakis, Ruth Hershberger, Peer Bork, Francesca D Ciccarelli, Michael A Patton, Victor A McKusick, and Andrew H Crosby. 2002. "SPG20 Is Mutated in Troyer Syndrome, an Hereditary Spastic Paraplegia." *Nature Genetics* 31 (4): 347–48. doi:10.1038/ng937.

Pool, Madeline, Joachim Thiemann, Amit Bar-Or, and Alyson E Fournier. 2008. "NeuriteTracer: A Novel ImageJ Plugin for Automated Quantification of Neurite Outgrowth." *Journal of Neuroscience Methods* 168 (1): 134–39. doi:10.1016/j.jneumeth.2007.08.029.

Popko, Jonathan, Adelaide Fernandes, Dora Brites, and Lorene M Lanier. 2009. "Automated Analysis of NeuronJ Tracing Data." *Cytometry. Part A : The Journal of the International Society for Analytical Cytology* 75 (4). NIH Public Access: 371–76. doi:10.1002/cyto.a.20660.

Prè, Deborah, Michael W. Nestor, Andrew a. Sproul, Samson Jacob, Peter Koppensteiner, Vorapin Chinchalongporn, Matthew Zimmer, Ai Yamamoto, Scott a. Noggle, and Ottavio Arancio. 2014. "A Time Course Analysis of the Electrophysiological Properties of Neurons Differentiated from Human Induced Pluripotent Stem Cells (IPSCs)." *PLoS ONE* 9 (7). doi:10.1371/journal.pone.0103418.

Prüfer, Kirsten, and Jeanne Boudreaux. 2007. “Nuclear Localization of Liver X Receptor Alpha and Beta Is Differentially Regulated.” *Journal of Cellular Biochemistry* 100: 69–85. doi:10.1002/jcb.21006.

Qiang, Liang, Wenqian Yu, Mei Liu, Joanna M Solowska, and Peter W Baas. 2010. “Basic Fibroblast Growth Factor Elicits Formation of Interstitial Axonal Branches via Enhanced Severing of Microtubules.” *Molecular Biology of the Cell* 21: 334–44. doi:10.1091/mbc.E09.

Rainier, Shirley, Melanie Bui, Erin Mark, Donald Thomas, Debra Tokarz, Lei Ming, Colin Delaney, et al. 2008. “Neuropathy Target Esterase Gene Mutations Cause Motor Neuron Disease.” *American Journal of Human Genetics* 82 (3): 780–85. doi:10.1016/j.ajhg.2007.12.018.

Rainier, Shirley, Jing-Hua Chai, Debra Tokarz, Robert D Nicholls, and John K Fink. 2003. “NIPA1 Gene Mutations Cause Autosomal Dominant Hereditary Spastic Paraplegia (SPG6).” *American Journal of Human Genetics* 73 (4): 967–71. doi:10.1086/378817.

Ran, F Ann, Patrick D Hsu, Chie-yu Lin, Jonathan S Gootenberg, Alexandro Trevino, David a Scott, Azusa Inoue, Shogo Matoba, Yi Zhang, and Feng Zhang. 2014. “Double Nicking by RNA-Guided CRISPR Cas9 for Enhanced Genome Editing Specificity.” *Cell* 154 (6). doi:10.1016/j.cell.2013.08.021.Double.

Rash, Brian G, H David Lim, Joshua J Breunig, and Flora M Vaccarino. 2011. “FGF Signaling Expands Embryonic Cortical Surface Area by Regulating Notch-Dependent Neurogenesis.” *The Journal of Neuroscience : The Official Journal of the Society for Neuroscience* 31 (43): 15604–17. doi:10.1523/JNEUROSCI.4439-11.2011.

Read, David J, Yong Li, Moses V Chao, John B Cavanagh, and Paul Glynn. 2009. “Neuropathy Target Esterase Is Required for Adult Vertebrate Axon Maintenance.” *The Journal of Neuroscience : The Official Journal of the Society for Neuroscience* 29 (37): 11594–600. doi:10.1523/JNEUROSCI.3007-09.2009.

Reid, Evan, James Connell, Thomas L. Edwards, Simon Duley, Stephanie E. Brown, and Christopher M. Sanderson. 2005. “The Hereditary Spastic Paraplegia Protein Spastin Interacts with the ESCRT-III Complex-Associated Endosomal Protein CHMP1B.” *Human Molecular Genetics* 14 (1): 19–38. doi:10.1093/hmg/ddi003.

Reid, Evan, Mark Kloos, Allison Ashley-Koch, Lori Hughes, Simon Bevan, Ingrid K Svenson, Felicia Lennon Graham, et al. 2002. “A Kinesin Heavy Chain (KIF5A) Mutation in Hereditary Spastic Paraplegia (SPG10).” *American Journal of Human Genetics* 71 (5): 1189–94. doi:10.1086/344210.

Reinhardt, Peter, Benjamin Schmid, Lena F. F. Burbulla, David C. C. Schöndorf, Lydia Wagner, Michael Glatza, Susanne Höing, et al. 2013a. “Genetic Correction of a LRRK2 Mutation in Human IPSCs Links Parkinsonian Neurodegeneration to ERK-Dependent Changes in Gene Expression.” *Cell Stem Cell* 12 (3): 354–67. doi:10.1016/j.stem.2013.01.008.

Reinhardt, Peter, Benjamin Schmid, Lena F. Burbulla, David C. Schöndorf, Lydia Wagner, Michael Glatza, Susanne Höing, et al. 2013b. “Genetic Correction of a LRRK2 Mutation in Human IPSCs Links Parkinsonian Neurodegeneration to ERK-Dependent Changes in Gene Expression.” *Cell Stem Cell* 12 (3): 354–67. doi:10.1016/j.stem.2013.01.008.

Renton, Alan E., Elisa Majounie, Adrian Waite, Javier Simón-Sánchez, Sara Rollinson, J. Raphael Gibbs, Jennifer C. Schymick, et al. 2011. “A Hexanucleotide Repeat Expansion in C9ORF72 Is the Cause of Chromosome 9p21-Linked ALS-FTD.” *Neuron* 72 (2): 257–68. doi:10.1016/j.neuron.2011.09.010.

Renvoisé, Benoît, and Craig Blackstone. 2010. “Emerging Themes of ER Organization in the Development and Maintenance of Axons.” *Current Opinion in Neurobiology* 20 (5): 531–37. doi:10.1016/j.conb.2010.07.001.

Renvoisé, Benoît, Jaerak Chang, Rajat Singh, Sayuri Yonekawa, Edmond J FitzGibbon, Ami Mankodi, Adeline Vanderver, et al. 2014. “Lysosomal Abnormalities in Hereditary Spastic Paraplegia Types SPG15 and SPG11.” *Annals of Clinical and Translational Neurology* 1 (6): 379–89. doi:10.1002/acn3.64.

Riano, Elena, Monica Martignoni, Giuseppe Mancuso, Daniele Cartelli, Francesca Crippa, Irene Toldo, Gabriele Siciliano, et al. 2009. “Pleiotropic Effects of Spastin on Neurite Growth Depending on Expression Levels.” *Journal of Neurochemistry* 108 (5): 1277–88. doi:10.1111/j.1471-4159.2009.05875.x.

Rinaldi, Carlo, Thomas Schmidt, Alan J Situ, Janel O Johnson, Philip R Lee, Ke-Lian Chen, Laura C Bott,

et al. 2015. “Mutation in CPT1C Associated With Pure Autosomal Dominant Spastic Paraplegia.” *JAMA Neurology* 72 (5): 561–70. doi:10.1001/jamaneurol.2014.4769.

Rouhani, Foad J, Serena Nik-Zainal, Arthur Wuster, Yilong Li, Nathalie Conte, Hiroko Koike-Yusa, Natsuhiko Kumasaka, Ludovic Vallier, Kosuke Yusa, and Allan Bradley. 2016. “Mutational History of a Human Cell Lineage from Somatic to Induced Pluripotent Stem Cells.” *PLoS Genetics* 12 (4): e1005932. doi:10.1371/journal.pgen.1005932.

Ruano, Luis, Claudia Melo, M. Carolina Silva, and Paula Coutinho. 2014. “The Global Epidemiology of Hereditary Ataxia and Spastic Paraplegia: A Systematic Review of Prevalence Studies.” *Neuroepidemiology* 42 (3): 174–83. doi:10.1159/000358801.

Ruschel, J., F. Hellal, K. C. Flynn, S. Dupraz, D. A. Elliott, A. Tedeschi, M. Bates, et al. 2015. “Systemic Administration of Epothilone B Promotes Axon Regeneration after Spinal Cord Injury.” *Science*, March. doi:10.1126/science.aaa2958.

Salinas, Sara, Christos Proukakis, Andrew Crosby, and Thomas T Warner. 2008. “Hereditary Spastic Paraplegia: Clinical Features and Pathogenetic Mechanisms.” *Lancet Neurology* 7 (12). Elsevier Ltd: 1127–38. doi:10.1016/S1474-4422(08)70258-8.

Sánchez-Danés, Adriana, Yvonne Richaud-Patin, Iria Carballo-Carbajal, Senda Jiménez-Delgado, Carles Caig, Sergio Mora, Claudia Di Guglielmo, et al. 2012. “Disease-Specific Phenotypes in Dopamine Neurons from Human IPS-Based Models of Genetic and Sporadic Parkinson’s Disease.” *EMBO Molecular Medicine* 4 (5): 380–95. doi:10.1002/emmm.201200215.

Sasai, Y, B Lu, H Steinbeisser, D Geissert, L K Gont, and E M De Robertis. 1994. “Xenopus Chordin: A Novel Dorsalizing Factor Activated by Organizer-Specific Homeobox Genes.” *Cell* 79 (5): 779–90.

Saugier-Veber, P, A Munnich, D Bonneau, J M Rozet, M Le Merrer, R Gil, and O Boespflug-Tanguy. 1994. “X-Linked Spastic Paraplegia and Pelizaeus-Merzbacher Disease Are Allelic Disorders at the Proteolipid Protein Locus.” *Nature Genetics* 6 (3): 257–62. doi:10.1038/ng0394-257.

Sbaschnig-Agler, M, K H Pfenninger, and R W Ledeen. 1988. “Gangliosides and Other Lipids of the Growth Cone Membrane.” *Journal of Neurochemistry* 51 (1): 212–20.

Schüle, Rebecca, and Ludger Schöls. 2011. “Genetics of Hereditary Spastic Paraplegias.” *Seminars in Neurology* 31 (5): 484–93. doi:10.1055/s-0031-1299787.

Schüle, Rebecca, Teepu Siddique, Han-Xiang Deng, Yi Yang, Sandra Donkervoort, Magnus Hansson, Ricardo E Madrid, Nailah Siddique, Ludger Schöls, and Ingemar Björkhem. 2010. “Marked Accumulation of 27-Hydroxycholesterol in SPG5 Patients with Hereditary Spastic Paresis.” *Journal of Lipid Research* 51 (4). American Society for Biochemistry and Molecular Biology: 819–23. doi:10.1194/jlr.M002543.

Schüle, Rebecca, Sarah Wiethoff, Peter Martus, Kathrin N. Karle, Susanne Otto, Stephan Klebe, Sven Klimpe, et al. 2016. “Hereditary Spastic Paraplegia: Clinicogenetic Lessons from 608 Patients.” *Annals of Neurology* 79 (4): 646–58. doi:10.1002/ana.24611.

Schuurs-Hoeijmakers, Janneke H M, Michael T Geraghty, Erik-Jan Kamsteeg, Salma Ben-Salem, Susanne T de Bot, Bonnie Nijhof, Ilse I G M van de Vondervoort, et al. 2012. “Mutations in DDHD2, Encoding an Intracellular Phospholipase A(1), Cause a Recessive Form of Complex Hereditary Spastic Paraplegia.” *American Journal of Human Genetics* 91 (6): 1073–81. doi:10.1016/j.ajhg.2012.10.017.

Schwartz, Charles E, Melanie M May, Nancy J Carpenter, R Curtis Rogers, Judith Martin, Martin G Bialer, Jewell Ward, et al. 2005. “Allan-Herndon-Dudley Syndrome and the Monocarboxylate Transporter 8 (MCT8) Gene.” *American Journal of Human Genetics* 77 (1): 41–53. doi:10.1086/431313.

Schwarz, Nele, Amanda Jayne Carr, Amelia Lane, Fabian Moeller, Li Li Chen, Mònica Aguilà, Britta Nommiste, et al. 2015. “Translational Read-through of the RP2 Arg120stop Mutation in Patient IPSC-Derived Retinal Pigment Epithelium Cells.” *Human Molecular Genetics* 24 (4): 972–86. doi:10.1093/hmg/ddu509.

Shaffer, Lisa G., and Bassem A. Bejjani. 2004. “A Cytogeneticist’s Perspective on Genomic Microarrays.” *Human Reproduction Update* 10 (3): 221–26. doi:10.1093/humupd/dmh022.

Sherwood, Nina Tang, Qi Sun, Mingshan Xue, Bing Zhang, and Kai Zinn. 2004. “Drosophila Spastin Regulates Synaptic Microtubule Networks and Is Required for Normal Motor Function.” *PLoS Biology* 2 (12): e429. doi:10.1371/journal.pbio.0020429.

REFERENCES

Shi, Yichen, Peter Kirwan, James Smith, Hugh P C Robinson, and Frederick J Livesey. 2012. “Human Cerebral Cortex Development from Pluripotent Stem Cells to Functional Excitatory Synapses.” *Nature Neuroscience* 15 (3). Nature Publishing Group: 477–86. doi:10.1038/nn.3041.

Simon-Sanchez, Javier, Sonja Scholz, Hon-Chung Fung, Mar Matarin, Dena Hernandez, J Raphael Gibbs, Angela Britton, et al. 2007. “Genome-Wide SNP Assay Reveals Structural Genomic Variation, Extended Homozygosity and Cell-Line Induced Alterations in Normal Individuals.” *Human Molecular Genetics* 16 (1): 1–14. doi:10.1093/hmg/ddl436.

Simpson, Michael A, Harold Cross, Christos Proukakis, Anna Pryde, Ruth Hershberger, Arnaud Chatonnet, Michael A Patton, and Andrew H Crosby. 2003. “Maspardin Is Mutated in Mast Syndrome, a Complicated Form of Hereditary Spastic Paraplegia Associated with Dementia.” *American Journal of Human Genetics* 73 (5): 1147–56. doi:10.1086/379522.

Słabicki, Mikołaj, Mirko Theis, Dragomir B Krastev, Sergey Samsonov, Emeline Mundwiller, Magno Junqueira, Maciej Paszkowski-Rogacz, et al. 2010. “A Genome-Scale DNA Repair RNAi Screen Identifies SPG48 as a Novel Gene Associated with Hereditary Spastic Paraplegia.” *PLoS Biology* 8 (6). Public Library of Science: e1000408. doi:10.1371/journal.pbio.1000408.

Smith, Joseph R, Ludovic Vallier, Giuseppe Lupo, Morgan Alexander, William A Harris, and Roger A Pedersen. 2008. “Inhibition of Activin/Nodal Signaling Promotes Specification of Human Embryonic Stem Cells into Neuroectoderm.” *Developmental Biology* 313 (1): 107–17. doi:10.1016/j.ydbio.2007.10.003.

Smith, W C, and R M Harland. 1992. “Expression Cloning of Noggin, a New Dorsalizing Factor Localized to the Spemann Organizer in Xenopus Embryos.” *Cell* 70 (5): 829–40. http://www.ncbi.nlm.nih.gov/pubmed/1339313.

Solowska, Joanna M., and Peter W. Baas. 2015. “Hereditary Spastic Paraplegia SPG4: What Is Known and Not Known about the Disease.” *Brain* 138 (9): 2471–84. doi:10.1093/brain/awv178.

Solowska, Joanna M., Mitchell D’Rozario, Daphney C. Jean, Michael W. Davidson, Daniel R. Marenda, and Peter W. Baas. 2014. “Pathogenic Mutation of Spastin Has Gain-of-Function Effects on Microtubule Dynamics.” *The Journal of Neuroscience : The Official Journal of the Society for Neuroscience* 34 (5): 1856–67. doi:10.1523/JNEUROSCI.3309-13.2014.

Solowska, Joanna M, James Y Garbern, and Peter W Baas. 2010. “Evaluation of Loss of Function as an Explanation for SPG4-Based Hereditary Spastic Paraplegia.” *Human Molecular Genetics* 19 (14): 2767–79. doi:10.1093/hmg/ddq177.

Solowska, Joanna M, Gerardo Morfini, Aditi Falnikar, B Timothy Himes, T Scott, Dongyang Huang, Peter W Baas, Scott T Brady, Dongyang Huang, and Peter W Baas. 2008. “Quantitative and Functional Analyses of Spastin in the Nervous System: Implications for Hereditary Spastic Paraplegia.” *The Journal of Neuroscience : The Official Journal of the Society for Neuroscience* 28 (9): 2147–57. doi:10.1523/JNEUROSCI.3159-07.2008.

Spits, Claudia, Ileana Mateizel, Mieke Geens, Afroditi Mertzanidou, Catherine Staessen, Yves Vandeskelde, Josiane Van der Elst, Inge Liebaers, and Karen Sermon. 2008. “Recurrent Chromosomal Abnormalities in Human Embryonic Stem Cells.” *Nature Biotechnology* 26 (12): 1361–63. doi:10.1038/nbt.1510.

Stadtfeld, Matthias, Masaki Nagaya, Jochen Utikal, Gordon Weir, and Konrad Hochedlinger. 2008. “Induced Pluripotent Stem Cells Generated Without Viral Integration.” *Nature Biotechnology* 945 (September): 945–49. doi:10.1126/science.1162494.

Štefková, Kateřina, Jiřina Procházková, and Jiří Pacherník. 2015. “Alkaline Phosphatase in Stem Cells.” *Stem Cells International* 2015 (January): 628368. doi:10.1155/2015/628368.

Stevanin, Giovanni, Filippo M Santorelli, Hamid Azzedine, Paula Coutinho, Jacques Chomilier, Paola S Denora, Elodie Martin, et al. 2007. “Mutations in SPG11, Encoding Spatacsin, Are a Major Cause of Spastic Paraplegia with Thin Corpus Callosum.” *Nature Genetics* 39 (3): 366–72. doi:10.1038/ng1980.

Stone, Michelle C., Kavitha Rao, Kyle W. Gheres, Seahee Kim, Juan Tao, Caroline La Rochelle, Christin T. Folker, Nina T. Sherwood, and Melissa M. Rolls. 2012. “Normal Spastin Gene Dosage Is Specifically Required for Axon Regeneration.” *Cell Reports* 2 (5). The Authors: 1340–50. doi:10.1016/j.celrep.2012.09.032.

Su, Kimmy G, Gary Banker, Dennis Bourdette, and Michael Forte. 2009. “Axonal Degeneration in Multiple Sclerosis: The Mitochondrial Hypothesis.” *Current Neurology and Neuroscience Reports* 9 (5). NIH Public Access: 411–17. http://www.ncbi.nlm.nih.gov/pubmed/19664372.

Szymanski, Kimberly M, Derk Binns, René Bartz, Nick V Grishin, Wei-Ping Li, Anil K Agarwal, Abhimanyu Garg, Richard G W Anderson, and Joel M Goodman. 2007. “The Lipodystrophy Protein Seipin Is Found at Endoplasmic Reticulum Lipid Droplet Junctions and Is Important for Droplet Morphology.” *Proceedings of the National Academy of Sciences of the United States of America* 104 (52): 20890–95. doi:10.1073/pnas.0704154104.

Tagliaferro, Patricia, and Robert E. Burke. 2016. “Retrograde Axonal Degeneration in Parkinson Disease.” *Journal of Parkinson’s Disease* 6 (1): 1–15. doi:10.3233/JPD-150769.

Takahashi, Kazutoshi, Koji Tanabe, Mari Ohnuki, Megumi Narita, Tomoko Ichisaka, Kiichiro Tomoda, Shinya Yamanaka, et al. 2007. “Induction of Pluripotent Stem Cells from Adult Human Fibroblasts by Defined Factors.” *Cell* 131 (5): 861–72. doi:10.1016/j.cell.2007.11.019.

Takahashi, Kazutoshi, and Shinya Yamanaka. 2006. “Induction of Pluripotent Stem Cells from Mouse Embryonic and Adult Fibroblast Cultures by Defined Factors.” *Cell* 126 (4): 663–76. doi:10.1016/j.cell.2006.07.024.

Tallaksen, C M, A Dürr, and A Brice. 2001. “Recent Advances in Hereditary Spastic Paraplegia.” *Current Opinion in Neurology* 14 (4): 457–63.

Tarrade, Anne, Coralie Fassier, Sabrina Courageot, Delphine Charvin, Jérémie Vitte, Leticia Peris, Alain Thorel, et al. 2006. “A Mutation of Spastin Is Responsible for Swellings and Impairment of Transport in a Region of Axon Characterized by Changes in Microtubule Composition.” *Human Molecular Genetics* 15 (24): 3544–58. doi:10.1093/hmg/ddl431.

Tesson, Christelle, Magdalena Nawara, Mustafa A M Salih, Rodrigue Rossignol, Maha S Zaki, Mohammed Al Balwi, Rebecca Schule, et al. 2012. “Alteration of Fatty-Acid-Metabolizing Enzymes Affects Mitochondrial Form and Function in Hereditary Spastic Paraplegia.” *American Journal of Human Genetics* 91 (6): 1051–64. doi:10.1016/j.ajhg.2012.11.001.

Thomsen, Bo, Peter H. Nissen, Jørgen S. Agerholm, and Christian Bendixen. 2010. “Congenital Bovine Spinal Dysmyelination Is Caused by a Missense Mutation in the SPAST Gene.” *Neurogenetics* 11 (2): 175–83. doi:10.1007/s10048-009-0214-0.

Thomson, J. A., J Itskovitz-Eldor, S.S. S Shapiro, M.A. A Waknitz, J J Swiergiel, V.S. S Marshall, J M Jones, et al. 1998. “Embryonic Stem Cell Lines Derived from Human Blastocysts.” *Science* 282 (5391): 1145–47. doi:10.1126/science.282.5391.1145.

Traynor, B. J., L. Bruijn, R. Conwit, F. Beal, G. O'Neill, S. C. Fagan, M. E. Cudkowicz, G. O’Neill, S. C. Fagan, and M. E. Cudkowicz. 2006. “Neuroprotective Agents for Clinical Trials in ALS: A Systematic Assessment.” *Neurology* 67 (1): 20–27. doi:10.1212/01.wnl.0000223353.34006.54.

Tsang, Hilda T H, Thomas L. Edwards, Xinnan Wang, James W. Connell, Rachel J. Davies, Hannah J. Durrington, Cahir J. O’Kane, J. Paul Luzio, and Evan Reid. 2009. “The Hereditary Spastic Paraplegia Proteins NIPA1, Spastin and Spartin Are Inhibitors of Mammalian BMP Signalling.” *Human Molecular Genetics* 18 (20): 3805–21. doi:10.1093/hmg/ddp324.

Tsankov, Alexander M, Veronika Akopian, Ramona Pop, Sundari Chetty, Casey A Gifford, Laurence Daheron, Nadejda M Tsankova, and Alexander Meissner. 2015. “A QPCR ScoreCard Quantifies the Differentiation Potential of Human Pluripotent Stem Cells.” *Nature Biotechnology* 33 (11). Nature Research: 1182–92. doi:10.1038/nbt.3387.

Tsaousidou, Maria K, Karim Ouahchi, Tom T Warner, Yi Yang, Michael A Simpson, Nigel G Laing, Philip A Wilkinson, et al. 2008. “Sequence Alterations within CYP7B1 Implicate Defective Cholesterol Homeostasis in Motor-Neuron Degeneration.” *American Journal of Human Genetics* 82 (2): 510–15. doi:10.1016/j.ajhg.2007.10.001.

Valdmanis, Paul N, Inge A Meijer, Annie Reynolds, Adrienne Lei, Patrick MacLeod, David Schlesinger, Mayana Zatz, et al. 2007. “Mutations in the KIAA0196 Gene at the SPG8 Locus Cause Hereditary Spastic Paraplegia.” *American Journal of Human Genetics* 80 (1): 152–61. doi:10.1086/510782.

Varga, Rita-Eva, Mukhran Khundadze, Markus Damme, Sandor Nietzsche, Birgit Hoffmann, Tobias Stauber, Nicole Koch, et al. 2015. “In Vivo Evidence for Lysosome Depletion and Impaired Autophagic

Clearance in Hereditary Spastic Paraplegia Type SPG11." *PLoS Genetics* 11 (8): e1005454. doi:10.1371/journal.pgen.1005454.

Wakatsuki, T, B Schwab, N C Thompson, and E L Elson. 2001. "Effects of Cytochalasin D and Latrunculin B on Mechanical Properties of Cells." *Journal of Cell Science* 114 (Pt 5): 1025–36.

Wang, Guohua, Xiaoyan Jiang, Hongjian Pu, Wenting Zhang, Chengrui An, Xiaoming Hu, Anthony Kian Fong Liou, Rehana K. Leak, Yanqin Gao, and Jun Chen. 2013. "Scriptaid, a Novel Histone Deacetylase Inhibitor, Protects Against Traumatic Brain Injury via Modulation of PTEN and AKT Pathway: Scriptaid Protects Against TBI via AKT." *Neurotherapeutics* 10 (1): 124–42. doi:10.1007/s13311-012-0157-2.

Warren, Luigi, Philip D Manos, Tim Ahfeldt, Yuin-Han Loh, Hu Li, Frank Lau, Wataru Ebina, et al. 2010. "Highly Efficient Reprogramming to Pluripotency and Directed Differentiation of Human Cells with Synthetic Modified MRNA." *Cell Stem Cell* 7 (5): 618–30. doi:10.1016/j.stem.2010.08.012.

Watanabe, Kiichi, Morio Ueno, Daisuke Kamiya, Ayaka Nishiyama, Michiru Matsumura, Takafumi Wataya, Jun B Takahashi, et al. 2007. "A ROCK Inhibitor Permits Survival of Dissociated Human Embryonic Stem Cells." *Nature Biotechnology* 25 (6): 681–86. doi:10.1038/nbt1310.

Welch, Ellen M, Elisabeth R Barton, Jin Zhuo, Yuki Tomizawa, Westley J Friesen, Panayiota Trifillis, Sergey Paushkin, et al. 2007. "PTC124 Targets Genetic Disorders Caused by Nonsense Mutations." *Nature* 447 (7140): 87–91. doi:10.1038/nature05756.

White, Susan Roehl, Katia J. Evans, Jeffrey Lary, James L. Cole, and Brett Lauring. 2007. "Recognition of C-Terminal Amino Acids in Tubulin by Pore Loops in Spastin Is Important for Microtubule Severing." *Journal of Cell Biology* 176 (7): 995–1005. doi:10.1083/jcb.200610072.

Windpassinger, Christian, Michaela Auer-Grumbach, Joy Irobi, Heema Patel, Erwin Petek, Gerd Hörl, Roland Malli, et al. 2004. "Heterozygous Missense Mutations in BSCL2 Are Associated with Distal Hereditary Motor Neuropathy and Silver Syndrome." *Nature Genetics* 36 (3): 271–76. doi:10.1038/ng1313.

Winkler, C., Christian Eggert, Dietmar Gradl, Gunter Meister, Marieke Giegerich, Doris Wedlich, Bernhard Laggerbauer, and Utz Fischer. 2005. "Reduced U SnRNP Assembly Causes Motor Axon Degeneration in an Animal Model for Spinal Muscular Atrophy." *Genes & Development* 19 (19): 2320–30. doi:10.1101/gad.342005.

Witte, Harald, Dorothee Neukirchen, and Frank Bradke. 2008. "Microtubule Stabilization Specifies Initial Neuronal Polarization." *The Journal of Cell Biology* 180 (3): 619–32. doi:10.1083/jcb.200707042.

Wójcicka, Grażyna, Anna Jamroz-wiśniewska, and Krzysztof Horoszewicz. 2007. "Liver X Receptors (LXRs). Part I : Structure , Function , Regulation of Activity , and Role in Lipid Metabolism Receptory Wątrobowe X (LXR). Część I : Budowa , Funkcja , Regulacja Aktywności i Znaczenie w Metabolizmie Lipidów." *Postepy Hig Dosw* 61: 736–59.

Wonders, Carl P, and Stewart a Anderson. 2006. "The Origin and Specification of Cortical Interneurons." *Nature Reviews. Neuroscience* 7 (9): 687–96. doi:10.1038/nrn1954.

Wood, Jonathan D., Jennifer a. Landers, Megan Bingley, Christopher J. McDermott, Vickie Thomas-McArthur, Lisa J. Gleadall, Pamela J. Shaw, and Vincent T. Cunliffe. 2006. "The Microtubule-Severing Protein Spastin Is Essential for Axon Outgrowth in the Zebrafish Embryo." *Human Molecular Genetics* 15 (18): 2763–71. doi:10.1093/hmg/ddl212.

Wrana, J L, and L Attisano. "The Smad Pathway." *Cytokine & Growth Factor Reviews* 11 (1–2): 5–13.

Wright, Andrew J, and Peter W Andrews. 2009. "Surface Marker Antigens in the Characterization of Human Embryonic Stem Cells." *Stem Cell Research* 3 (1): 3–11. doi:10.1016/j.scr.2009.04.001.

Xu, C, M S Inokuma, J Denham, K Golds, P Kundu, J D Gold, and M K Carpenter. 2001. "Feeder-Free Growth of Undifferentiated Human Embryonic Stem Cells." *Nature Biotechnology* 19 (10): 971–74. doi:10.1038/nbt1001-971.

Xu, Ren-He, Ruthann M Peck, Dong S Li, Xuezhu Feng, Tenneille Ludwig, and James A Thomson. 2005. "Basic FGF and Suppression of BMP Signaling Sustain Undifferentiated Proliferation of Human ES Cells." *Nature Methods* 2 (3): 185–90. doi:10.1038/nmeth744.

Ye, K, Y Ke, N Keshava, J Shanks, J a Kapp, R R Tekmal, J Petros, and H C Joshi. 1998. "Opium Alkaloid

Noscapine Is an Antitumor Agent That Arrests Metaphase and Induces Apoptosis in Dividing Cells." *Proceedings of the National Academy of Sciences of the United States of America* 95 (4): 1601–6. doi:10.1073/pnas.95.4.1601.

Yu, Junying, Maxim A Vodyanik, Kim Smuga-Otto, Jessica Antosiewicz-Bourget, Jennifer L Frane, Shulan Tian, Jeff Nie, et al. 2007. "Induced Pluripotent Stem Cell Lines Derived from Human Somatic Cells." *Science (New York, N.Y.)* 318 (5858): 1917–20. doi:10.1126/science.1151526.

Yu, L., J. York, K. von Bergmann, D. Lutjohann, J. C. Cohen, and H. H. Hobbs. 2003. "Stimulation of Cholesterol Excretion by the Liver X Receptor Agonist Requires ATP-Binding Cassette Transporters G5 and G8." *Journal of Biological Chemistry* 278 (18). American Society for Biochemistry and Molecular Biology: 15565–70. doi:10.1074/jbc.M301311200.

Zago, Stefano, Barbara Poletti, Claudia Morelli, Alberto Doretti, and Vincenzo Silani. 2011. "Amyotrophic Lateral Sclerosis and Frontotemporal Dementia (ALS-FTD)." *Archives Italiennes de Biologie* 149 (1): 39–56. http://www.ncbi.nlm.nih.gov/pubmed/21412715.

Zanetta, Chiara, Monica Nizzardo, Chiara Simone, Erika Monguzzi, Nereo Bresolin, Giacomo P Comi, and Stefania Corti. 2014. "Molecular Therapeutic Strategies for Spinal Muscular Atrophies: Current and Future Clinical Trials." *Clinical Therapeutics* 36 (1). Elsevier: 128–40. doi:10.1016/j.clinthera.2013.11.006.

Zhang, Chuanling, Dan Li, Yan Ma, Jinting Yan, Baiqing Yang, Peng Li, Aiping Yu, Cailing Lu, and Xu Ma. 2012. "Role of Spastin and Protrudin in Neurite Outgrowth." *Journal of Cellular Biochemistry* 113 (7): 2296–2307. doi:10.1002/jcb.24100.

Zhang, Dongshan, Ruhao Yang, Shixuan Wang, and Zheng Dong. 2014. "Paclitaxel: New Uses for an Old Drug." *Drug Design, Development and Therapy* 8: 279–84.

Zhao, X, D Alvarado, S Rainier, R Lemons, P Hedera, C H Weber, T Tukel, et al. 2001. "Mutations in a Newly Identified GTPase Gene Cause Autosomal Dominant Hereditary Spastic Paraplegia." *Nature Genetics* 29 (3): 326–31. doi:10.1038/ng758.

Zhou, Hongyan, Shili Wu, Jin Young Y Joo, Saiyong Zhu, Dong Wook W Han, Tongxiang Lin, Sunia Trauger, et al. 2009. "Generation of Induced Pluripotent Stem Cells Using Recombinant Proteins." *Cell Stem Cell* 4 (5): 381–84. doi:10.1016/j.stem.2009.04.005.

Zhu, Peng-Peng Peng, Cynthia Soderblom, Jung-Hwa H. Tao-Cheng, Julia Stadler, and Craig Blackstone. 2006. "SPG3A Protein Atlastin-1 Is Enriched in Growth Cones and Promotes Axon Elongation during Neuronal Development." *Human Molecular Genetics* 15 (8): 1343–53. doi:10.1093/hmg/ddl054.

Zivony-Elboum, Yifat, Wendy Westbroek, Nehama Kfir, David Savitzki, Yishay Shoval, Assnat Bloom, Raya Rod, et al. 2012. "A Founder Mutation in Vps37A Causes Autosomal Recessive Complex Hereditary Spastic Paraparesis." *Journal of Medical Genetics* 49 (7): 462–72. doi:10.1136/jmedgenet-2012-100742.

Züchner, Stephan, Gaofeng Wang, Khanh-Nhat Tran-Viet, Martha a Nance, Perry C Gaskell, Jeffery M Vance, Allison E Ashley-Koch, et al. 2006. "Mutations in the Novel Mitochondrial Protein REEP1 Cause Hereditary Spastic Paraplegia Type 31." *American Journal of Human Genetics* 79 (2): 365–69. doi:10.1086/505361.

6 FIGURES

Figure 1.1 Illustration of HSP proteins and their cellular compartments ... 3
Figure 1.2 Scheme of the microtubule severing protein spastin ... 5
Figure 1.3 Formula for the z-factor ... 13
Figure 2.1 INCell analysis ... 35
Figure 3.1 SNP analyses of HSP22f iPSC lines ... 38
Figure 3.2 SNP analysis of HSP23m iPSC line ... 39
Figure 3.3 SNP analyses of HSP24m iPSC lines ... 40
Figure 3.4 Sequencing analysis of mutated region in the *SPAST* gene ... 41
Figure 3.5 Pluripotency-associated markers ... 42
Figure 3.6 *In vivo* differentiation potential of SPG4 iPSCs ... 43
Figure 3.7 *In vitro* differentiation potential of SPG4 iPSCs ... 44
Figure 3.8 Scorecard analysis ... 45
Figure 3.9 Validation of transgene silencing ... 46
Figure 3.10 Cortical differentiation scheme ... 46
Figure 3.11 Differentiation of iPSCs to cortical progenitors and neurons ... 47
Figure 3.12 Validation of iPSC-derived cortical neurons ... 48
Figure 3.13 Marker quantification of cortical neurons ... 49
Figure 3.14 Layer identity of cortical neurons after three months on mouse astrocytes ... 50
Figure 3.15 Electrophysiological properties of cortical neurons ... 50
Figure 3.16 Assessment of spastin expression ... 52
Figure 3.17 Neurite outgrowth assay ... 53
Figure 3.18 Growth cone area of SPG4 neurons ... 54
Figure 3.19 Taxol induces Tau1-positive axonal structures ... 55
Figure 3.20 Analysis of axonal swellings in cortical HSP and control neurons ... 57
Figure 3.21 Derivation of GABAergic neurons ... 59
Figure 3.22 Electrophysiological properties of GABAergic neurons ... 60
Figure 3.23 Analysis of neurite outgrowth and growth cone area in GABAergic neurons ... 61
Figure 3.24 Assessment of swellings in GABAergic neurons ... 62
Figure 3.25 Comparative qPCR analysis of cortical and GABAergic neurons ... 63
Figure 3.26 The effect of read-through molecules on spastin expression ... 65
Figure 3.27 Timeline for drug treatment in the neurite outgrowth and growth cone assay ... 67
Figure 3.28 Neurite outgrowth modulation in SPG4 neurons ... 68
Figure 3.29 Growth cone area modulation in SPG4 neurons ... 70
Figure 3.30 Examples for successful neurite outgrowth and growth cone area modulation. 71
Figure 3.31 Timeline for drug treatment in the axonal swelling assay ... 72
Figure 3.32 Overview of axonal swelling modulation in SPG4 neurons ... 73

Figure 3.33 Examples of axonal swelling modulation in SPG4 neurons..... 74
Figure 3.34 Neurite outgrowth assay using cryopreserved neurons..... 76

7 TABLES

Table 2.1 Cell lines 15
Table 2.2 Cell culture instruments 15
Table 2.3 Cell culture materials 16
Table 2.4 Cell culture media 17
Table 2.5 Cell culture reagents 19
Table 2.6 Molecular biology instruments 26
Table 2.7 Molecular biology materials 26
Table 2.8 Molecular biology reagents 27
Table 2.9 Molecular biology kits 28
Table 2.10 Molecular biology buffers 28
Table 2.11 Primary antibodies and dyes 29
Table 2.12 Secondary antibodies 29
Table 2.13 Primer Sequences 30
Table 2.14 Analysis software 31
Table 2.15 Quick Extract cycle program 31
Table 2.16 Reverse transcription 31
Table 2.17 Sequencing PCR 32
Table 2.18 Scorecard PCR 32
Table 2.19 Semi-quantitative PCR (GoTaq) 33
Table 2.20 quantitative PCR (GoTaq) 33
Table 2.21 quantitative PCR (Taq) 33
Table 3.1 Generation of SPG4 patient iPSC clones 37
Table 3.2 Overview of tested small molecules 67
Table 3.3 Overview of tested small molecules and p-values obtained for SPG4 neurons ... 75

8 APPENDIX

8.1 Abbreviations

Abbreviation	Full name
AAA	ATPase associated with various cellular activities
ABCA1	ATP-binding cassette transporter
AD	Alzheimer's disease
AFP	α-fetoprotein
ALS	amyotrophic lateral sclerosis
ApoE	apolipoprotein E
AraC	Cytosine β-D-arabinofuranoside hydrochloride
B4GALNT1	β-1,4-N-acetyl-galactosaminyl transferase 1
BAF	B allele frequency
BAF	B allele frequency
BMP	bone morphogenetic protein
CHMP1B	charged multi-vascular body protein 1B
CNVs	copy number variations
COX-2	cyclooxygenase-2
CRISPR	clustered regularly interspaced short palindromic repeats
CSMN	corticospinal motor neurons
CYP7B1	cytochrome P450-7B1
DNA	deoxyribonucleic acid
E8	essential 8
EBs	embryoid bodies
EGFR	epidermal growth factor receptor
EHS	Engelbreth-Holm-Swarm
EpiSCs	epiblast derived stem cells
ER	endoplasmic reticulum
ESCRT	endosomal sorting complex required for transport
ESCs	embryonic stem cells
FA2H	fatty acid 2-hydroxylase
FCS	fetal call serum
FGF	fibroblast growth factor
GAD	glutamate decarboxylase
GFR	growth factor reduced
GGPP	geranylgeranylpyrophosphate
gRNA	guide RNA
HSP	hereditary spastic paraplegia
HSP60	heat shock protein 60
IPSC	Induced pluripotent stem cell
IST1	increased sodium tolerance
Lif	leukemia inhibitory factor
LRR	Log R ratio
LXR	liver X receptor
MG	Matrigel
min	minutes
MIT	microtubule interacting and trafficking
mPTP	mitochondrial permeability pore
MTBD	microtubule-binding domain
NEAA	Non-essential amino acids
NMJ	neuromuscular junction
PBS	phosphate buffered saline
PLP1	proteolipid protein 1
PSCs	pluripotent stem cells
QC	quality control
REEP1	receptor expression-enhancing protein 1
RNA	ribonucleic acid
ROCK	Rho-associated protein kinase

RT	room temperature
RTN1	reticulon 1
s	seconds
Shh	sonic hedgehog
SMA	smooth muscle actin
SNP	single nucleotide polymorphism
SPG4	Spastic paraplegia 4
TECPR2	tectonin beta propeller repeat containing protein 2
TGF-β	transforming growth factor beta
TTX	tetrodotoxin
TUBB3	β-III-tubulin
vGLUT1	vesicular glutamate transporter 1
VAPB	synaptobrevin-associated membrane protein B
WASH	Wiskott–Aldrich syndrome protein and scar homolog

8.2 Acknowledgements

Firstly, I am grateful to Prof. Oliver Brüstle for giving me the opportunity to work on this exciting project, for the supervision, the support and for the opportunity to visit international conferences. I am especially grateful for the chance to be part of the COSYN consortium and prove myself in the context of neuropsychiatric diseases with international partners.

Secondly, I want to thank Dr. Michael Peitz for being my direct supervisor.

Additionally, I am indebted to Johannes Jungverdorben for his advice and countless scientific discussions.

Furthermore, I thank my second supervisor Walter Witke for guidance and for recommending and providing the actin-destabilizing small molecules.

I am thankful to the whole AG Peitz, my great colleagues at Life&Brain and to everyone at the institute for the nice atmosphere during the long hours in the cell culture, the office and during coffee brakes and “happy hours”.

Many thanks go to Caro Schuster, Laura Stappert, Marthe-Siobhán Hecke and Beate Roese-Körner for the years of friendship and for proof-reading this thesis.

I thank all my fantastic friends for the wonderful distraction on the weekends and during holidays and Mona Matthews for the stress relief during “bunning”.

Last but not least, I thank my parents and my wonderful husband Jakob for supporting me throughout these often difficult years. I could not have done it without you!

8.3 Declaration

I hereby confirm, that the work conducted in this thesis has been carried out by myself at the Institute of Reconstructive Neurobiology at the University of Bonn. This thesis was prepared under the supervision of Prof. Dr. Oliver Brüstle in fulfillment of the requirements of the doctoral degree of natural sciences of the University of Bonn. I declare that I have written this thesis independently and marked any data that has been collected as part of collaborative projects. I further declare that this work has not been submitted to another university and I have not applied for a doctorate previously.

Bonn,

_____

Kristina Rehbach

8.4 Publications

Scientific reports, under review
K. Rehbach, J. Kesavan, S. Hauser, S. Ritzenhofen, J. Jungverdorben, L. Schöls, M. Peitz, O. Brüstle:
“Rapid multiparametric phenotype assessment as basis for target identification in human SPG4 neurons”

Brain - A Journal of Neurology, June 2017
M. Minnerop, D. Kurzwelly, H.Wagner, A. Soehn, J. Reichbauer, F. Tao, T.W. Rattay, M. Peitz, **K. Rehbach**, … O. Brüstle, T. Klopstock, K.D. Mathews, M.E. Shy, P. de Jonghe, P.F. Chinnery, R. Horvath, J. Kohlhase, I. Schmitt, M. Wolf, S. Greschus, K. Amunts, W. Maier, L. Schöls, P. Nürnberg, S. Zuchner, T. Klockgether, A. Ramirez, R. Schüle:
“Hypomorphic mutations in POLR3A are a frequent cause of sporadic and recessive spastic ataxia”

Cellular and Molecular Life Sciences, November 2015
L. Heesen, M. Peitz, L. Torres-Benito, I. Hölker, K. Hupperich, **K. Dobrindt**, J. Jungverdorben, S. Ritzenhofen,B. Weykopf, D. Eckert, SM. Hosseini-Barkooie, M. Storbeck, N. Fusaki, R. Lonigro, R. Heller, MJ. Kye, O. Brüstle, B. Wirth:
“Plastin 3 is upregulated in iPSC-derived motoneurons from asymptomatic SMN1-deleted individuals”

Science, March 2015
J. Ruschel, F. Hellal, K. C. Flynn, S. Dupraz, D. A. Elliott, A. Tedeschi, M. Bates, C. Sliwinski, G. Brook, **K. Dobrindt**, M. Peitz, O. Brüstle, M. D. Norenberg, A. Blesch, N. Weidner, M. B. Bunge, J. L. Bixby, F. Bradke:
“Systemic Administration of Epothilone B Promotes Axon Regeneration after Spinal Cord Injury”